HAL open science

Asymptotic modeling and discretisation of magnetic components in eddy current problems

Mohammad Issa

To cite this version:

Mohammad Issa. Asymptotic modeling and discretisation of magnetic components in eddy current problems. Electromagnetism. Université Paul Sabatier - Toulouse III, 2019. English. NNT : 2019TOU30177 . tel-02500653

HAL Id: tel-02500653

https://theses.hal.science/tel-02500653v1

Submitted on 6 Mar 2020

HAL is a multi-disciplinary open access archive for the deposit and dissemination of scientific research documents, whether they are published or not. The documents may come from teaching and research institutions in France or abroad, or from public or private research centers.

L'archive ouverte pluridisciplinaire **HAL**, est destinée au dépôt et à la diffusion de documents scientifiques de niveau recherche, publiés ou non, émanant des établissements d'enseignement et de recherche français ou étrangers, des laboratoires publics ou privés.

THÈSE

En vue de l'obtention du

DOCTORAT DE L'UNIVERSITÉ DE TOULOUSE

Délivré par : *l'Université Toulouse 3 Paul Sabatier (UT3 Paul Sabatier)*

Présentée et soutenue le *30/10/2019* **par :**

Mohammad ISSA

Modélisation asymptotique et discrétisation des composants magnétiques dans les problèmes de courant de Foucault.

JURY

Ruth V. SABARIEGO	Professeur d'Université	Rapporteur
Stéphane CLÉNET	Professeur d'Université	Rapporteur
Olivier COULAUD	Directeur de Recherche	Examinateur
Yvan LEFEVRE	Chargé de Recherche	Examinateur
Ronan PERRUSSEL	Chargé de Recherche	Directeur de thèse
Jean-René POIRIER	Maître de Conférence	Co-Directeur de thèse
Laurent KRÄHENBÜHL	Directeur de Recherche	Invité

École doctorale et spécialité :
GEET : Électromagnétisme et Systèmes Haute Fréquence
Unité de Recherche :
LAPLACE - LAboratoire PLAsma et Conversion d'Énergie
Directeur de Thèse :
Ronan PERRUSSEL
Rapporteurs :
Ruth V. SABARIEGO et *Stéphane CLÉNET*

Remerciements

Il me sera très difficile de remercier tout le monde car c'est grâce à l'aide de nombreuses personnes que j'ai pu mener cette thèse à son terme.

Les travaux de thèse présentés dans ce mémoire ont été effectués au LAboratoire PLAsma et Conversion d'Energie (LAPLACE) dans le Groupe de Recherche en Electromagnétisme (GRE), en collaboration avec le Groupe de Convertisseurs Statiques (CS) du même laboratoire, et avec le laboratoire de Génie Électrique de Grenoble (G2Elab).

Je remercie Monsieur Stéphane CLENET, professeur à ParisTech-école nationale supérieure d'arts et métiers et Madame Ruth Vazquez SABARIEGO, professeure à l'université catholique de Louvain d'avoir accepté de rapporter ma thèse. Je vous remercie pour votre lecture attentive, rigoureuse ainsi que pour vos chaleureux commentaires. Vos remarques et conseils ont permis d'améliorer la clarté de la présentation des idées véhiculées par le présent manuscrit.

Je remercie également Monsieur Olivier COULAUD, Directeur de recherche à l'INRIA de Bordeaux, et Monsieur Yvan LEFEVRE, chargé de recherche au LAPLACE-TOULOUSE, qui ont bien voulu être examinateurs dans mon jury de thèse.

Je remercie chaleureusement Monsieur Ronan PERRUSSEL, mon directeur de thèse pour son écoute, son soutien, et ses conseils tout au long de cette thèse et qui m'a fait partager ses brillantes intuitions. Je le remercie aussi pour les nombreuses réflexions que nous avons pu mener ensemble et au travers desquelles il a partagé une partie de son expérience avec moi. Qu'il soit aussi remercié pour sa gentillesse, sa disponibilité permanente, sa patience et pour les nombreux encouragements qu'il m'a prodigué. Tu étais mon directeur, mon frère, et mon ami. Tout simplement merci!

J'adresse mes meilleurs sentiments à Monsieur Jean-René POIRIER, mon Co-directeur de thèse pour son aide constante et ses conseils judicieux tant du point de vue scientifique et académique. Tout au long de ces années de thèse, il m'a donné non seulement des conseils scientifiques, et l'expérience pédagogique mais aussi beaucoup d'encouragements. Je lui en suis très reconnaissant.

Je remercie Monsieur Laurent Krähenbühl pour l'honneur qu'il m'a fait d'être dans mon jury de thèse. Merci pour les informations précieuses à chaque discussion lors d'une partie importante de la thèse.

Je remercie Monsieur Emmanuel SARRAUTE pour son encadrement durant ma thèse, pour la discussion et les explications fructueuses, notamment sur l'aspect physique du

problème.

Je tiens à remercier Monsieur Olivier Chadebec, directeur de recherche à G2Elab de Grenoble, de m'avoir aidé à réaliser la partie numérique de ma thèse. Je remercie également Monsieur Gérard Meunier, merci de m'avoir accordé du temps. Votre compétence et complémentarité m'ont aussi beaucoup apporté. Merci également à tous les membres de l'équipe "MAGE" de G2Elab de m'avoir accueilli durant de nombreux séjours là-bas, plus particulièrement merci à Bertrand Bannwarth.

Je tiens à remercier Monsieur Victor Péron, maître de conference à l'université de Pau et des Pays de l'Adour pour son aide, et sa coopération lors d'une partie théorique de ma thèse. Je remercie également Monsieur Clair Poignard, directeur de recherche à l'inria Bordeaux de m'avoir aidé à réaliser la dernière partie de ma thèse. La collaboration avec lui a été productive et réussie.

Durant ces années de thèse, j'ai eu l'occasion de faire la connaissance de nombreuses personnes au contact desquelles j'ai beaucoup appris. Les échanges avec les membres de l'équipe au labo ont toujours été enrichissant et sympa : merci à Nathalie Raveu (merci pour ton soutien et tes remarques), Anne-Laure Franc, Hamza Kaouach, et Olivier Pigaglio. Je salue notre collègues du labo Frédéric Messine, il m'a soutenu pendant toute cette période et il m'a beaucoup aidé dans le cadre d'enseignement et a partagé avec moi son expérience pédagogique, Alors Merci ! Je salue bien sûr mes collègues avec qui on a passé que des bons moments : Priscillia, Jing-yi, Wencong et plus particulièrement à ma meilleure amie Lucille avec qui j'ai passé la plus longue durée au Labo. Merci de m'avoir tenu compagnie pendant ces dernier trois ans, de m'avoir encouragé, et pour toutes les discussions. Un grand Merci pour tout !

Je tiens à exprimer ma gratitude à Monsieur Paul ARMAND et à Monsieur Olivier Ruatta pour leur extrême disponibilité, et les discussions qui m'ont orienté vers ce sujet de thèse.

Je salue tous mes amis qui m'ont encouragé pendant ces années : Abdalah, Hamza, Ali, Hicham, Nouh, Farah, Iman, Fatima, André, Andrea, ... Mes remerciements vont naturellement à mes amies les plus proches, Abbas Hamadi, Bilal Fakih et Mohanad Alchaar. Ils m'ont supporté jusqu'au dernier moment, ils étaient ma source d'optimisme, de sécurité, et de pouvoir. Merci pour votre gentillesse, votre bienveillance.

Enfin, je souhaite remercier tous mes proches et toute ma famille qui m'on supporté dès le premier battement de coeur et surtout pour avoir accepté la distance géographique qui nous sépare, en particulier mes parents, Ibrahim et Hala, tous mes frères et soeurs, Saiid, Mahmoud, Manal, Zeinab, et Kawthar, ma fiancée Farah, mes beaux frères et belles soeurs, Ahmad, A. Badran, A. kamal, Amani, et Reef, ainsi que mes petites nièces et petits neveux.

Bien entendu merci à tous les autres que j'ai probablement oublié involontairement, et pour cela je m'en excuse.

Abstract

Modeling of integrated magnetic components in electrical engineering (such as high frequency transformers) leads to several issues related to frequency increase. This frequency increase induces eddy currents in conducting material which require very fine meshes and consequently, it leads to large systems of equations and prohibit computational cost, especially for 3D structures. The commercial scientific software only partially tackle these issues due notably to the presence of airgaps (modeling "infinite" medium by radiating conditions), the presence of thin layers (very heterogeneous meshes), and the inclusion of winding multi-layers.

To deal with these difficulties, dedicated tools have been implemented. The primary issue that is the presence of airgaps is treated by solving a coupled "Finite Element Method (FEM)/ Boundary Element Method (BEM)" system in 3D. The BEM is adapted to general field problems with unbounded structures because no artificial boundaries are needed, this is not the case for the FEM. Moreover, the BEM requires only a surface discretisation which reduces the number of unknowns and then the computational time.

The secondary issue is to deal with thin conductive layers used in a wide range of applications for shielding purpose. Modeling such conductive regions require very fine volume discretisation due to the rapid decay of fields through the surface for high frequencies. To avoid this difficulty, we derive an equivalent model for 3D Eddy Current problem with a conductive thin layer of slight thickness, where the conductive sheet is replaced by its mid-surface, and its shielding behaviour is satisfied by an equivalent transmission condition which connects the electric and magnetic fields around the surface. In addition, an efficient discretisation using the BEM is provided to solve numerically the problem with the transmission condition.

The last issue is to tackle the foil winding problems. We proceed by considering the simple case of a problem of laminar stacks. We provide an effective modeling of the laminar stacks in 1D and 2D by deriving the classical homogenisation in the domain of the laminar stacks. Then, we study the influence of the interface (with air) on the vector potential to treat the problem in the whole domain. We also consider the case where the skin depth is kept less than or equal to the thickness of the metal sheet.

Résumé

La modélisation de composants magnétiques intégrés en génie électrique (ex. les transformateurs hautes fréquences) conduit à un certain nombre de problèmes liés à l'augmentation de la fréquence. Cette augmentation de fréquence induit notamment des courants de Foucault dans les pièces conductrices qui nécessitent des maillages très fins et conduit de grands systèmes d'équations et donc souvent à des temps de calcul prohibitifs, notamment pour les structures 3D. Les outils de calcul numérique commerciaux ne répondent que partiellement à ces difficultés, induites notamment par la présence d'entrefers (modélisation du milieu «infini» par une condition de radiation), la présence des couches minces (maillages très hétérogènes) et la prise en compte d'enroulements multi-couches.

Pour répondre à ces difficultés, on se propose de développer des outils dédiés. Une première action a été menée pour répondre au problème de grands entrefers en résolvant un système avec deux techniques couplées : la méthode des éléments finis volumiques (FEM) et la méthode des éléments finis de frontière (BEM) en 3D. La BEM est bien adaptée aux problèmes avec des structures non bornées, car aucune condition aux limites artificielle n'est nécessaire, ce qui n'est pas le cas pour la FEM. De plus, la BEM ne nécessite qu'une discrétisation de surface, ce qui réduit le nombre d'inconnues et généralement le temps de calcul.

Une autre problématique sera de traiter les couches conductrices minces utilisées dans un large éventail d'applications à des fins de blindage. La modélisation de telles régions conductrices requiert une discrétisation volumique très fine en raison de la décroissance rapide des champs vers la surface pour les hautes fréquences. Pour éviter cette difficulté, nous dérivons un modèle équivalent pour le problème des courants de Foucault en 3D avec une couche mince conductrice de faible épaisseur, dans laquelle la feuille conductrice est remplacée par sa surface médiane, et son comportement de blindage est satisfait par une condition de transmission équivalente qui relie les champs électrique et magnétique autour de la surface. De plus, une discrétisation efficace utilisant la BEM est proposée pour résoudre numériquement le problème avec la condition de transmissions.

La dernière problématique est de traiter les problèmes d'enroulements. Nous procédons en considérant le cas plus simple d'un problème d'empilement de tôles. Nous fournissons une modélisation efficace des empilements des tôles en 1D et 2D en utilisant l'homogénéisation classique dans le domaine des empilements. Ensuite, nous étudions l'influence de l'interface (avec l'air) pour traiter le problème dans le domaine entier. Nous considérons le cas où la profondeur de pénétration est maintenue inférieure ou égale à l'épaisseur de la tôle.

Contents

Remerciements iii

Abstract v

Résumé vii

Table des matières xii

Figures xiv

Tableaux xv

Notations xvii

Introduction 1
- 0.1 Objective . . . 3
- 0.2 Plan of the thesis . . . 4
- 0.3 Contributions . . . 4

1 Introduction to Eddy-Current Problems and Discretisation Techniques 7
- 1.1 Maxwell's equations . . . 8
- 1.2 Eddy-current approximation of Maxwell's equations . . . 12
- 1.3 Formulations of eddy current problems . . . 12
  - 1.3.1 An Electric Field Formulation . . . 14
  - 1.3.2 A Magnetic Field Formulation . . . 14
  - 1.3.3 $E - H$ Formulation . . . 15
  - 1.3.4 $E - \Phi$ Formulation . . . 15
  - 1.3.5 A Magnetic Vector Potential Formulation A . . . 16
- 1.4 Finite Element Method . . . 16
  - 1.4.1 Example . . . 17
  - 1.4.2 Advantages and disadvantages of the Finite Element Method . . . 19
- 1.5 Boundary Element Method . . . 19
  - 1.5.1 Boundary Integral Equation by Scalar Form of Green's Identity . . . 20
  - 1.5.2 Example . . . 23
  - 1.5.3 Advantages and disadvantages of the Boundary Element Method . . . 24
- 1.6 Shape functions . . . 25
  - 1.6.1 Nodal shape functions - H(grad) . . . 26
  - 1.6.2 Edge shape functions - H(curl) . . . 27
  - 1.6.3 Cell shape functions . . . 27

2 FEM/BEM coupling for Magnetostatic and Eddy Current problems **29**
2.1 Why FEM/BEM ? . . . 30
2.1.1 Setting of the problem . . . 31
2.2 $\Phi - \Phi$ Formulation for Magnetostatic Field Equations . . . 32
2.2.1 Weak formulation for Φ in Ω_C . . . 32
2.2.2 Integral equation for Φ in Ω_A . . . 33
2.2.3 Coupled variational formulation . . . 33
2.2.4 FEM/BEM discretisation . . . 35
2.2.5 Numerical results . . . 36
2.3 $A - \Phi$ Formulation for Magnetodynamique Field Equations . . . 37
2.3.1 Weak formulation for A in Ω_C . . . 39
2.3.2 Integral equation for Φ in Ω_A . . . 40
2.3.3 Coupled variational formulation . . . 40
2.3.4 FEM/BEM discretisation . . . 41
2.3.5 Numerical results . . . 42
2.4 Conclusion and Perspectives . . . 43

3 Boundary Element Method for 3D Conductive Thin Layers in Eddy-Current Problems **45**
3.1 Introduction . . . 47
3.2 Mathematical Model . . . 49
3.2.1 Notations . . . 49
3.2.2 Eddy Current Problem for a Thin Layer . . . 50
3.2.3 $\mathbf{E}^\varepsilon_\pm/\mathbf{H}^\varepsilon_0$ Hybrid Formulation . . . 52
3.2.4 Objective . . . 54
3.3 Multiscale Expansion and Equivalent Models with Transmission Conditions 55
3.3.1 Equations of the coefficients of $E^\varepsilon_\pm/H^\varepsilon_0$ . . . 56
3.4 Equivalent Models up to order 2 . . . 59
3.4.1 Equivalent Model of Order 1 . . . 59
3.4.2 Equivalent Model of Order 2 . . . 60
3.5 Discretisation by the Boundary Element Method . . . 63
3.5.1 Functional Spaces . . . 64
3.5.2 Potentials . . . 64
3.5.3 Boundary Integral Equations . . . 65
3.5.4 Equivalent Model of Order 1 . . . 66
3.5.5 Strong Formulation for E_1 . . . 68
3.5.6 Equivalent Model of Order 2 . . . 69
3.5.7 Implementation . . . 71
3.6 Numerical Results . . . 71
3.6.1 Validation of Integral Equations . . . 72
3.6.2 Verification of the consistency of H^1_ε with H_0 and $H_0 + \varepsilon H_1$ . . . 73
3.6.3 Example 1 . . . 73
3.6.4 Example 2 . . . 75
3.6.5 Example 3 . . . 77
3.6.6 Example 4 . . . 79
3.7 Conclusion . . . 80

4 Homogenisation and boundary correction of laminar stacks in vector potential formulation. 83
4.1 Mathematical Formulation . . . 86
4.2 Procedure . . . 88
4.3 The 1D model problem . . . 88
4.3.1 Expansion of $\mathcal{M}^\varepsilon$ . . . 89
4.3.2 Classical homogenisation of the laminar stacks in Ω_L . . . 89
4.3.3 Numerical validation in Ω_L . . . 91
4.3.4 Accounting of the interface . . . 92
4.3.5 Numerical validation in Ω . . . 94
4.4 The 2D model problem . . . 95
4.4.1 Expansion of $\mathcal{M}^\varepsilon$ . . . 96
4.4.2 Classical homogenisation of the laminar stacks in Ω_L . . . 96
4.4.3 Recombination of the results . . . 100
4.4.4 Numerical results . . . 100
4.5 Conclusion . . . 101

Conclusion 103

A Annex 105
A.1 Expansion of differential operators inside the conductive sheet Ω_0^ε [59, section 5.1] . . . 105
A.2 . . . 106
A.3 . . . 107
A.4 . . . 107
A.5 . . . 107
A.6 Calculation of the External Field . . . 108
A.6.1 First term H_0 . . . 108
A.6.2 Second term H_1 . . . 108
A.6.3 Second order H_ε^1 . . . 109
A.7 Analytical Solution of the Eddy-Current Problem for a Sphere with a Thin Layer in 3D . . . 109
A.7.1 Formulation of the problem . . . 109
A.7.2 Mathematical Analysis . . . 111
A.8 Analytical Solution of the Eddy-Current Problem for a Sphere without Thin Layer . . . 112

Annexes 105

B Annex 115
B.1 Appendix . . . 115
B.1.1 . . . 115
B.1.2 . . . 115
B.1.3 . . . 115
B.1.4 Analytical solution of A_ε in the domain of lamination stack Ω_L . . . 116
B.1.5 Approximation of the derivative of A_ε along x_2 by the asymptotic expansion in power series of δ . . . 116

Publications **119**

List of Figures

1 1
2 An anechoic chamber used to measure antenna characterisation. https://www.comsol.fr 1
3 The skin effect in a thin layer. 2
4 A mesh consists of 825,207 elements and 10,956,146 DOF. It needs a storage of 69,77GB, and 37 mins 6 secs to be created. 3

1.1 10
1.2 The different sides of the interface Γ. 11
1.3 A cross section of the domain Ω. 13
1.4 The mesh in 2D for the Finite Element Method 20
1.5 The mesh in 2D for the Boundary Element Method 25
1.6 First order tetrahedral nodal finite element in local coordinates. 26

2.1 A cross section of the two sub-domains Ω_A and Ω_c and their corresponding appropriate numerical methods. 31
2.2 37
2.3 The x and z components of H_{Comsol}, and H_{Mipse}. 38
2.4 Potential Φ on the sphere. 38
2.5 Normal induction B_n on the sphere. 38
2.6 Magnetic field on the sphere. 38
2.7 The x and z components of the real part of the magnetic fields H_{Mipse} using cell shape functions, and H_{Comsol} in 2D axisymmetry. 43
2.8 The x and z components of the real part of the magnetic fields H_{Mipse} using nodal shape functions, and H_{Comsol} in 2D axisymmetry. 43

3.1 A cross section of the domain Ω 49
3.2 A cross section of the domain Ω 51
3.3 The cross sections of the domain of the main problem $\Omega_-^\varepsilon \cup \overline{\Omega_0^\varepsilon} \cup \Omega_+^\varepsilon$ and of the approximate problem $\Omega_- \cup \Omega_+$ 54
3.4 Normalised domain 56
3.5 Taylor expansion around the mid-surface. 56
3.6 Basis function of H_h associated with a vertex 67
3.7 A cross section of the domain 72
3.8 The magnetic field H_0 on the arc of radius 1.3m compared to the analytical solution 72
3.9 L^2 error of the solution H_ε^1 with respect to H_0 and $H_0 + \varepsilon H_1$ 73
3.10 The real and imaginary part $\gamma^+ E_\varepsilon^1$ and $\gamma^- E_\varepsilon^1$ for a spherical thin layer of radius 0.99m and thickness 0.02m. 74

3.11 The magnetic fields H_0 and H^1_ε on the arc of radius 1.3m compared to the analytical solution. 75
3.12 The magnetic fields $H_{analytic}$ and H^1_ε in the interior domain of the sphere. . 76
3.13 Relative L^2 errors of the solutions H_0 and H^1_ε of the equivalent models of order 1 and 2 versus the parameter $\tilde{\sigma}$ for $\varepsilon = 4$cm 76
3.14 A spherical thin sheet with a cylindrical Coil 77
3.15 The real part of $\gamma^+_N E^1_\varepsilon$ 77
3.16 The imaginary part of $\gamma^+_N E^1_\varepsilon$ 77
3.17 The x component of H_0, H_{Comsol}, and the source field H_s. 78
3.18 The x component of H^1_ε, H_{Comsol}, and the source field H_s. 78
3.19 The z component of H_0, H_{Comsol}, and the source field H_s. 78
3.20 The z component of H^1_ε, H_{Comsol}, and the source field H_s. 78
3.21 Meshing the domain in Comsol 79
3.22 A cylindrical thin layer with an exterior spire 80
3.23 The magnetic fields H_0 and H^1_ε on the segment compared to Comsol (H_{com}) 80
3.24 The $x-$component of the real part of the total magnetic fields H^1_ε, the reduced magnetic fields $H^1_{\varepsilon Reduced}$ and the source field H_{Source}. 81
3.25 The $z-$component of the real part of the total magnetic fields H^1_ε, the reduced magnetic fields $H^1_{\varepsilon Reduced}$ and the source field H_{Source}. 81

4.1 Representation of the whole domain Ω which consists of an air domain Ω_A and a lamination stack Ω_L. A global magnetic flux and a current source will be enforced. 86
4.2 The magnetic vector potential in Ω_L for $\omega = 50$. 92
4.3 The magnetic vector potential in Ω_L for $\omega = 10^3$. 92
4.4 Relative L^2-errors of the solution A^1_ε versus the thickness ε. 93
4.5 The magnetic vector potential in Ω for $\omega = 50$ 94
4.6 The magnetic vector potential in Ω for $\omega = 10^3$ 94
4.7 Relative L^2-errors of the solution A^1_ε versus the thickness ε. 95
4.8 Relative L^2-errors of the solution A^1_ε versus $\bar{\alpha}$. 96
4.9 99
4.10 The magnetic vector potential A^1_ε in Ω_L compared to the numerical solution A_{FDM}. 101

A.1 A cross section of the domain 109
A.2 A cross section of the domain 113

List of Tables

2.1 Relative L^2-errors of the solution H_{Mipse}. 37
2.2 Relative L^2-errors of the solution H_{Mipse}. 42

3.1 L^2-relative errors of H_0 and H^1_ε 78
3.2 L^∞-errors of H_0 and H^1_ε 80
3.3 Computational time of our models comparing with Comsol 80

4.1 Relative L^2-errors of the solution A^1_ε for several ω. 92

Notations

E	Electric field (V/m).
H	Magnetic field (A/m).
B	Magnetic induction (T).
D	Electric induction (C/m^2).
J	Current density (A/m^2).
A	Magnetic vector potential (Wb/m).
Φ	Scalar potential.
μ	Magnetic permeability (H/m).
σ	Electric conductivity (S/m).
ω	Angular frequency (rad/s).
f	Frequency (Hz).
$\times$	Cross product.
$\mathbb{I}d$	Identity operator.
ε	Thickness of the thin layer.
δ	The skin depth.
$[\,\cdot\,]_\Gamma$	The Jump through Γ.
$\{\cdot\}_\Gamma$	The mean.
$\gamma_D\cdot$	Dirichlet trace.
$\gamma_N\cdot$	Neumann trace.
$\gamma_n\cdot$	Normal trace.
$L^2(\Gamma)$	square integrable vector fields.
$H_{\parallel}^{\frac{1}{2}}(\Gamma)$	Vector fields with tangential continuity.
$H_{\perp}^{\frac{1}{2}}(\Gamma)$	Vector fields with normal continuity.
H_{Mipse}	Magnetic field calculated by simulations done in Mipse.
H_{Comsol}	Magnetic field calculated by simulations done in Comsol.
L^2-error	$\|\|U-V\|\|_2 = \sqrt{\sum_i (U_i - V_i)^2}$
L$^\infty$-error	$\|\|U-V\|\|_\infty = \max_i \|U_i - V_i\|$
$\langle\cdot,\cdot\rangle_\Omega$	$\langle f, g\rangle_\Gamma = \int_\Omega f(x)g(x)d\Omega(x)$

Introduction

Eddy currents appear in various electrical systems, for example in motors, or in power electronics devices. Thin conductive layers also appear in many of these devices: for instance, shielding of transformers, casing of devices, foil windings, or constructing a chamber to measure antenna features (see Figures 1 and 2).

The phenomenon of eddy currents was discovered by the French physicist Léon Foucault in 1851. Supplying an electric current creates a time-varying magnetic field, that will induce eddy currents in the conductive domain (according to Faraday's law). An induced magnetic field is then produced which is opposite to the excitation field, and then reduces the total magnetic field (according to Ampère's law). The subject of this thesis is about asymptotic modeling and discretisation of magnetic components in eddy-current problems, especially in the presence of thin layers.

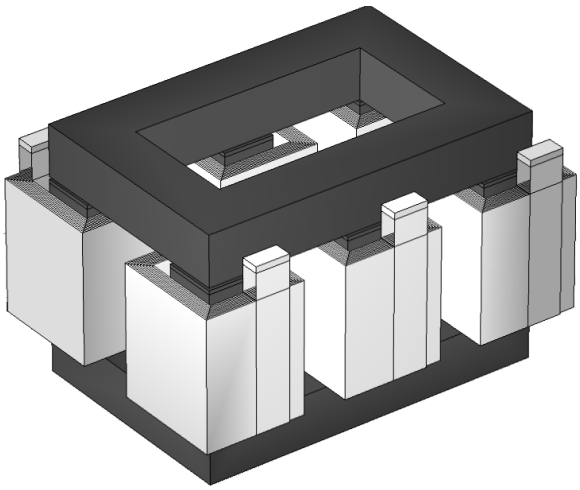

Figure 1

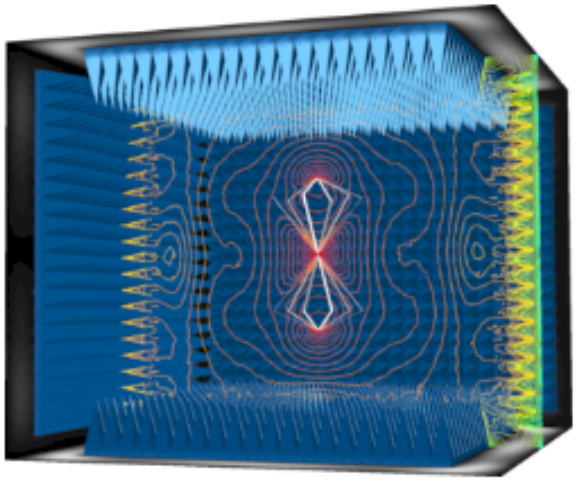

Figure 2: An anechoic chamber used to measure antenna characterisation. https://www.comsol.fr

An accurate calculation of the magnetic field distribution is necessary to optimise the design of the electrical devices. At a high frequency, the incoming electromagnetic fields do not penetrate completely into the interior of the material. In this case, the current will circulate exclusively on the surface of the conductors. This is often called "the skin effect". In this case, very fine meshes are required in the conducting material which lead to a large system of equations and prohibitive computational times, especially for 3D structures. Moreover, in the presence of large homogeneous volumes like the exterior

air, it will be more expensive if we consider numerical methods which require a volume discretisation (like the finite element method, or the finite difference method).

The phenomenon of skin effect restricts the current to the skin depth calculated as follows:

$$\delta = \sqrt{\frac{2}{\mu\sigma\omega}},$$

where μ is the magnetic permeability (H/m), σ is the electric conductivity (S/m), and ω is the angular frequency (rad/s). Thus, δ is equal to the distance where the majority of the current density circulates in a conductor (around 63% of the current density). The current density in the conducting medium is described by the following formula:

$$J(r) = J_0 e^{-r/\delta},$$

where r is the depth from the surface. Consequently, the current density decreases exponentially from its initial value at the surface J_0.

In Figure 3, we show the flow of current in a thin layer with respect to its thickness and skin depth (according to the possible cases $\delta \ll \varepsilon$, $\delta \approx \varepsilon$, and $\delta \gg \varepsilon$). For $\delta \ll \varepsilon$, this is the case for high frequencies, the density current circulates only near the interface which makes the simulation more problematic because the field decays rapidly near the interface. Mesh of $\delta/2$ maximum element size is then needed to reach a minimal accuracy.

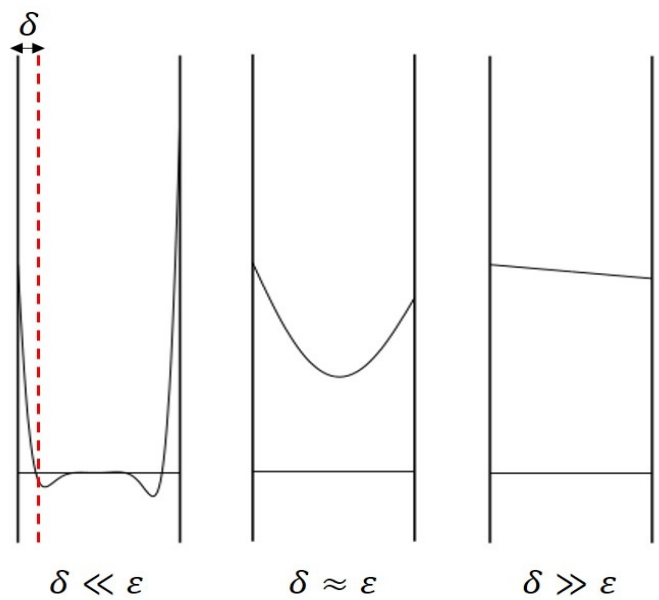

Figure 3: The skin effect in a thin layer.

Based on that, numerical simulations of structures containing thin layers is still a challenge for many reasons:

- It is difficult to mesh by some mesh generators.

- Heterogeneous meshes can lead to ill-conditioned matrices, and regular meshes will lead to a high number of degrees of freedom.

In fact, a lot of commercial softwares exist for simulating 3D structures in eddy-current problems, but there are still also many issues which are only partially tackled. In this thesis, we handle partially the issues related to the presence of large homogeneous mediums, the presence of thin layers, and the inclusion of winding multi-layers.

0.1 Objective

In the context of this thesis, we will focus on the modeling of thin layers by asymptotic expansion and an appropriate discretisation in eddy-current problems. The objectives of this thesis are:

1. To treat the presence of infinite domain considering the appropriate numerical methods in order to reduce the computational time. The coupling of the Finite Element Method (FEM) and the Boundary Element Method (BEM) will be proposed for this reason.

2. To model and discretise the conductive thin layers in eddy-current problems in order to avoid the difficulties of meshing and dealing with strongly refined meshes (see Figure 4). These difficulties can be treated by deriving an equivalent model with transmission conditions that replace the thin layer by its mid-surface, and using a well-adapted method of discretisation as the boundary element method.

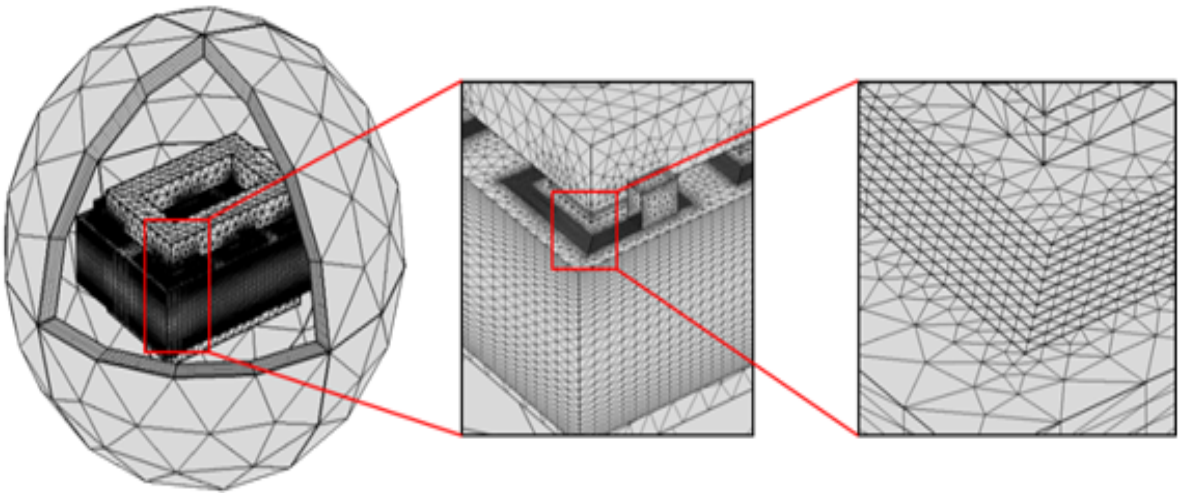

Figure 4: A mesh consists of 825,207 elements and 10,956,146 DOF. It needs a storage of 69,77GB, and 37 mins 6 secs to be created.

3. To deal with the treatment of the foil windings. In this thesis, we start by considering the more simple case of laminar stacks. A homogenisation technique with an

interface correction is derived.

Throughout this thesis, we consider the case where the skin depth is kept less than or equal to the thickness of the metal sheet.

0.2 Plan of the thesis

The thesis manuscript is organized as follows:

1. In the first chapter, we recall briefly the Maxwell equations, as well as its eddy-current approximation. We give some mathematical formulations of the eddy-current problems. We recall the principles of the finite element method and the boundary element method. Finally, we give some shape functions used to approximate the vector fields in the second chapter.

2. In the second chapter, we present the mathematical formulation of the magnetostatic and the eddy-current problems using the magnetic potentials. Both formulations have been discretised using the FEM/BEM coupling. Results are validated in comparison to the analytical solutions.

3. In the third chapter, we present the hybrid formulation of 3D eddy current problems with a thin layer. We provide a formal calculus using the asymptotic expansion in a power series of a small parameter ε (the layer thickness) in order to obtain the equivalent models of the first and second order. We apply the BEM to calculate the first term of the expansion (model of the first order), the second term, and the model of the second order. Some examples are provided to check the accuracy of the models, as well as the efficiency of the discretisation method.

4. In the last chapter, a formulation of the eddy-current problem in laminar stacks using the magnetic vector potential is presented. We demonstrate our procedure concerning the homogenisation in the domain composed of sheets, and the correction at the interface. Some examples are also provided to validate our approach.

Complementary elements including the calculation of analytical solutions and post-processing calculations of the exterior field are given in the appendices.

0.3 Contributions

Various parts of this work make an original contribution to the modelisation and numerical simulations in electromagnetism. In particular, we contribute to the following aspects:

- The modeling of a conductive thin layer for 3D eddy-current problems using a hybrid formulation. The equivalent models with the transmission conditions which replace the layer offer less complexity in discretising the problem [83].

- An efficient discretisation using the BEM in the interior and the exterior domain of the layer is provided for the equivalent models of a conductive thin layer. It validates the accuracy of these models, as well as saving computational time requiring only a surface discretisation. [82 ; 84 ; 85].

- An effective modeling of a lamination stack in 1D using two-scale homogenisation and a correction for the interface between the air and the lamination stack is proposed. This procedure is validated in 1D and shows a agreement comparing with an analytical solution. [101]. Using the same procedure, we proceed to treat the case in 2D that is actually in progress.

CHAPTER 1

Introduction to Eddy-Current Problems and Discretisation Techniques

Contents

1.1 Maxwell's equations **8**

1.2 Eddy-current approximation of Maxwell's equations **12**

1.3 Formulations of eddy current problems **12**

1.3.1 An Electric Field Formulation 14

1.3.2 A Magnetic Field Formulation 14

1.3.3 $E - H$ Formulation 15

1.3.4 $E - \Phi$ Formulation 15

1.3.5 A Magnetic Vector Potential Formulation A 16

1.4 Finite Element Method **16**

1.4.1 Example 17

1.4.2 Advantages and disadvantages of the Finite Element Method . 19

1.5 Boundary Element Method **19**

1.5.1 Boundary Integral Equation by Scalar Form of Green's Identity 20

1.5.2 Example 23

1.5.3 Advantages and disadvantages of the Boundary Element Method 24

1.6 Shape functions **25**

1.6.1 Nodal shape functions - H(grad) 26

1.6.2 Edge shape functions - H(curl) 27

1.6.3 Cell shape functions 27

Electromagnetic phenomena are described by Maxwell's equations, a system of partial differential equations satisfied by the electromagnetic field. In electrical engineering, we often focus on the diffusion of the magnetic field by neglecting the current displacement introduced by Maxwell, this approximation is often called the Eddy-Current Problem.

Discretisation methods play an important role in the solution of eddy current problems. Among these methods, the finite element method is the most widespread. However, the boundary element method can also be considered to approximate the eddy current problems using less unknowns.

In this chapter, we recall the system of Maxwell's equations, and the eddy-current problem in sections 1.1 and 1.2, respectively. In section 1.3, we compare several formulations of the eddy-current problems. Then, we provide the main elements for the numerical simulation of these formulations in sections 1.4, 1.5, and 1.6.

1.1 Maxwell's equations

Maxwell's equations describe the interactions of components of the electromagnetic field. The system of equations can be written in differential form as follows [2]:

- Maxwell-Ampère's law:
$$\frac{\partial \mathcal{D}}{\partial t} + \mathcal{J} = \mathrm{curl}\mathcal{H}, \tag{1.1}$$
which describes the magnetic field $\mathcal{H}$ resulting from the displacement current $\frac{\partial \mathcal{D}}{\partial t}$ and the total current $\mathcal{J}$.

- Faraday's law:
$$\frac{\partial \mathcal{B}}{\partial t} + \mathrm{curl}\mathcal{E} = 0, \tag{1.2}$$
which describes the electric field $\mathcal{E}$ induced by the time variations of the magnetic induction field $\mathcal{B}$.

- Gauss' electrical law:
$$\mathrm{div}\mathcal{D} = \rho, \tag{1.3}$$

which indicates that the charges ρ are the source of the electric displacement field $\mathcal{D}$.

- Gauss' magnetic law:

$$\mathrm{div}\mathcal{B} = 0, \tag{1.4}$$

which indicates that the magnetic induction is solenoidal.

In the previous equations, all the quantities are functions of the space coordinates $x \in \mathbb{R}^3$, and of the time $t \in \mathbb{R}^+$.

Material laws

To complete the system (1.1)-(1.4), relations between ($\mathcal{D}$,$\mathcal{B}$) and ($\mathcal{E}$,$\mathcal{H}$) are introduced for isotropic, homogeneous and linear materials in the form:

$$\mathcal{D} = \varepsilon\mathcal{E}, \tag{1.5}$$

$$\mathcal{B} = \mu\mathcal{H}. \tag{1.6}$$

In addition, the Ohm law expresses the current density in terms of the electric field:

$$\mathcal{J} = \sigma\mathcal{E}, \tag{1.7}$$

where σ denotes the electric conductivity, ε is the electric permittivity, and μ is the magnetic permeability.

Note that when a given current density $\mathcal{J}_s$ is applied, we need to consider the general Ohm law [2]:

$$\mathcal{J} = \sigma\mathcal{E} + \mathcal{J}_s, \tag{1.8}$$

assuming that $\mathrm{div}\mathcal{J}_s = 0$ in any non-conducting region, by reason of the Maxwell-Ampère and Gauss electrical equations.

Eventually, the full Maxwell system of equations can be written in the following form:

$$\begin{cases} \dfrac{\partial\varepsilon\mathcal{E}}{\partial t} + \sigma\mathcal{E} + \mathcal{J}_s &= \mathrm{curl}\mathcal{H}, \\ \dfrac{\partial\mu\mathcal{H}}{\partial t} + \mathrm{curl}\mathcal{E} &= 0, \\ \mathrm{div}\varepsilon\mathcal{E} &= \rho, \\ \mathrm{div}\mu\mathcal{H} &= 0. \end{cases} \tag{1.9}$$

Integral form of Maxwell's Equations

Here, we present the integral form of Maxwell's equations [8]. This form can be shown to be equivalent to the differential forms through the use of the general Stokes' Theorem.

$$\begin{aligned}
\oint_C \mathcal{H} \cdot dl &= \int_S \mathcal{J} \cdot ds + \int_S \frac{\partial \mathcal{D}}{\partial t} \cdot ds, \\
\oint_C \mathcal{E} \cdot dl &= -\int_S \frac{\partial \mathcal{B}}{\partial t} \cdot ds, \\
\oint_S \mathcal{D} \cdot ds &= \int_V \rho dv, \\
\oint_S \mathcal{B} \cdot ds &= 0,
\end{aligned}$$

where $C = \partial S$, $S = \partial V$, and V represent the line integral, surface integral, and volume integral, repectively (see Figure 1.1).

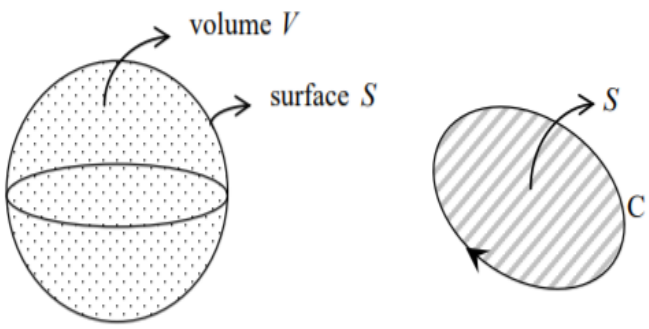

Figure 1.1

The time-harmonic Maxwell's equations

In this thesis, we deal with the time-harmonic fields. Ordinarily, this happens when the excitation fields are time-harmonic. Using this assumption, the applied current density $\mathcal{J}_s$ is an alternating current that has the form

$$\mathcal{J}_s(x,t) = Re[J_s(x)e^{i\omega t}], \tag{1.10}$$

where J_s is a complex-valued vector function called phasor and $\omega \neq 0$ is the angular frequency.

Consequently, we look for a time-harmonic solution through the usual relationship:

$$\mathcal{E}(x,t) = Re[E(x)e^{i\omega t}], \tag{1.11}$$

$$\mathcal{H}(x,t) = Re[H(x)e^{i\omega t}], \tag{1.12}$$

where E, and H are phasors representing the electric and magnetic fields.
By inserting this representation (1.10)-(1.12) into the time-dependent Maxwell equations (1.9) we obtain the following set of the time-harmonic Maxwell's equations:

$$\begin{cases} \mathrm{curl} H - i\omega\varepsilon E &= J, \\ \mathrm{curl} E + i\omega\mu H &= 0, \\ \mathrm{div} D &= \rho, \\ \mathrm{div} B &= 0. \end{cases} \tag{1.13}$$

Transmission conditions

We consider the transmission conditions on the interface between two subdomains (see Figure 1.2). The tangential components of the electric and magnetic fields are continuous:

$$H^+ \times n_{|\Gamma} = H^- \times n_{|\Gamma}, \tag{1.14}$$

$$E^+ \times n_{|\Gamma} = E^- \times n_{|\Gamma}. \tag{1.15}$$

The normal components of the electric displacement field and the magnetic induction are continuous:

$$D^+ \cdot n_{|\Gamma} = D^- \cdot n_{|\Gamma}, \tag{1.16}$$

$$B^+ \cdot n_{|\Gamma} = B^- \cdot n_{|\Gamma}, \tag{1.17}$$

where the signs indicate the different sides of the interface Γ and n is the normal vector of Γ (see Figure 1.2).

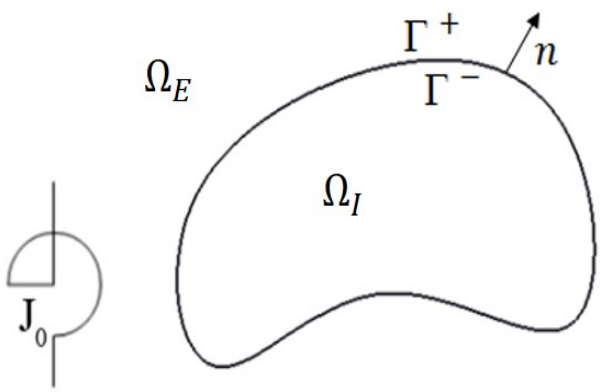

Figure 1.2: The different sides of the interface Γ.

1.2 Eddy-current approximation of Maxwell's equations

The system of equations obtained when the displacement current term $\frac{\partial D}{\partial t}$ (or $i\omega\varepsilon E$ in the time-harmonic regime) can be neglected is called the eddy current approximation or magnetoquasistatic approximation of Maxwell's equations [1]

$$\begin{aligned}
\mathrm{curl} H &= J \text{ in } \mathbb{R}^3, && (1.18)\\
i\omega B + \mathrm{curl} E &= 0 \text{ in } \mathbb{R}^3, && (1.19)\\
B &= \mu H \text{ in } \mathbb{R}^3, && (1.20)\\
J &= \sigma E + J_s \text{ in } \mathbb{R}^3, && (1.21)\\
\mathrm{div} B &= 0 \text{ in } \mathbb{R}^3, && (1.22)\\
\mathrm{div} \varepsilon E &= 0 \text{ in } \mathbb{R}^3. && (1.23)
\end{aligned}$$

To complement this system, we consider the continuity of the tangential traces of the magnetic and electric fields across any interface Γ, as well as the limit condition at infinity

$$\left\{\begin{array}{lll}
[E \times n]_\Gamma & = 0 & \text{on } \Gamma,\\
[H \times n]_\Gamma & = 0 & \text{on } \Gamma,\\
|H(x)| + |E(x)| & = O(|x|^{-2}) & |x| \longrightarrow \infty.
\end{array}\right. \tag{1.24}$$

1.3 Formulations of eddy current problems

In this section, we denote by $\Omega \subset \mathbb{R}^3$ the domain of study, which is composed of two domains

$$\Omega = \Omega_I \cup \Omega_E,$$

where Ω_I is the conductive region and Ω_E the exterior region (air). Let also Γ be the boundary of the domain Ω_I (see Figure 1.3).

There are various ways to reformulate the initial eddy-current problem. By eliminating the electric field [32] (H-Based Formulation), eliminating the magnetic field [33] (E-Based Formulation), or by considering hybrid formulations [20 ; 31].

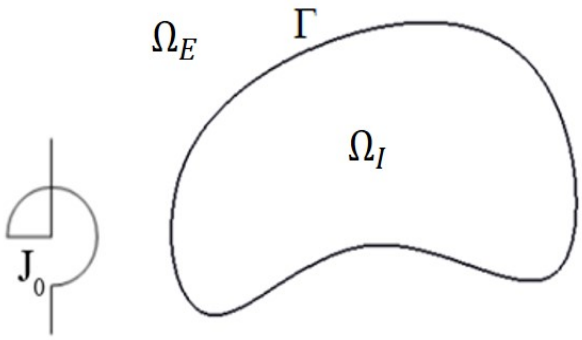

Figure 1.3: A cross section of the domain Ω.

Hybrid formulations are the case where the eliminated field in the conducting region is different from the one eliminated in the exterior domain. Thus there are two possibilities if we consider only the electrical and the magnetic field, the first one is to use a "E-Based formulation" inside Ω_I and a "H-Based formulation" in Ω_E, the second one is to use a "H-Based formulation" inside Ω_I and a "E-Based formulation" in Ω_E.
In addition, we may consider the formulations in terms of the potentials that describe the E and H fields [19 ; 22], i.e. the magnetic vector potential or the scalar magnetic potential for instance.

Boundary conditions

When electromagnetic problems are defined in an unbounded domain, a boundary far away from the electromagnetic device should be considered with either Dirichet or Neumann boundary conditions [10], asymptotic boundary conditions [11], Robin boundary conditions [9], Kelvin transformation [12], or shell transformation [13].
In the case of solving the unbounded problem using some numerical methods (like the finite element method), a fictitious boundary has to be introduced. A suitable boundary condition must be written also as a compromise between the accuracy, the implementation, and the computational efficiency.

On the other hand, using the boundary element method does not require a boundary surface. It is sufficient to consider that the fields vanish as $|x| \to \infty$

$$|E(x)| = O\Big(\frac{1}{|x|^2}\Big) \text{ as } |x| \to \infty, \tag{1.25}$$

$$|H(x)| = O\Big(\frac{1}{|x|^2}\Big) \text{ as } |x| \to \infty. \tag{1.26}$$

1.3.1 An Electric Field Formulation

Multiplying equation (1.18) by iω and substituting (1.21) and the curl of (1.19), we obtain:

$$\text{curl}(\mu^{-1}\text{curl}E) + i\omega\sigma E = -i\omega J_s \text{ in } \Omega. \tag{1.27}$$

As the whole domain Ω is subdivided into a conductive region Ω_I free of any source current and the air region Ω_E possibly containing source currents. Hence, the final system can be written as:

$$\begin{cases} \text{curl}(\mu^{-1}\text{curl}E) + i\omega\sigma E &= 0 & \text{in } \Omega_I, \\ \text{curl}(\text{curl}E) &= -i\omega J_s & \text{in } \Omega_A, \\ \text{div}E &= 0 & \text{on } \mathbb{R}^3, \\ [E \times n]_\Gamma &= 0 & \text{on } \Gamma, \\ |E(x)| &= O(|x|^{-2}) & \text{as } |x| \to \infty. \end{cases} \tag{1.28}$$

1.3.2 A Magnetic Field Formulation

Applying curl to the equation (1.18) and substituting (1.21), we obtain:

$$\text{curl}(\frac{1}{\sigma}\text{curl}H) = \text{curl}E + \text{curl}\frac{1}{\sigma}J_s \text{ in } \Omega_I, \tag{1.29}$$

replacing (1.19) and (1.20) in (1.29), we get:

$$\text{curl}(\frac{1}{\sigma}\text{curl}H) = -i\omega\mu H + \text{curl}\frac{1}{\sigma}J_s \text{ in } \Omega_I. \tag{1.30}$$

Similarly, substituting the electromagnetic properties in both regions of Ω, we end with the following system:

$$\begin{cases} \text{curl}(\sigma^{-1}\text{curl}H) + i\omega\mu H &= 0 & \text{in } \Omega_I, \\ \text{curl}(\text{curl}H) &= \text{curl}(J_s) & \text{in } \Omega_A, \\ \text{div}H &= 0 & \text{on } \mathbb{R}^3, \\ [H \times n]_\Gamma &= 0 & \text{on } \Gamma, \\ [\partial_n H]_\Gamma &= 0 & \text{on } \Gamma, \\ |H(x)| &= O(|x|^{-2}) & \text{as } |x| \to \infty. \end{cases} \tag{1.31}$$

1.3.3 $E - H$ Formulation

In what follows, we consider the "E-Based Formulation" inside Ω_I and the "H-Based Formulation" inside Ω_E. In this case, the problem is formulated as follows:

$$\begin{cases} \text{curl}(\mu^{-1}\text{curl}E) + i\omega\sigma E &= 0 & \text{in } \Omega_I, \\ \text{curl}(\text{curl}H) &= \text{curl}(J_s) & \text{in } \Omega_A, \\ \text{div}H &= 0 & \text{on } \mathbb{R}^3, \\ [E \times n]_\Gamma &= 0 & \text{on } \Gamma, \\ [H \times n]_\Gamma &= 0 & \text{on } \Gamma, \\ |E(x)| + |H(x)| &= O(|x|^{-2}) & \text{as } |x| \to \infty. \end{cases} \tag{1.32}$$

1.3.4 $E - \Phi$ Formulation

In this section, we present another formulation which depends on a combination of the electric field considered in the conductive domain Ω_I, and the magnetic scalar potential considered in Ω_E.

In Ω_E, the magnetic field can be written as $H = H_r + H_0$, where H_0 represents the source terms and satisfies $\text{curl}H_0 = J_s$, and H_r is the reaction magnetic field that satisfies $\text{curl}H_r = 0$. Considering a simple geometry and using the fact that $\text{curl}H_r = 0$ in Ω_E, we can write $H_r = -\nabla\Phi$ where Φ is a magnetic scalar potential.
As $\text{div}H_r = 0$ in Ω_E, then $\text{div}(\nabla\Phi) = 0$, which gives that $\Delta\Phi = 0$.

The overall formulation is then represented by the following model:

$$\begin{cases} \text{curl}(\mu^{-1}\text{curl}E) + i\omega\sigma E &= 0 & \text{in } \Omega_I, \\ \Delta\Phi &= 0 & \text{in } \Omega_A, \\ [E \times n]_\Gamma &= 0 & \text{on } \Gamma, \\ [\Phi]_\Gamma &= 0 & \text{on } \Gamma, \\ |\Phi(x)| &= O(|x|^{-1}) & \text{as } |x| \to \infty. \end{cases} \tag{1.33}$$

1.3.5 A Magnetic Vector Potential Formulation A

Starting from (1.22)

$$\text{div}B = 0 \qquad \text{in } \Omega, \tag{1.34}$$

we can express magnetic induction B in terms of the magnetic vector potential A

$$B = \text{curl}A \qquad \text{in } \Omega. \tag{1.35}$$

Replacing (1.35) in (1.19), we obtain that $A = (i\omega)^{-1}E$. Here A is subjected to the so-called temporal gauge that makes the scalar potential vanish.
Replacing (1.20), (1.21), (1.35) and $E = i\omega A$ in (1.18), we obtain the A-based formulation

$$\text{curl}(\mu^{-1}\text{curl}A) + i\omega\sigma A = J_s \text{ in } \Omega. \tag{1.36}$$

In order to assure the uniqueness of the solution of A, it is sufficient to add the following conditions

$$\text{div}A = 0 \qquad \text{in } \Omega, \tag{1.37}$$

$$\int_\Gamma A \cdot n d\Gamma = 0 \qquad \text{on } \Gamma. \tag{1.38}$$

Adding the continuity condition, the complete system can be written as follows:

$$\begin{cases} \text{curl}(\mu^{-1}\text{curl}A) + i\omega\sigma A &= J_s & \text{in } \Omega_I, \\ [A \times n]_\Gamma &= 0 & \text{on } \Gamma, \\ \text{div}A &= 0 & \text{on } \mathbb{R}^3, \\ \int_\Gamma A \cdot n d\Gamma &= 0 & \text{on } \Gamma. \\ |A(x)| &= O(|x|^{-2}) & \text{as } |x| \to \infty. \end{cases} \tag{1.39}$$

1.4 Finite Element Method

The Finite Element Method (FEM) is a standard numerical technique for solving partial differential equations. It became one of the most effective and widely used methods for

numerical computation in electromagnetics [3–5]. The starting idea of the FEM is to write a weak variational formulation of the problem. Then, we divide the domain of study into elements (called finite elements) to generate a finite element mesh. There are several types of element shapes, for example meshes may consist of triangles in two dimensions and tetrahedra in three dimensions. Then, the unknown scalar or vector functions are approximated by shape functions defined over each element to represent the behaviour of the unknown variables (see section 1.6). The shape function is a continuous function defined over a single finite element (such as nodes and edges). According to Galerkin's method, we then replace test functions by the same basis functions. Finally, we solve the linear system to find the approximate solution.

1.4.1 Example

Consider the Poisson equation on a domain Ω with homogeneous Dirichlet boundary condition

$$\begin{cases} -\Delta u &= f \quad \text{in } \Omega, \\ u &= 0 \quad \text{on } \partial\Omega. \end{cases} \tag{1.40}$$

1. Weak formulation:
   To obtain the weak formulation of the problem (1.40), we multiply by an arbitrary function v (called the test function). Then, we integrate over Ω

$$-\int_\Omega (\Delta u) v d\Omega = \int_\Omega f v d\Omega. \tag{1.41}$$

   Using Green's theorem, we can rewrite (1.41) as follows

$$\int_\Omega \nabla u \cdot \nabla v d\Omega - \int_{\partial\Omega} (n \cdot \nabla u) v d\partial\Omega = \int_{\Omega_I} f v d\Omega. \tag{1.42}$$

   Choosing v such that $v_{|\partial\Omega} = 0$, we get

$$\int_\Omega \nabla u \cdot \nabla v d\Omega = \int_\Omega f v d\Omega. \tag{1.43}$$

   Thus, if we choose the functional space

$$V = \{v \in H^1(\Omega), v_{|\partial\Omega} = 0\} = H_0^1(\Omega),$$

   where [14]

$$H^1(\Omega) = \{v \in L^2(\Omega), \partial_{x_i} v \in L^2(\Omega), 1 \leq i \leq 3\},$$

we can write the weak formulation in the following form

$$\begin{cases} \text{Find} & u \in V, \\ \text{such that} & a(u,v) = l(v), \quad \forall v \in V, \end{cases} \tag{1.44}$$

where $a(u,v) = \int_\Omega \nabla u \nabla v d\Omega$ is a bilinear form, and $l(v) = \int_\Omega f v d\Omega$ is a bounded linear functional on V.

The weak formulation reduces the requirement to only first order partial derivatives. The choice of the functional space V can be justified by the form of the weak formulation that requires functions in $H^1(\Omega)$, and the boundary conditions of the strong formulation (1.40).

2. Galerkin's method:
   The variational problems are usually solved by the Galerkin method. To approximate the unknowns, we should define a vector subspace V_h of V generated by the basis functions $\phi_1, \phi_2, .., \phi_n$. Then, we approximate the solution u as a linear combination of these basis functions

$$u_h(x) = \sum_{i=1}^{n} u_i \phi_i(x), \tag{1.45}$$

   and the test functions came from the same space. Then, the Galerkin formulation is written as

$$\begin{cases} \text{Find} & u_h \in V_h, \\ \text{such that} & a(u_h, v_h) = l(v_h), \quad \forall v_h \in V_h. \end{cases} \tag{1.46}$$

   Using the basis (ϕ_j) of V_h, it is also equivalent to

$$\begin{cases} \text{Find} & u_h \in V_h, \\ \text{such that} & a(u_h, \phi_j) = l(\phi_j), \quad \forall j \in [1, n]. \end{cases} \tag{1.47}$$

3. Linear system:

Replacing (1.45) in (1.47), we obtain the following linear system

$$\begin{bmatrix} A_{11} & A_{12} & \cdots & A_{1n} \\ A_{21} & A_{22} & \cdots & A_{2n} \\ \vdots & \vdots & \ddots & \vdots \\ A_{n1} & A_{n2} & \cdots & A_{nn} \end{bmatrix} \begin{bmatrix} u_1 \\ u_2 \\ \vdots \\ u_n \end{bmatrix} = \begin{bmatrix} L_1 \\ L_2 \\ \vdots \\ L_n \end{bmatrix},$$

where $A_{ji} = a(\phi_i, \phi_j)$ and $L_j = l(\phi_j)$.

1.4.2 Advantages and disadvantages of the Finite Element Method

As is the case for other numerical methods, the FEM has some advantages and drawbacks.

Advantages of the Finite Element Method

1. The FEM is simple, for that it is widely popular among the engineering community.
2. Modeling of complex geometries as a wide range of element shapes exist for discretising the domain (unstructured mesh) [7].
3. Non-Linear Analysis : non-homogeneous materials can be easily considered.
4. The sparsity of the generated matrix system.

Drawbacks and limitations of the Finite Element Method

1. Volume discretisation : FEM requires a volume disretization, and so it may lead to a large number of unknowns (see Fig. 1.4).
2. It can require large memory because of the volume discretisation.
3. Finite domains: additional boundaries must be added in free-space problems with appropriate boundary conditions to limit the studied domain.

1.5 Boundary Element Method

The Boundary Element Method (BEM) is also a numerical method for solving the eddy-current problems, that play an important role in the modern numerical computation in the engineering science. It is more convenient than many numerical methods such as the

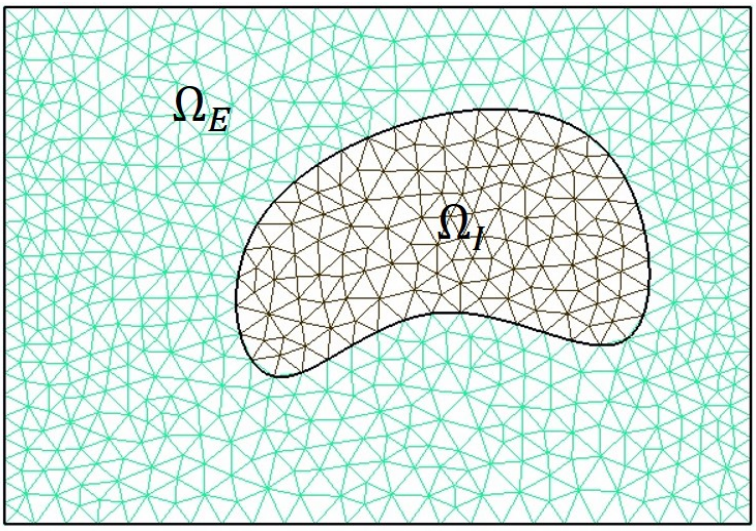

Figure 1.4: The mesh in 2D for the Finite Element Method

FEM and the Finite Difference Method, as it reduces the number of elements and often the computational time while maintaining accuracy.
The Boundary Element Method is just FEM applied to an integral equation. For this reason, it is convenient to introduce the Boundary Integral Equations (BIE).

1.5.1 Boundary Integral Equation by Scalar Form of Green's Identity

The BIE's are reformulations of the partial differential equations on a simple smooth boundary. Obtaining these equations consists of defining the mathematical model, the representational formula of the unknowns, then passing through limits toward the boundary. Here, we introduce the most popular BIE formulation for the Laplace equation, as it will be considered in section 2.2.2.

- Mathematical model:
  The magnetic scalar potential Φ which derives from the field H in absence of current satisfies
  $$-\operatorname{div}(\mu \operatorname{grad}\Phi) = 0. \tag{1.48}$$
  As we are interested to apply BEM in an air region or any linear-isotropic medium, then Φ verifies in this case the Laplace equation
  $$\Delta\Phi = 0. \tag{1.49}$$

Let $u = \Phi$, the mathematical model is formulated as follows:

$$\Delta u = 0 \text{ in } \Omega_E, \tag{1.50}$$

$$|u(x)| = O\Big(\frac{1}{|x|^2}\Big) \text{ as } |x| \to \infty. \tag{1.51}$$

- Representation formula:
  Firstly, let us recall the fundamental solution of the PDE (1.50),

$$G(x,y) = -\frac{1}{2\pi}\log|x-y| \quad \text{for x, y} \in \mathbb{R}^2, \tag{1.52}$$

$$G(x,y) = \frac{1}{4\pi|x-y|} \quad \text{for x, y} \in \mathbb{R}^3. \tag{1.53}$$

The solution of the partial differential equation (1.50) can be represented in terms of boundary potentials. In potential theory we have [27]:

$$u(x) = -\int_\Gamma \partial_{n(y)} G(x,y)[u(y)]_\Gamma d\Gamma_y + \int_\Gamma G(x,y)[\partial_{n(y)} u(y)]_\Gamma d\Gamma_y, \tag{1.54}$$

for $x \in \mathbb{R}^n \setminus \Gamma$. Here ∂_n denotes the normal derivative, where n is the unit normal vector on Γ oriented from the interior domain enclosed by Γ towards the outer domain.

The representation formula in Ω_E can be obtained depending on the assumption of u in Ω_I, $u = 0$ in $\mathbb{R}^n \setminus \Omega_E$, we obtain

$$u(x) = -\int_\Gamma \partial_{n(y)} G(x,y) u(y) d\Gamma_y + \int_\Gamma G(x,y) \partial_{n(y)} u(y) d\Gamma_y \tag{1.55}$$

for $x \in \Omega_E$.

We can rewrite the equation (1.55) in the following form:

$$u(x) = S(\partial_n u)(x) - D(u)(x), \tag{1.56}$$

where,

$$(S\phi)(\tilde{x}) = \int_\Gamma G(\tilde{x},y)\phi(y) d\Gamma, \tag{1.57}$$

is the scalar single layer potential, and

$$(D\phi)(\tilde{x}) = \int_\Gamma \partial_{n(y)} G(\tilde{x},y)\phi(y) d\Gamma, \tag{1.58}$$

is the scalar double layer potential, for all $\tilde{x} \in \Omega_E$ and $y \in \Gamma$.

- Integral Equations:
  The solution u in the domain Ω_E is given by the representational formula (1.56). Using this representational formula, we must pass through limits toward the surface Γ in order to obtain the boundary integral equations. Taking the limits of the single layer potential S from both sides, we obtain [27]:

$$\lim_{\Omega_+ \ni \tilde{x} \to x \in \Gamma} (S\phi)(\tilde{x}) = \int_\Gamma G(x,y)\phi(y)d\Gamma, \tag{1.59}$$

and

$$\lim_{\Omega_- \ni \tilde{x} \to x \in \Gamma} (S\phi)(\tilde{x}) = \int_\Gamma G(x,y)\phi(y)d\Gamma, \tag{1.60}$$

for all $x \in \Gamma$ and $y \in \Gamma$.

Similarly for the double layer potential D, we get:

$$\lim_{\Omega_+ \ni \tilde{x} \to x \in \Gamma} (D\phi)(\tilde{x}) = -\frac{1}{2}\phi(x) + \int_\Gamma \partial_{n(y)} G(x,y)\phi(y)d\Gamma, \tag{1.61}$$

and

$$\lim_{\Omega_- \ni \tilde{x} \to x \in \Gamma} (D\phi)(\tilde{x}) = +\frac{1}{2}\phi(x) + \int_\Gamma \partial_{n(y)} G(x,y)\phi(y)d\Gamma, \tag{1.62}$$

for all $x \in \Gamma$ and $y \in \Gamma$.

Applying the limits (1.59-1.61) on (1.56), we obtain the following boundary integral equation

$$\frac{1}{2}u(x) = -\int_\Gamma \left(u(y)\frac{\partial G(x,y)}{\partial n} - G(x,y)\frac{\partial u(y)}{\partial n} \right) d\Gamma. \tag{1.63}$$

We can rewrite the integral equation as follows

$$\frac{1}{2}u(x) = S(\partial_n u)(x) - (Du)(x). \tag{1.64}$$

for all $x \in \Gamma$.

The solution of the problem as well as its gradients or even high order derivatives are then given by the application of the representation formula, this method based on Green's formula is called the direct BEM approach. Another possibility is to use the property that single or double layer potentials solve the partial differential equation exactly for any given density function. In any case, passing through limits of the representational formula give

the boundary integral equations. Then, as for the FEM, a numerical procedure applied to the boundary integral equation leads to a linear system of algebraic equations.

1.5.2 Example

Consider the Poisson equation on the domain Ω_I with Dirichlet boundary condition

$$\begin{cases} -\Delta u &= f \quad \text{in } \Omega_I, \\ u &= f \quad \text{on } \Gamma. \end{cases} \tag{1.65}$$

1. Representational formula:
   By considering the single layer potential, the solution u is given by

$$u(\tilde{x}) = S(\partial_n u)(\tilde{x}) = \int_\Gamma G(\tilde{x}, y)\partial_{n(y)} u(y) d\Gamma_y \text{ for all } \tilde{x} \in \Omega_I, \text{ and } y \in \Gamma, \tag{1.66}$$

   where u and $\partial_n u$ are the unknowns.

2. Integral Equation:
   Passing through limits, we obtain:

$$f(x) = V(\partial_n u)(x) = \int_\Gamma G(x, y)\partial_{n(y)} u(y) d\Gamma_y \text{ for all } x \text{ and } y \in \Gamma, \tag{1.67}$$

   where $p = \partial_n u$ is the only unknown to find.

3. Galerkin's method:
   Considering $V^f = \{v \in H^1(\Gamma), v_{|\Gamma} = f\}$ as an admissible vector space. The integral equation (1.67) is equivalent to the variational formulation (1.68)

$$\int_\Gamma \int_\Gamma G(x, y)p(y)q(x) d\Gamma_y d\Gamma_x = \int_\Gamma f(x)q(x) d\Gamma_x, \tag{1.68}$$

   for all $q \in V^f$. Similarly, as for the FEM (section 1.4.1). To approximate the unkown $p(y)$ using Galerkin's method, we should define a vector subspace V_h^f of V^f generated by the basis functions $\psi_1, \psi_2, .., \psi_n$. Then, we approximate the solution p as a linear combination of these basis functions

$$p_h(y) = \sum_{i=1}^{n} p_i \psi_i(y), \tag{1.69}$$

   and the test functions are considered from the same functional space. Then, the Galerkin formulation is written as
   Find $p_h \in V_h^f$, such that

$$\int_\Gamma \int_\Gamma G(x,y) p_h(y) \psi_j(x) d\Gamma_y d\Gamma_x = \int_\Gamma f(x)\psi_j(x)\Gamma_x, \quad \forall j \in [1,n]. \tag{1.70}$$

4. Linear system:
   Replacing (1.69) in (1.70), we obtain a linear system

$$Ap = b,$$

   where

$$A_{ji} = \int_{\Gamma_j} \int_{\Gamma_i} G(x,y)\psi_i \psi_j d\Gamma_y d\Gamma_x,$$

$$p = \begin{bmatrix} p_1 \\ p_2 \\ \vdots \\ p_n \end{bmatrix},$$

   and

$$b_j = \int_{\Gamma_j} f(x)\psi_j \Gamma_x.$$

1.5.3 Advantages and disadvantages of the Boundary Element Method

The BEM has also some advantages and drawbacks.

Advantages of Boundary Element Method

1. Only boundary discretisation is required (see Figure 1.5).
2. Less data and less memory storage: it is a direct result from the first point. Only the surface is discretised, so less number of elements are used.
3. Unbounded domains are treated in the same way as the bounded domains.

Disadvantages of Boundary Element Method

1. Non linearity: In general, the non-linear problems cannot be treated simply by pure BEM, as it normally requires the discretisation of the interior domain to take into account the non-homogeneous parameters. Then, a coupling of BEM with another numerical method can be an appropriate solution [21], or obtaining the solution as a sum of homogeneous solution and one particular non-homogeneous one [28 ; 29].

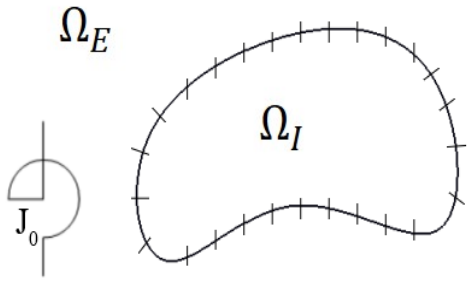

Figure 1.5: The mesh in 2D for the Boundary Element Method

2. Fully populated matrix: Matrices obtained by the BEM may be unsymmetrical and fully populated with non-zero coefficients. It can lead to specific difficulties for the solution. To handle these difficulties, a compression and preconditioning techniques can be used [16–18], or using an iterative solution method without the dense matrix but with approximately the same accuracy [45].

3. Singular kernels: the numerical solution requires the evaluation of integrals having singular kernels which must have a patricular treatment [15].

1.6 Shape functions

Numerical methods, such as the finite element method and the boundary element method, are used to find approximate solutions of partial differential equations. The unknowns of these equations which are scalar or vector functions are approximated by continuous functions defined over each single element of the mesh. These functions defined over a single element called "shape functions" are combined over all the mesh to form the basis functions. In the following, we introduce the usual nodal, edge, and cell shape functions.

In 1980, some families of finite elements in $\mathbb{R}^3$ were introduced by Nédélec [24]. For the $H(\text{curl})-$conforming elements that provide the continuity of the tangential component of a vector function, new complementary families are introduced in [30]. In [25], it exposed the relevance of the linear edge elements for numerical calculations as well as their disadvantages. A comparison was done with the tetrahedral low order edge elements, and the more accurate and efficient solutions are obtained with the linear edge elements and the

nodal elements. Concerning storage requirements, nodal elements are less expensive than linear edge elements.

1.6.1 Nodal shape functions - H(grad)

For a nodal element, a scalar or a vector function is approximated by a linear combination of shape functions associated with vertices (see Figure 1.6). Within an element, a scalar function u is approximated as:

$$u = \sum_{i=1}^{n} u_i N_i, \tag{1.71}$$

where N_i is the nodal shape function corresponding to a node i, n is the number of nodes in the element, and u_i's are the coefficients of u at nodes $i = 1, .., n$.
For a vector function W, it is approximated by considering three scalar components:

$$W = \sum_{i=1}^{n} W_i N_i = \sum_{i=1}^{n} (W_i^x \vec{x} + W_i^y \vec{y} + W_i^z \vec{z}) N_i, \tag{1.72}$$

where W_i^x, W_i^y, and W_i^z are the components of W_i in the cartesian coordinates. When two elements share a node i, the nodal values W_i at node i are equal, consequently the vector function W is normally and tangentially continuous across all element interfaces.

Considering a tetrahedral element for example, the nodal shape functions in local coor-

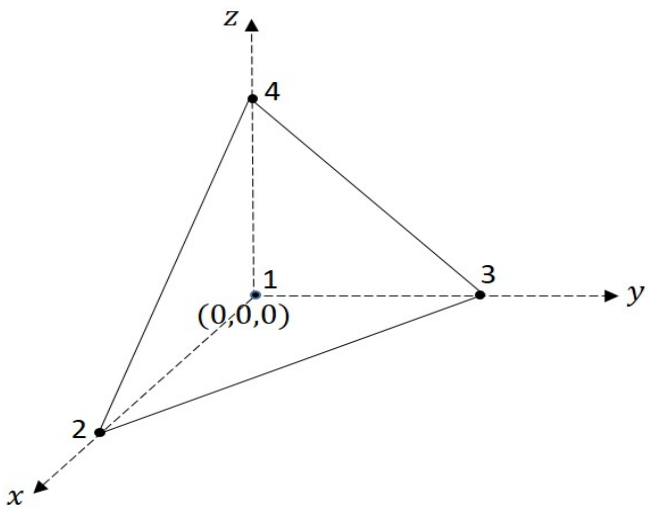

Figure 1.6: First order tetrahedral nodal finite element in local coordinates.

dinates can be written as [23]:

$$N_1 = \lambda_1 = 1 \pm x \pm y \pm z,$$

$$N_2 = \lambda_2 = x,$$

$$N_3 = \lambda_3 = y,$$

$$N_4 = \lambda_4 = z,$$

where λ_1, λ_2, λ_3 and λ_4 are the barycentric coordinates of nodes 1, 2, 3 and 4. Within the element, the nodal shape function N_i equals unity at node i and zero at all other nodes.

1.6.2 Edge shape functions - H(curl)

As the nodal element has one shape function associated with each of the vertices of the element, the edge element has one shape function for each of the edges of the element. The edge shape functions in local coordinates for the tetrahedral element can be written as:

$$E_i = \lambda_k \nabla \lambda_l \pm \lambda_l \nabla \lambda_k,$$

where the edge i goes from the node k to the node l. Within the element, the line integral of an edge shape function E_i along edge i equals unity and is zero along all other edges. The tangential component of a vector function approximated by edge shape functions is continuous across the element boundaries, however the normal component is not necessarily continuous. For the lowest order edge elements in a tetrahedron, the divergence of the edge shape functions is zero [26]. Thus, the vector function approximated by edge shape functions is divergence free in this element. However, that does not imply that the vector field approximated by the edge basis functions is globally divergence free since the normal components of these functions are not continuous.

1.6.3 Cell shape functions

The cell shape functions are zero order shape functions correspond to the scalar cell space function. This function is well suited to approximate densities. Note that there is no continuity properties between elements.

CHAPTER 2

FEM/BEM coupling for Magnetostatic and Eddy Current problems

Contents

2.1 Why FEM/BEM ? **30**

2.1.1 Setting of the problem 31

2.2 $\Phi - \Phi$ Formulation for Magnetostatic Field Equations **32**

2.2.1 Weak formulation for Φ in Ω_C 32

2.2.2 Integral equation for Φ in Ω_A 33

2.2.3 Coupled variational formulation 33

2.2.4 FEM/BEM discretisation 35

2.2.5 Numerical results 36

2.3 $A - \Phi$ Formulation for Magnetodynamique Field Equations . **37**

2.3.1 Weak formulation for A in Ω_C 39

2.3.2 Integral equation for Φ in Ω_A 40

2.3.3 Coupled variational formulation 40

2.3.4 FEM/BEM discretisation 41

2.3.5 Numerical results 42

2.4 Conclusion and Perspectives **43**

In this chapter, we couple the Finite Element Method (FEM) and the Boundary Element Method (BEM) for solving 3D magnetostatic and magnetodynamic problems. This coupling is provided to treat one of the objectives of this thesis concerning the presence of infinite homogeneous domains. We justify the use of this coupling in section (2.1). We provide the $\Phi-\Phi$ formulation for the magnetostatic case in section (2.2) and the $A-\Phi$ formulation to consider magnetodynamic problems in section (2.3), the magnetic vector potential is denoted by A and Φ is the magnetic scalar potential.

2.1 Why FEM/BEM ?

The Finite Element Method and the Boundary Element Method are widespread discretisation techniques for computing approximate solutions of the partial differential equations that appear in engineering. However, each method has some drawbacks in terms of computational costs and some complementary advantages. Consequently, the whole domain of the problem can be divided into subdomains, so that we may choose the most appropriate discretisation technique in each subdomain. In this way, we mainly keep the advantages of each method [55 ; 56].

In [34], the FEM/BEM coupling has been proposed for the first time using the standard collocation BEM. Before, many papers adopted this coupling method until they became used to habituated the coupling based on the symmetric Galerkin BEM [35–42]. The symmetric coupling of FEM and BEM has been used to treat many problems [54]. It is also used for transient electro-quasistatic field simulations in the time domain, as well as for electrostatic simulations of 3D high voltage technnical devices [47].

An accurate field computation is needed for modeling the design and the optimisation of some devices. Therefore, the FEM/BEM coupling is used in [48] to facilitate the modeling of large hadron collider (LHC) superconducting magnets. It is also used to model the propagation of interacting acoustic-acoustic/acoustic-elastic waves through axisymmetric media [49].

Considering movement is also one of the situations where using FEM/BEM is attractive. In [44], The FEM/BEM coupling has been applied on 3D eddy-current problems with moving bodies which can arise from the modeling of electromechanical systems. Similar approach applied on the electrodynamic levitation device [43]. It is used as well for the modeling of induction heating processes including moving parts [46].

For an eddy current problem, the equations inside the conductor region Ω_C can be non-linear, it is not the case in a homogeneous medium (such as the infinite exterior region that corresponds to the air in our case). In addition, there is no need for an extra artificial boundary conditions if we consider the BEM in the exterior domain and only a surface discretisation is required. This is why the proposed coupling is useful for eddy current problems and becomes more important in 3D [50–53].

2.1.1 Setting of the problem

We divide the domain Ω into two subdomains: Ω_C which is a conductive or magnetic bounded domain, and Ω_A which is the exterior domain (Air). It leads to a natural FEM/BEM coupling, where the BEM is applied in the exterior domain and the FEM in the interior domain (see Fig. 2.1). Let Γ be the common interface $\Gamma = \partial\Omega_c \cap \partial\Omega_A$.

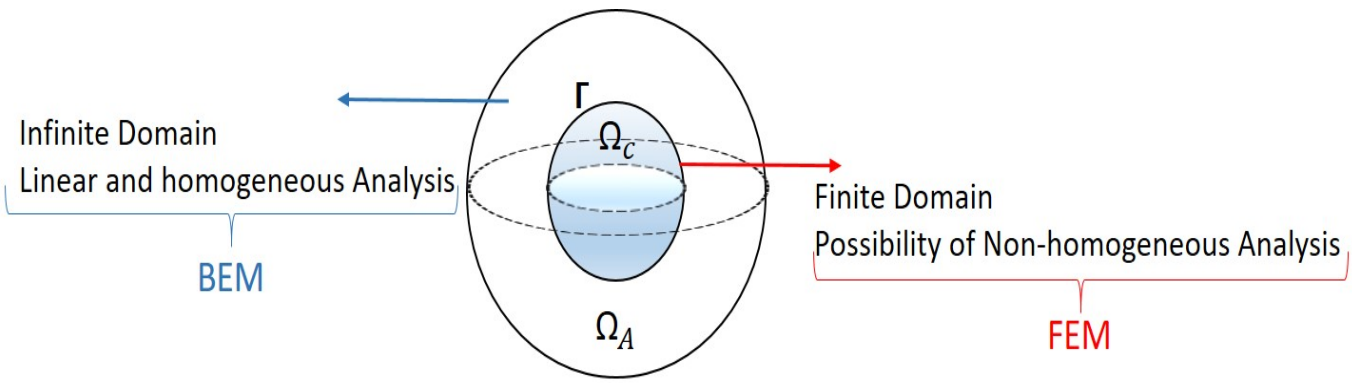

Figure 2.1: A cross section of the two sub-domains Ω_A and Ω_c and their corresponding appropriate numerical methods.

2.2 $\Phi - \Phi$ Formulation for Magnetostatic Field Equations

The magnetostatic problem can be written as follows:

$$\begin{aligned}
\mathrm{curl}H &= J_s \quad \text{in } \Omega, && (2.1)\\
\mathrm{div}B &= 0 \quad \text{in } \Omega, && (2.2)\\
B &= \mu H \quad \text{in } \Omega, && (2.3)\\
[B \cdot n]_\Gamma &= 0, \quad \text{in } \Gamma, && (2.4)\\
|H(x)| &= O\Big(\frac{1}{|x|^2}\Big) \text{ as } |x| \to \infty. && (2.5)
\end{aligned}$$

The magnetic field H in Ω_A can be expressed as the sum of two fields:

$$H = H_s + H_r, \tag{2.6}$$

where H_s is the field produced by the source current that satisfies:

$$\mathrm{curl}H_s = J_s, \tag{2.7}$$

and, H_r is the remaining part produced by the magnetised material (reaction magnetic field) given by:

$$\mathrm{curl}H_r = 0. \tag{2.8}$$

The equation (2.8) implies that there exists a magnetic scalar potential Φ such that $H_r = -\mathrm{grad}\Phi$, and so H can be written as:

$$H = H_s - \mathrm{grad}\Phi. \tag{2.9}$$

2.2.1 Weak formulation for Φ in Ω_C

Starting from (2.2), multiplying by a test function $\alpha \in$H(grad) and integrating over Ω_C:

$$\int_{\Omega_c} \alpha(\mathrm{div}B) d\Omega_c = 0, \tag{2.10}$$

and using the divergence theorem:

$$-\int_{\Omega_c}(\mathrm{div}\phi)\phi' = \int_{\Omega_c}\phi(\mathrm{grad}\phi') - \int_{\Gamma} n\cdot\phi\phi', \tag{2.11}$$

we get:

$$\int_{\Omega_c}(\mathrm{grad}\alpha)\cdot B d\Omega_c - \int_{\Gamma}(n\cdot B)\alpha d\Gamma = 0. \tag{2.12}$$

Using (2.3) and (2.9) in (2.12), we obtain:

$$\int_{\Omega_c}(\mathrm{grad}\alpha)\cdot\mu(\mathrm{grad}\Phi)d\Omega_c + \int_{\Gamma} B_n\alpha d\Gamma = \int_{\Omega_c}(\mathrm{grad}\alpha)\cdot\mu H_s d\Omega_c, \tag{2.13}$$

where $B_n = B\cdot n$ is the normal component of the magnetic induction.

2.2.2 Integral equation for Φ in Ω_A

The potential Φ derives from the magnetic field H and in absence of the current satisfies

$$-\mathrm{div}(\mu\mathrm{grad}\Phi) = 0.$$

As we consider just an air region or any linear-homogeneous medium, Φ verifies in this case the Laplace equation

$$\Delta\Phi = 0. \tag{2.14}$$

Therefore, we can write the boundary integral equation as follows (see section 1.5.1)

$$c\Phi = -\int_{\Gamma}\left(\Phi\frac{\partial G}{\partial n} - G\frac{\partial\Phi}{\partial n}\right)d\Gamma, \tag{2.15}$$

where $c = -\frac{1}{2}$.

2.2.3 Coupled variational formulation

Both methods should be linked by considering the same unknowns. For coupling the integral equation (2.15) with the weak form (2.13), we have to evoke the normal component of the magnetic flux density [57]. Thus, if we substitute the magnetic scalar potential:

$$B_{n_r} = \mu(-\mathrm{grad}\Phi\cdot n), \tag{2.16}$$

in (2.15), we get:

$$c\Phi = -\int_\Gamma (\Phi \frac{\partial G}{\partial n} - G(\frac{-B_{n_r}}{\mu}))d\Gamma. \tag{2.17}$$

However,

$$B_n = B \cdot n = \mu(H_s - \text{grad}\Phi) \cdot n, \tag{2.18}$$

then:

$$\frac{B_n}{\mu} = H_s \cdot n - \text{grad}\Phi \cdot n = H_s \cdot n + \frac{B_{n_r}}{\mu}. \tag{2.19}$$

From (2.15) and (2.19), we end with the following integral equation:

$$c\Phi = -\int_\Gamma \Big(\Phi \frac{\partial G}{\partial n} + G\Big(\frac{B_n}{\mu} - H_s \cdot n\Big)\Big)d\Gamma. \tag{2.20}$$

The final set of equations for both domains Ω_C and Ω_A, which are connected at a common interface Γ, can be written as:

$$\begin{cases} \displaystyle\int_{\Omega_c} (\text{grad}\alpha)\mu(\text{grad}\Phi)d\Omega_c + \int_\Gamma B_n \alpha d\Gamma = \int_{\Omega_c} (\text{grad}\alpha)\mu H_s d\Omega_c, \\ \displaystyle c\Phi + \int_\Gamma \Phi \frac{\partial G}{\partial n} d\Gamma - \int_\Gamma G \frac{B_n}{\mu} d\Gamma = -\int_\Gamma G.H_s \cdot n d\Gamma. \end{cases} \tag{2.21}$$

The complete variational formulation can be written as:

Find $\Phi \in H(\text{grad}, \Omega_c)$ and $B_n \in H(\text{div}, \Gamma)$, such that:

$$\begin{cases} \langle \mu \text{grad}\Phi, \text{grad}\alpha \rangle_{\Omega_c} + \langle B_n, \alpha \rangle_\Gamma = \langle \mu H_s, \text{grad}\alpha \rangle_{\Omega_c}, \\ \langle (cI + D)\Phi, \beta \rangle_\Gamma - \langle \mu^{-1} S(B_n), \beta \rangle_\Gamma = -\langle S(\beta), H_s \cdot n \rangle_\Gamma, \end{cases} \tag{2.22}$$

for all $\alpha \in H(\text{grad}, \Omega_c)$ and $\beta \in H(\text{div}, \Gamma)$.

where, as defined in subsection 1.5.1,

$$(S\phi)(x) = \int_\Gamma G(x, y)\phi(y)d\Gamma, \tag{2.23}$$

and

$$(D\phi)(x) = \int_\Gamma \partial_{n(y)} G(x, y)\phi(y)d\Gamma, \tag{2.24}$$

for all $x \in \Gamma$ and $y \in \Gamma$.
And note that $\langle f, g\rangle_\Gamma = \int_\Gamma f(x)g(x)d\Gamma(x)$ and $\langle f, g\rangle_{\Omega_C} = \int_{\Omega_C} f(x) \cdot g(x)d\Omega_C$.

2.2.4 FEM/BEM discretisation

In Ω_C, Φ can be approximated by a linear combination of shape functions associated with the nodes:

$$\Phi_h = \sum_{i=1}^{n} \Phi_i \alpha_i,$$

where n is the number of nodes, the coefficients Φ_i's are the values of Φ_h at node i, and α_i is the nodal shape function of degree 1 corresponding to node i. Note that when using the conforming elements in $H(\text{grad}, \Omega_c)$, the degrees of freedom are associated with the nodes (see section 1.6.1).

B_n is approximated using scalar cell shape function (0-order shape function), those functions are equal to a constant on the face of the tetrahedral on the boundary and zero elsewhere. B_n is approximated by:

$$B_{n_h} = \sum_{i=1}^{m} B_{n_j} \beta_j,$$

where m is the number of faces of tetrahedrals, the coefficients B_{n_j}'s are the values of B_{n_h} at face j, and β_j is the scalar cell shape function of degree 0 corresponding to face j.

Applying Galerkin's Method, we can write the discretised formulation as:

Find $\Phi_j \in \mathbb{R}^n$ and $B_n \in \mathbb{R}^n$, such that

$$\sum_{j=1}^{n} \Phi_i \langle \mu \text{grad}\alpha_i, \text{grad}\alpha_l\rangle_{\Omega_c} + \sum_{j=1}^{m} B_{n_j} \langle \beta_j, \alpha_l\rangle_\Gamma = \langle \mu H_s, \text{grad}\alpha_l\rangle_{\Omega_c}, \tag{2.25}$$

$$\sum_{i=1}^{n} \Phi_i \langle (cI + D)\alpha_i, \beta_k\rangle_\Gamma - \sum_{j=1}^{m} B_{n_j} \langle \mu^{-1} S(\beta_j), \beta_k\rangle_\Gamma = -\langle S(\beta_k), H_s \cdot n\rangle_\Gamma, \tag{2.26}$$

for $l = 1, \ldots, n$, and $k = 1, \ldots, m$.

Matrix assembly:

We end up with the following system of linear equations

$$\left(\begin{array}{c|c|c} F^1 & & 0 \\ & & F^2 \\ \hline 0 & B^1 & B^2 \end{array}\right)\left(\begin{array}{c} \Phi_{\Omega_c} \\ \Phi_\Gamma \\ \hline B_n \end{array}\right) = \left(\begin{array}{c} S^1 \\ S^2 \end{array}\right),$$

where Φ_{Ω_c} represents the values of Φ on the nodes inside the domain Ω_c, Φ_Γ represents the values of Φ on the nodes on the boundary Γ,

$F^1_{li}=$

$$\int_{\Omega_c} (\text{grad}\alpha_i) \cdot \mu \text{grad}\alpha_l d\Omega_c,$$

$F^2_{lj}=$

$$\int_\Gamma \alpha_l \beta_j d\Gamma,$$

$B^1_{ki}=$

$$c\int_\Gamma \beta_i \beta_k d\Gamma + \int_\Gamma \beta_i \frac{\partial G}{\partial n} \beta_k d\Gamma,$$

$B^2_{kj}=$

$$\int_\Gamma \frac{1}{\mu} \beta_i G \beta_j d\Gamma,$$

$S^1_l=$

$$\int_{\Omega_c} \text{grad}\alpha_l \cdot (\mu H_s) d\Omega_c,$$

$S^2_k=$

$$\int_\Gamma G(H_s \cdot n) d\Gamma.$$

2.2.5 Numerical results

We consider a sphere with a radius of $1m$, and a source current excited by a uniform magnetic field $H_S = 1\vec{z}$ (see Figure 2.2).

We implement this formulation in the platform «MIPSE» of the G2Elab. A LU-preconditioning method is used to solve the problem using an iterative solver, and the BEM Matrix is approximated by a H-matrix [58]. With these results, we compute the external magnetic field H_{Mipse} on an arc of circle at radius $1.3m$ and we compare the results to the analytical solution. In table (2.1), we calculate the relative L^2-error $\left(\frac{||H_{analytic}-H_{Mipse}||_2}{||H_{analytic}||_2}\right)$ on this arc for a range of values of the relative permeability. These errors show a harmonised agreement as the error is less than 2% and the time of simulation is around $8s$. The considered mesh consists of 322 nodes and 458 cell elements on the boundary.

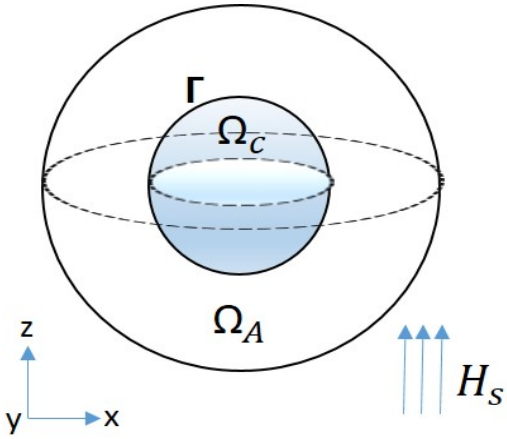

Figure 2.2

μ_r	$\|\|H_{analytic} - H_{Mipse}\|\|$
10^2	0.0159
10^3	0.0108
10^4	0.01027
10^5	0.01022

Table 2.1: Relative L^2-errors of the solution H_{Mipse}.

We also compare the magnetic field H_{Mipse} with the results of a simulation done by Comsol in 2D axisymmetry H_{Comsol} for $\mu_r = 10^3$ H/m. In Fig. (2.3), we represent both components H_x and H_z of the field calculated on the segment that connects the two points $(1.1, 0, -1)$ and $(1.1, 0, +1)$. In the figures (2.4-2.6), it is shown the magnetic scalar potential Φ, the normal component of the magnetic induction B_n, and the magnetic field in the sphere, respectively.

2.3 $A - \Phi$ Formulation for Magnetodynamique Field Equations

Recall the eddy-current problem (1.18-1.23).
Starting from the fact that div$B = 0$, then B can be written as:

$$B = \text{curl}A,$$

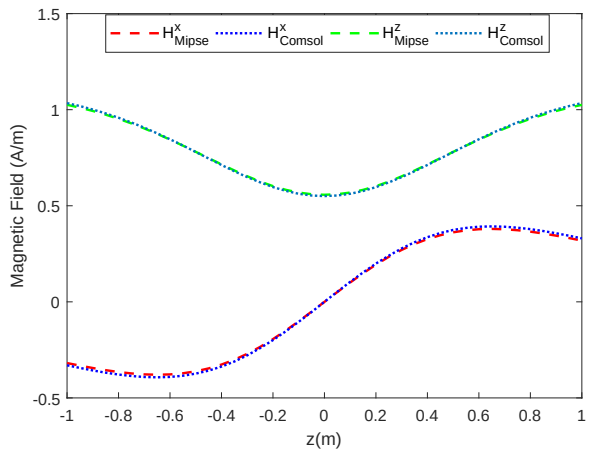

Figure 2.3: The x and z components of H_{Comsol}, and H_{Mipse}.

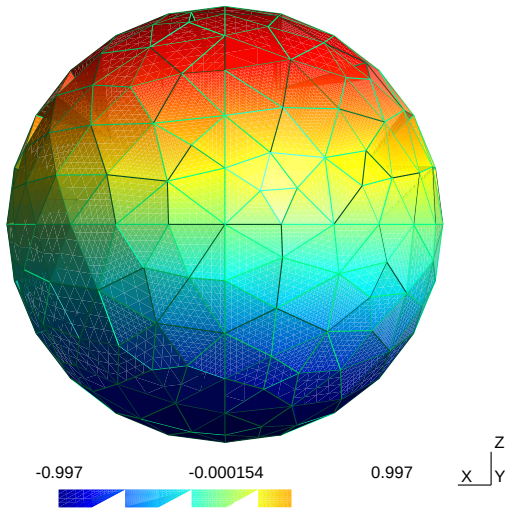

Figure 2.4: Potential Φ on the sphere.

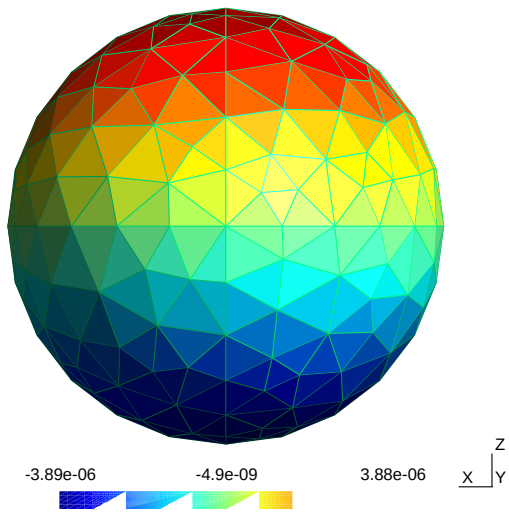

Figure 2.5: Normal induction B_n on the sphere.

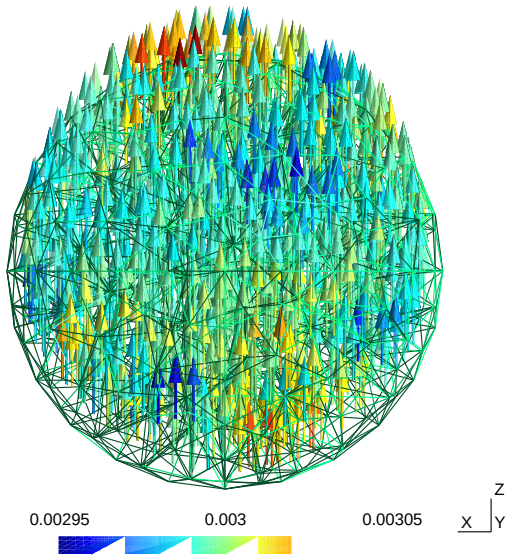

Figure 2.6: Magnetic field on the sphere.

where A is the magnetic vector potential. Therefore, H can be written in the following two forms:

$$H = \nu \mathrm{curl} A, \tag{2.27}$$

and

$$H = H_s - \mathrm{grad}\Phi. \tag{2.28}$$

where $\nu = \mu^{-1}$.

2.3.1 Weak formulation for A in Ω_C

We consider $J_s = 0$ in Ω_C, we have

$$\mathrm{curl} H = \sigma E. \tag{2.29}$$

Multiplying (2.29) by a test function W and integrating over Ω_c

$$\int_{\Omega_c} W \cdot \mathrm{curl} H d\Omega_c = \int_{\Omega_c} (\sigma E) \cdot W d\Omega, \tag{2.30}$$

and using the property $\mathrm{div}(A \times B) = B \cdot (\mathrm{curl} A) - A \cdot (\mathrm{curl} B)$, we get

$$\int_{\Omega_c} H \cdot \mathrm{curl} W d\Omega_c + \int_{\Omega_c} \mathrm{div}(H \times W) d\Omega_c = \int_{\Omega_c} (\sigma E) \cdot W d\Omega, \tag{2.31}$$

$$\int_{\Omega_c} H \cdot \mathrm{curl} W d\Omega_c - \int_{\Omega_c} \mathrm{div}(W \times H) d\Omega_c = \int_{\Omega_c} (\sigma E) \cdot W d\Omega. \tag{2.32}$$

Using the fact that

$$\int_{\Omega_c} \mathrm{div}(W \times H) d\Omega_c = \int_{\Gamma} (W \times H) \cdot n d\Gamma,$$

we obtain,

$$\int_{\Omega_c} H \cdot \mathrm{curl} W d\Omega_c - \int_{\Gamma} (W \times H) \cdot n d\Gamma = \int_{\Omega_c} (\sigma E) \cdot W d\Omega. \tag{2.33}$$

Substitute $H = \nu \mathrm{curl} A$, implies

$$\int_{\Omega_c} \mathrm{curl} W \cdot \nu \mathrm{curl} A d\Omega_c - \int_{\Omega_c} (\sigma E) \cdot W d\Omega - \int_{\Gamma} (W \times H) \cdot n d\Gamma = 0, \tag{2.34}$$

then substitute $H = H_s - \mathrm{grad}\Phi$, we get

$$\int_{\Omega_c} \mathrm{curl} W \cdot \nu \mathrm{curl} A d\Omega_c - \int_{\Omega_c} (\sigma E) \cdot W d\Omega - \int_{\Gamma} (\mathrm{grad}\Phi \times W) \cdot n d\Gamma = \int_{\Gamma} (W \times H_s) \cdot n d\Gamma, \tag{2.35}$$

$$\int_{\Omega_c} \mathrm{curl} W \cdot \nu \mathrm{curl} A d\Omega_c - \int_{\Omega_c} (\sigma E) \cdot W d\Omega - \int_{\Gamma} (\mathrm{grad}\Phi \times W) \cdot n d\Gamma = \int_{\Gamma} W \cdot (H_s \times n) d\Gamma. \tag{2.36}$$

However

$$\int_\Gamma (\text{grad}\Phi \times W)\cdot n d\Gamma = -\int_\Gamma (n\times W)\text{grad}\Phi d\Gamma = \int_\Gamma \text{div}_\Gamma (n\times W)\Phi d\Gamma = -\int_\Gamma n\cdot \text{curl}W\Phi d\Gamma,$$

implies

$$\int_{\Omega_c} \text{curl}W\cdot \nu \text{curl}A d\Omega_c - \int_{\Omega_c}(\sigma E)\cdot W d\Omega + \int_\Gamma n\cdot \text{curl}W\Phi d\Gamma = \int_\Gamma W\cdot (H_s\times n)d\Gamma. \quad (2.37)$$

Using Faraday's equation, we can write $E=-i\omega A$, which gives that:

$$\int_\Omega \text{curl}W\cdot \nu \text{curl}A d\Omega + i\omega \int_{\Omega_c}(\sigma A)\cdot W d\Omega + \int_\Gamma (n\cdot \text{curl}W)\Phi d\Gamma = \int_\Gamma W\cdot (H_s\times n)d\Gamma. \quad (2.38)$$

2.3.2 Integral equation for Φ in Ω_A

Similarly as in section (2.2.2), the integral equation is written as follows

$$c\Phi + \int_\Gamma \Phi \frac{\partial G}{\partial n} d\Gamma - \int_\Gamma G\frac{B_n}{\mu} d\Gamma = -\int_\Gamma G.H_s\cdot n d\Gamma. \quad (2.39)$$

where $B_n = B\cdot n$ is the normal component of the magnetic induction.

2.3.3 Coupled variational formulation

Both methods are linked by the following interface condition:

$$B_n = B\cdot n = \text{curl}A\cdot n,$$

to get

$$\begin{cases} \int_{\Omega_c} \text{curl}W\nu\text{curl}A d\Omega + i\omega\int_{\Omega_c}(\sigma A)W d\Omega + \int_\Gamma n\cdot \text{curl}W\Phi d\Gamma = \int_\Gamma W\cdot(H_s\times n)d\Gamma, \\ c\Phi + \int_\Gamma \Phi\frac{\partial G}{\partial n}d\Gamma - \int_\Gamma G\frac{\text{curl}A\cdot n}{\mu}d\Gamma = -\int_\Gamma G.H_s\cdot n d\Gamma. \end{cases} \quad (2.40)$$

The variational formulation is written as:

Find $A\in H(\text{curl})$ and $\Phi\in\Big(\text{Cell or } H(\text{grad})\Big)$, such that

$$\begin{cases} \langle \nu\text{curl}A, \text{curl}W\rangle_{\Omega_c} + i\omega\langle \sigma A, W\rangle_{\Omega_c} + \langle \Phi, n\cdot\text{curl}W\rangle_\Gamma = \langle H_s\wedge n, W\rangle_\Gamma, \\ \langle \mu^{-1}S(\text{curl}A\cdot n), F\rangle_\Gamma - \langle (cI+D)\Phi, F\rangle_\Gamma = -\langle S(F), H_s\cdot n\rangle_\Gamma, \end{cases} \quad (2.41)$$

for all $W \in H(\text{curl})$ and $F \in \Big(\text{Cell or } H(\text{grad})\Big)$.
Where Cell is the function space of zero order shape functions (constants). Note that the aim of choosing Φ either in the functional space Cell or $H(\text{grad})$ is to test two ways of discretisation. The interest is to show that the cell shape functions can be sufficient in simple geometries, moreover it may reduce the computational time.

2.3.4 FEM/BEM discretisation

In Ω_C, A is approximated by a linear combination of shape functions associated with edges

$$A_h = \sum_{i=1}^{n} A_i W_i,$$

where the coefficient A_i is the value of A at edge i, and W_i is the edge shape function of degree 1 corresponding to edge i (see section 1.6.2).
When using the conforming elements in $H(\text{curl})$, the degree of freedom are associated with the edges.

Φ is approximated using nodal shape functions (first order shape function) or using cell shape functions (zero order shape functions).
Applying Galerkin Method, we state the discretised formulation knowing that Φ is approximated by:

$$\Phi_h = \sum_{j=1}^{m} \Phi_j N_j,$$

where N_j represents either the nodal shape function, or the cell shape function. Applying Galerkin's Method, we can write the discretised formulation as:

Find A_i and $\Phi_j \in \mathbb{R}^n$, such that

$$\begin{aligned}\textstyle\sum_{i=1}^{n} A_i < \nu \text{curl} W_i, \text{curl} W_l >_{\Omega_c} - \sum_{i=1}^{n} A_i < i\omega\sigma W_i, W_l >_{\Omega_c} \quad &+ \textstyle\sum_{j=1}^{m} \Phi_j < N_j, n \cdot \text{curl} W_l >_\Gamma \\ &=< H_s \wedge n, W_l >_\Gamma,\end{aligned} \tag{2.42}$$

$$\sum_{i=1}^{n} A_i < \mu^{-1} S(\text{curl} W_i \cdot n), N_k >_\Gamma - \sum_{j=1}^{m} \Phi_j < (cI + D) N_j, N_k >_\Gamma =< H_s \cdot n, S(N_k) >_\Gamma \tag{2.43}$$

for l=1..n, and k=1..m.

Matrix assembly:
We end up with the following system of linear equations:

$$\left(\begin{array}{c|c} F^1 & \begin{array}{c} 0 \\ \hline F^2 \end{array} \\ \hline 0 \;\Big|\; B^1 & B^2 \end{array}\right) \left(\begin{array}{c} A \\ \hline \Phi \end{array}\right) = \left(\begin{array}{c} S^1 \\ \hline S^2 \end{array}\right),$$

where

$$F^1_{il} = \int_{\Omega_c} (\mathrm{curl} W_i) \nu \mathrm{curl} W_l d\Omega + i\omega \int_{\Omega} W_i \sigma W_l d\Omega$$

$$F^2_{jl} = \int_{\Gamma} \mathrm{curl}(W_l \cdot n) N_j d\Gamma$$

$$B^1_{ik} = \int_{\Gamma} \frac{1}{\mu} (\mathrm{curl} W_i \cdot n) G N_k d\Gamma$$

$$B^2_{jk} = c \int_{\Gamma} N_j N_k d\Gamma + \int_{\Gamma} N_j \frac{\partial G}{\partial n} N_k d\Gamma$$

$$S^1_l = \int_{\Omega_c} (W_l) \cdot (H_s \wedge n) d\Omega$$

$$R^2_k = \int_{\Gamma} G (H_s \cdot n) d\Gamma$$

2.3.5 Numerical results

We consider a sphere with a radius of 1 m, $\mu_r = 10$ H/m, $\sigma = 5.5 \times 10^6$ S, $f = 10^3$ Hz. The source current is excited by a uniform magnetic field $H_s = 1\vec{z}$.
The simulation is performed by both ways of discretisation concerning Φ (Nodal and Cell), and using the same mesh. We calculate the external magnetic field H_{Mipse} on an arc of circle at radius 1.3m and we compare the results to the analytical solution. In Table (2.2), we provide the error obtained considering the discretisation of Φ by the nodal and cell shape functions, as well as their computational time.

	$\|\|H_{analytic} - H_{Mipse}\|\|$	Time
Φ_{cell}	0.003	11s
Φ_{nodal}	0.004	22s

Table 2.2: Relative L^2-errors of the solution H_{Mipse}.

We also compare the magnetic field H_{Mipse} with the results of a simulation done by Comsol in 2D axisymmetry H_{Comsol} for $\mu_r = 10^3$ H/m. In Figs. (2.7) and (2.8), we trace both fields calculated on the segment that connects the two points $(1.1, 0, -1)$ and $(1.1, 0, +1)$.

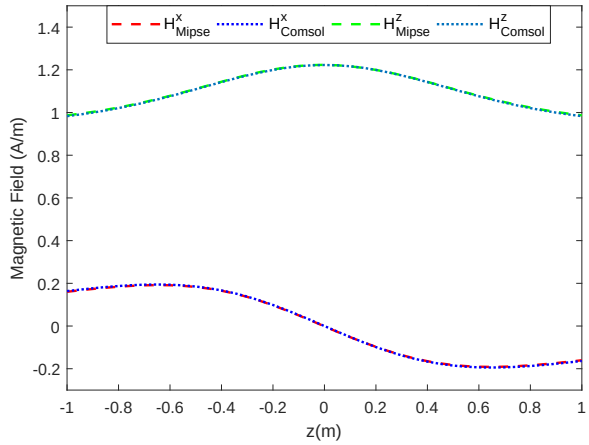

Figure 2.7: The x and z components of the real part of the magnetic fields H_{Mipse} using cell shape functions, and H_{Comsol} in 2D axisymmetry.

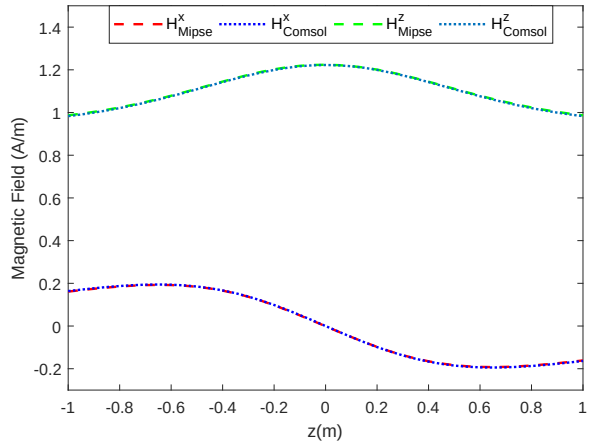

Figure 2.8: The x and z components of the real part of the magnetic fields H_{Mipse} using nodal shape functions, and H_{Comsol} in 2D axisymmetry.

2.4 Conclusion and Perspectives

Magnetostatic Maxwell equations are solved in 3D using the $\Phi - \Phi$ FEM/BEM coupling formulation and 3D magnetodynamic problem is solved using the $A - \Phi$ FEM/BEM coupling method. Note that, we consider here only linear and homogeneous materials.
One of the interests in choosing a FEM/BEM coupling is to treat the nonlinearity in the bounded domain using the FEM (see section 2.1). In addition, the initial project is represented by the discretisation of the magnetic circuit in the coupler (see Figure 1, section 0.1), thus one of our perspectives is to apply these formulations on non-linear problems.

CHAPTER 3

Boundary Element Method for 3D Conductive Thin Layers in Eddy-Current Problems

Contents

3.1 Introduction **47**

3.2 Mathematical Model **49**

3.2.1 Notations 49

3.2.2 Eddy Current Problem for a Thin Layer 50

3.2.3 $\mathbf{E}^{\varepsilon}_{\pm}/\mathbf{H}^{\varepsilon}_{\mathbf{0}}$ Hybrid Formulation 52

3.2.4 Objective 54

3.3 Multiscale Expansion and Equivalent Models with Transmission Conditions **55**

3.3.1 Equations of the coefficients of $E^{\varepsilon}_{\pm}/H^{\varepsilon}_{0}$ 56

3.4 Equivalent Models up to order 2 . . . . . **59**

3.4.1 Equivalent Model of Order 1 59

3.4.2 Equivalent Model of Order 2 60

3.5 Discretisation by the Boundary Element Method **63**

3.5.1 Functional Spaces 64

3.5.2 Potentials 64

3.5.3 Boundary Integral Equations 65

3.5.4 Equivalent Model of Order 1 66

3.5.5 Strong Formulation for E_1 68

3.5.6 Equivalent Model of Order 2 69

3.5.7 Implementation 71

3.6 Numerical Results **71**

3.6.1 Validation of Integral Equations 72

3.6.2 Verification of the consistency of H^1_{ε} with H_0 and $H_0 + \varepsilon H_1$ . . 73

3.6.3 Example 1 73

3.6.4 Example 2 75

3.6.5 Example 3 77
3.6.6 Example 4 79
3.7 Conclusion 80

3.1 Introduction

Many components are surrounded by conductive thin layers for shielding purposes such as the anechoic chamber used to measure antenna characterization, and the Helmholtz coils used to cancel the earth magnetic field and generate the required magnetic fields for experiments. Modeling these conducting regions requires a very fine volume discretisation because the fields decay rapidly through the surface due to the skin depth. Therefore, it may lead to a large system of equations (using the FEM) and then to prohibitive computational time especially for 3D structures. To prevent this difficulty, the conductive sheet can be replaced by a mid-surface with equivalent transmission conditions. The transmission conditions are derived asymptotically for vanishing sheet thickness ε where the skin depth is kept proportional to ε, in this way we will maintain the skin depth less than or equal to the sheet thickness.

In [68], an integral formulation using facet elements is presented for modeling a non-magnetic conductive thin sheet in the general case (the skin depth is smaller, larger, or equal to the thickness of the sheet).

In [77], a thin shell approximation that reduces the thin shell volume to an average surface situated halfway between the inner and outer surface of the shell is proposed. It is based on the treatment of the surface terms that appear in the finite element formulation. This treatment is done by establishing an appropriate impedance boundary conditions and a discretisation using Whitney edge elements. They assumed that the electromagnetic fields H and E have no components perpendicular to the surface of the shell. This approach is applied on the perforated magnetic shield for electric power applications in [79].

In [81], a time-domain approach with a magnetic field vector formulation is proposed to consider the presence of thin layers. It is based on the treatment of the surface term in the weak formulation of finite element method and the use of orthogonal polynomial basis functions to account for the variation of the magnetic flux and the current density through the shell thickness. A tangential vector fields are introduced on the average surface to take into account the time domain behavior of the thin shell. This work has been extended to the magnetic field formulation in [80], and an application on a shielded induction heater with a pulsed current is presented in [103].

In [65] two families of Impedance Transmission Conditions (ITC) for Eddy Current

Model in 2D have been derived using asymptotic expansions, ITC-1-N based on scaling the conductivity with the sheet thickness ε like $1/\varepsilon$ and ITC-2-N based on scaling the conductivity with the sheet thickness ε like $1/\varepsilon^2$, where $N+1$ is the order of convergence for these families. The robustness of the ITC-2-N family of transmission conditions is validated in [67] and it shows a higher accuracy in comparison with ITC-1-N. The ITC-2-N family thus adopted in [59] to derive an equivalent transmission conditions for the full time-harmonic Maxwell equations in 3D, where curved thin sheets are considered, and the material constants can take different values inside and outside the sheet.

In this work, the family ITC-2-N is considered, we present impedance transmission conditions derived asymptotically for eddy-current problems in 3D, for curved thin sheets, where the materials inside and outside the sheet are non-conductive. The difference between this work and the work in [64] is that we proceed with an hybrid (electric and magnetic fields) formulation, where in [64] the derivation of asymptotic models is based on a magnetic field formulation and a multi-scale expansion for the magnetic field and then impedance conditions are identified for the electric field.

We also study a discretization that can be the numerical relevant for ITCs. We avoid the volume mesh required in the Finite Element Method (FEM) by discretising the problem using the Boundary Element Method (BEM) that uses only a mesh on the surface. In addition, the BEM is well adapted to general field problems with unbounded structures because no artificial boundary is needed [66]. This is not the case for the FEM.

We validate the results by comparing them to an analytical solution, and to the same problem simulated in COMSOL and solved numerically using the Finite Element Method with very fine meshes.

This chapter is organized as follows: Sections 3.2.3 and 3.3 presents the hybrid formulation of the eddy current problem, and the mathematical demonstration of the equivalent models up to order 2. In Section 3.5 we provide the Boundary Element Method with specific basis functions to solve the problem. Numerical results are provided in Section 3.6, we validate our models and assumptions, and we study the computational time using the BEM.

3.2 Mathematical Model

3.2.1 Notations

Let Γ be any orientable and closed surface of $\mathbb{R}^3$, and let v be a vector field on Γ, then we denote by

$$v_T = n \times (v \times n)$$

the tangential component of v. Here n is the unit normal vector on Γ which is oriented from the interior domain enclosed by Γ towards the outer domain (see Figure 3.1).

We also denote by $\gamma_D \cdot$, $\gamma_N \cdot$ and $\gamma_n \cdot$ the Dirichlet, Neumann, and normal traces, respectively. They are defined as

$$\gamma_D v = v_T = n \times (v \times n)_{|\Gamma},$$

$$\gamma_N v = (\mathrm{curl} v \times n)_{|\Gamma},$$

$$\gamma_n v = (v \cdot n)_{|\Gamma}.$$

We denote by $\mathbf{curl}_\Gamma$ the tangential rotational operator and by curl_Γ the surface rotational

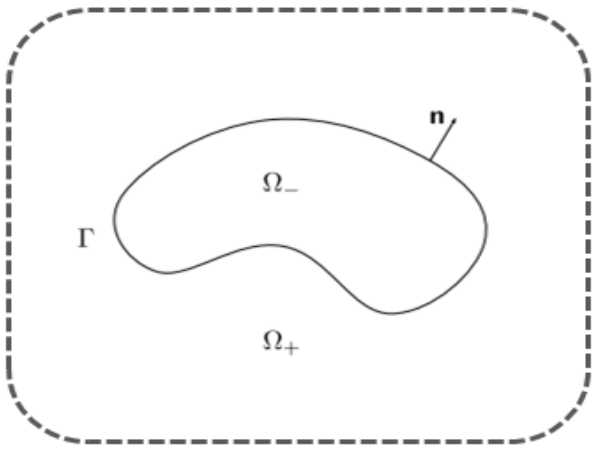

Figure 3.1: A cross section of the domain Ω

operator:

$$\forall f \in C^\infty(\Gamma), \quad \mathbf{curl}_\Gamma f = (\nabla_\Gamma f) \times n$$

$$\forall v \in (C^\infty(\Gamma))^3, \quad \mathrm{curl}_\Gamma v = \mathrm{div}_\Gamma (v \times n)$$

where ∇_Γ and div_Γ are respectively the tangential gradient and the surface divergence on Γ.

Denote also the space of L^2-integrable tangent vector fields by

$$L^2_t(\Gamma) = \{v \in (L^2(\Gamma))^3, v \cdot n = 0 \text{ on } \Gamma\}.$$

Let Ω_- and Ω_+ be two Lipschitz domains, and let $\Gamma := \partial\Omega_- \cup \partial\Omega_+$ be the common interface which is a closed set (see Figure 3.1).

Let Σ be any smooth surface, we denote by $[f]_\Sigma$ the jump of f across Σ

$$[f]_\Sigma = f_{|\Sigma+} - f_{|\Sigma-} \qquad \text{for} \qquad f \in C^\infty(\Omega_\pm)$$

where for all $x \in \Sigma$, the one sided traces are defined by:

$$f_{|\Sigma\pm} = \lim_{s \to 0\pm} f(x + sn).$$

Also we denote by $\{f\}_\Sigma$ the mean value of f across Σ

$$\{f\}_\Sigma = \frac{1}{2}(f_{|\Sigma+} + f_{|\Sigma-}) \qquad \text{for} \qquad f \in C^\infty(\Omega_\pm).$$

The same definitions can be extended to vector fields $v \in (C(\Omega_\pm))^3$.
For the tangential traces, we have the following relations:

$$\{v \times n\}_\Sigma = \{v\}_\Sigma \times n, \qquad [v \times n]_\Sigma = [v]_\Sigma \times n,$$

$$\{v_T\}_\Sigma = (\{v\}_\Sigma)_T, \qquad [v_T]_\Sigma = ([v]_\Sigma)_T.$$

3.2.2 Eddy Current Problem for a Thin Layer

Throughout this chapter, we denote by $\Omega \subset \mathbb{R}^3$ the domain of study, which is itself composed of three sub-domains

$$\Omega = \Omega^\varepsilon_- \cup \overline{\Omega^\varepsilon_0} \cup \Omega^\varepsilon_+$$

where Ω^ε_- is the interior domain that corresponds to any non-conductive linear material, Ω^ε_+ is the exterior of the structure domain, and the subdomain Ω^ε_0 is a conductive thin

layer of constant thickness ε surrounding the subdomain Ω_-^ε. Let Γ_-^ε and Γ_+^ε be the two smooth boundaries of the subdomains Ω_-^ε and $\overline{\Omega_-^\varepsilon} \cup \Omega_0^\varepsilon$ respectively (see Figure 3.2). As

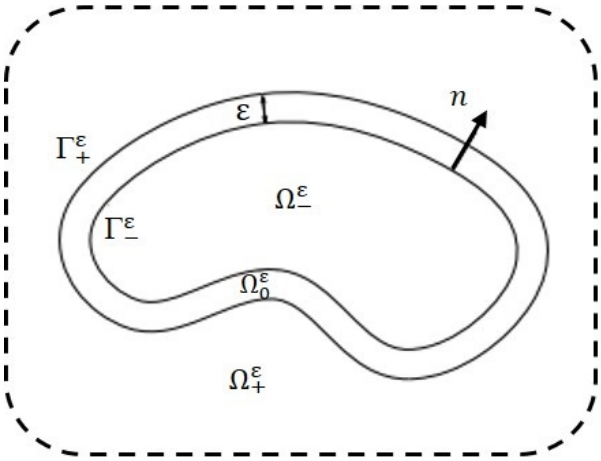

Figure 3.2: A cross section of the domain Ω

the three subdomains have different properties, we define μ^ε(magnetic permeability) and σ^ε(conductivity) as piecewise constant functions:

$$\mu^\varepsilon = \begin{cases} \mu_- & \text{in} \quad \Omega_-^\varepsilon, \\ \mu_0^c & \text{in} \quad \Omega_0^\varepsilon, \\ \mu_+ & \text{in} \quad \Omega_+^\varepsilon, \end{cases} \quad \text{and} \quad \sigma^\varepsilon = \begin{cases} 0 & \text{in} \quad \Omega_-^\varepsilon, \\ \sigma_0 & \text{in} \quad \Omega_0^\varepsilon, \\ 0 & \text{in} \quad \Omega_+^\varepsilon. \end{cases}$$

At high frequency, the skin depth $\delta = \sqrt{\frac{2}{\omega \mu_0^c \sigma_0}}$ becomes smaller than the thickness ε. In this case, very fast changing field near the interface will be observed, and the magnetic field does not penetrate completely in the interior of the layer. This skin effect makes the studying of the behavior of the magnetic field near the interface more problematic, as a very fine mesh is required. That is why we are interested in the case where the skin depth is smaller than ε or of the same order.

For studying the asymptotic behaviour, we assume an explicit dependence of the layer conductivity σ_0 on ε

$$\sigma_0 = \varepsilon^{-2}\bar{\sigma},$$

which comes from the fact that as the layer is thinner, the conductivity is larger and δ remains less than or equal to ϵ.

The general model of the eddy current problem is already presented in chapter 1, but we

recall it once again for clarity

$$\text{curl}H^\varepsilon = J \qquad \text{in } \Omega, \tag{3.1}$$

$$\text{curl}E^\varepsilon - i\omega\mu^\varepsilon H^\varepsilon = 0 \qquad \text{in } \Omega, \tag{3.2}$$

$$B^\varepsilon = \mu^\varepsilon H^\varepsilon \qquad \text{in } \Omega, \tag{3.3}$$

$$J = \sigma^\varepsilon E^\varepsilon + J_s \qquad \text{in } \Omega, \tag{3.4}$$

$$\text{div}E^\varepsilon = 0 \qquad \text{in } \Omega^\varepsilon_\pm, \tag{3.5}$$

$$\int_{\Gamma^\varepsilon_\pm} E^\varepsilon_\pm \cdot n dS = 0 \qquad \text{on } \Gamma^\varepsilon_\pm, \tag{3.6}$$

$$E^\varepsilon = O\Big(\frac{1}{|x|}\Big) \qquad \text{as } |x| \to \infty, \tag{3.7}$$

where ω is the angular frequency.

3.2.3 $\mathbf{E}^\varepsilon_\pm/\mathbf{H}^\varepsilon_0$ Hybrid Formulation

In [64] the formulations in H and E are adopted but it is also possible to do all the calculations in a hybrid formulation E/H.
Using Faraday's law (3.2), the magnetic field can be written in $\Omega^\varepsilon_\pm$ in function of the electric field as

$$H^\varepsilon_\pm = (i\omega)^{-1}(\mu^\varepsilon_\pm)^{-1}\text{curl}E^\varepsilon_\pm,$$

and substituting it in Ampère's law (3.1), we obtain an equation for the electric field in the insulator or air region $\Omega^\varepsilon_\pm$

$$\text{curlcurl}E^\varepsilon_\pm = i\omega\mu^\varepsilon_\pm J_s.$$

Similarly, using Ampère's law (3.1) the electric field can be written in Ω^ε_0 as

$$E^\varepsilon_0 = (\sigma_0)^{-1}(\text{curl}H^\varepsilon_0 - J_s),$$

and substituting it in Faraday's law (3.2), we obtain an equation for the magnetic field in the conductor Ω^ε_0

$$\text{curlcurl}H^\varepsilon_0 - i\omega\mu^\varepsilon_0\sigma_0 H^\varepsilon_0 = \text{curl}J_s.$$

Transmission conditions across the two conductor surfaces Γ_+^ε and Γ_-^ε are considered [70]

$$[H^\varepsilon \times n]_{\Gamma_\pm^\varepsilon} = 0 \qquad \text{on } \Gamma_\pm^\varepsilon, \tag{3.8}$$

$$[\mu H^\varepsilon \cdot n]_{\Gamma_\pm^\varepsilon} = 0 \qquad \text{on } \Gamma_\pm^\varepsilon. \tag{3.9}$$

Using Faraday's law and the tangential continuity of the magnetic field across the boundary, we obtain

$$i\omega(H_0^\varepsilon \times n) = i\omega(H_\pm^\varepsilon \times n) = \frac{1}{\mu_\pm^\varepsilon}\text{curl}E_\pm^\varepsilon \times n.$$

Using the continuity of the normal component of the magnetic induction (3.9) and the Faraday law, we get

$$\mu_0^\varepsilon H_0^\varepsilon \cdot n = \mu_\pm^\varepsilon H_\pm^\varepsilon \cdot n = \frac{1}{i\omega}\text{curl}E_\pm^\varepsilon \cdot n.$$

For simplicity, we assume that the source current term J_s is smooth enough and its support does not meet the layer Ω_0^ε ($J_s = 0$ in Ω_0^ε).
Therefore the hybrid eddy current model can be written

$$\begin{cases} \text{curlcurl}E_\pm^\varepsilon & = & i\omega\mu_\pm^\varepsilon J_s & \text{in} & \Omega_\pm^\varepsilon, \\ \text{curlcurl}H_0^\varepsilon - k_0^\varepsilon H_0^\varepsilon & = & 0 & \text{in} & \Omega_0^\varepsilon, \\ i\omega(H_0^\varepsilon \times n) & = & \frac{1}{\mu_\pm^\varepsilon}\text{curl}E_\pm^\varepsilon \times n & \text{on} & \Gamma_\pm^\varepsilon, \\ \mu_0 H_0^\varepsilon \cdot n & = & \frac{1}{i\omega}\text{curl}E_\pm^\varepsilon \cdot n & \text{on} & \Gamma_\pm^\varepsilon, \\ \text{div}E_\pm^\varepsilon & = & 0 & \text{in} & \Omega_\pm^\varepsilon, \\ \int_{\Gamma_\pm^\varepsilon} E_\pm^\varepsilon \cdot n dS & = & 0 & \text{on} & \Gamma_\pm^\varepsilon, \end{cases} \tag{3.10}$$

where k^ε is the complex wave number given by

$$(k^\varepsilon)^2(x) = i\omega\sigma^\varepsilon(x)\mu^\varepsilon(x).$$

It is defined as a piecewise constant function inside the three subdomains

$$k^\varepsilon = \begin{cases} 0 & \text{in} & \Omega_-^\varepsilon, \\ k_0 & \text{in} & \Omega_0^\varepsilon, \\ 0 & \text{in} & \Omega_+^\varepsilon, \end{cases}$$

where E_+^ε, E_-^ε and H_0^ε denote the restrictions of E^ε and H^ε to the respective domains Ω_+^ε, Ω_-^ε and Ω_0^ε.

3.2.4 Objective

The discretisation of the conducting sheet by the FEM is time-consuming as it requires meshing by very small cells due to the rapid decay of the field under high conductivity. To avoid meshing the thin layer Ω_0^ε, we suggest replacing it by an interface, usually its mid-surface Γ, on which appropriate conditions are set.

This is to say that we have to approximate new models defined on ε-independent domains

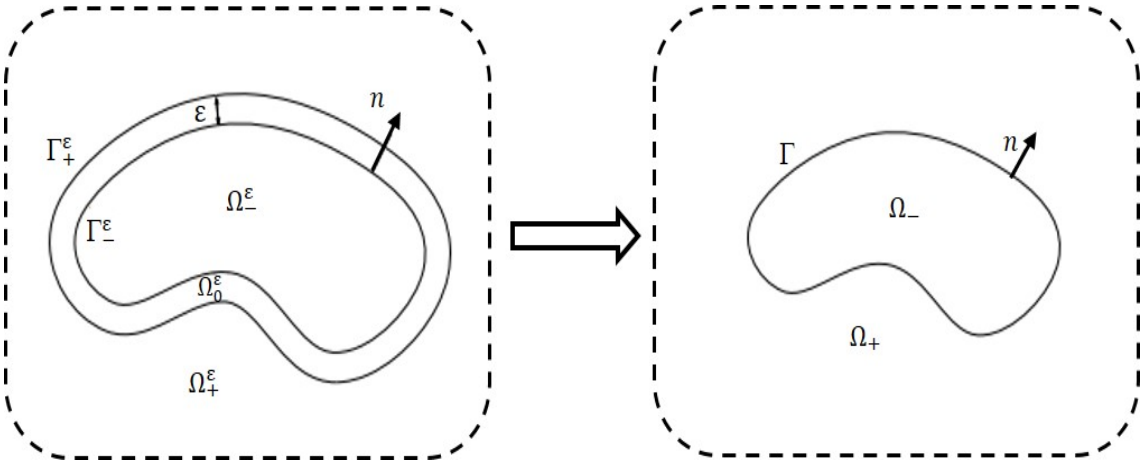

Figure 3.3: The cross sections of the domain of the main problem $\Omega_-^\varepsilon \cup \overline{\Omega_0^\varepsilon} \cup \Omega_+^\varepsilon$ and of the approximate problem $\Omega_- \cup \Omega_+$

Ω_- and Ω_+ (see Figure 3.3), where

$$\Omega_- = \lim_{\varepsilon \to 0} \Omega_-^\varepsilon,$$

and

$$\Omega_+ = \lim_{\varepsilon \to 0} \Omega_+^\varepsilon.$$

In the approximate model, we redefine the magnetic properties in the new subdomains by a simple extension of μ^ε and σ^ε outside the sheet. We obtain the new values:

$$\mu = \begin{cases} \mu_- & \text{in} \quad \Omega_-, \\ \mu_+ & \text{in} \quad \Omega_+, \end{cases}$$

and

$$\sigma = \begin{cases} \sigma_- = 0 & \text{in} \quad \Omega_-, \\ \sigma_+ = 0 & \text{in} \quad \Omega_+. \end{cases}$$

Similarly, we define k the extension of k^ε as

$$k = \begin{cases} 0 & \text{in} \quad \Omega_-, \\ 0 & \text{in} \quad \Omega_+. \end{cases}$$

3.3 Multiscale Expansion and Equivalent Models with Transmission Conditions

In problem (3.10), Ω_0^ε is a thin layer, and Γ its mediant-surface (Ω_0^ε is then a tubular neighborhood of Γ in $\Omega_- \cup \Omega_+$)
Assuming that Γ is a smooth curve, then it is possible to derive a multiscale expansion for the solution of the problem: It possesses an asymptotic expansion in power series of the small parameter ε [64]

$$E_\pm^\varepsilon(x) \approx E_0^\pm(x) + \varepsilon E_1^\pm(x) + \varepsilon^2 E_2^\pm(x) + ... + \mathcal{O}(\varepsilon^k), \tag{3.11}$$

$$H_0^\varepsilon(x) \approx \boldsymbol{\mathcal{H}}_0\Big(y_\alpha, \frac{h}{\varepsilon}\Big) + \varepsilon \boldsymbol{\mathcal{H}}_1\Big(y_\alpha, \frac{h}{\varepsilon}\Big) + ... + \mathcal{O}(\varepsilon^k), \tag{3.12}$$

where $\mathcal{O}(\varepsilon^k)$ means that the remainder is uniformly bounded by ε^k.
Here, $x \in \mathbb{R}^3$ are the cartesian coordinates, and (y_α, h) is the local coordinate system where $h \in (-\frac{\varepsilon}{2}, \frac{\varepsilon}{2})$ is the normal coordinate to Γ and y_α for $\alpha = 1, 2$ (i.e. (y_1, y_2)) are the tangential coordinates to Γ (see Figure 3.4). Note that, y_α is called the "slow" variable and h/ε is called the "fast" variable according to the normal coordinates.

The term $\boldsymbol{\mathcal{H}}_j$ are profiles defined on $\Gamma \times (-\frac{1}{2}, \frac{1}{2})$ and are smooth for all variables. These profiles describe the magnetic field in the thin layer Ω_0^ε according to the normal coordinate system.

The derivation is based on:

- the expansion of the differential operators inside the thin layer Ω_0^ε, (see Appendix A.1)
- the Taylor expansion of $E_j|_{\Gamma_\pm^\varepsilon}$ around the mid-surface Γ, (see Figure (3.5))
- the collection of the terms with the same power in ε in the PDE inside and outside the sheet, and the conditions for the Dirichlet and normal traces on $\Gamma_\pm^\varepsilon$.

Then, we can introduce a problem satisfied by an approximation E_ε^k of the expression $E_0(x) + \varepsilon E_1(x) + \varepsilon^2 E_2(x) + ... + \varepsilon^k E_k(x)$ up to a residual term $\mathcal{O}(\varepsilon^{k+1})$.

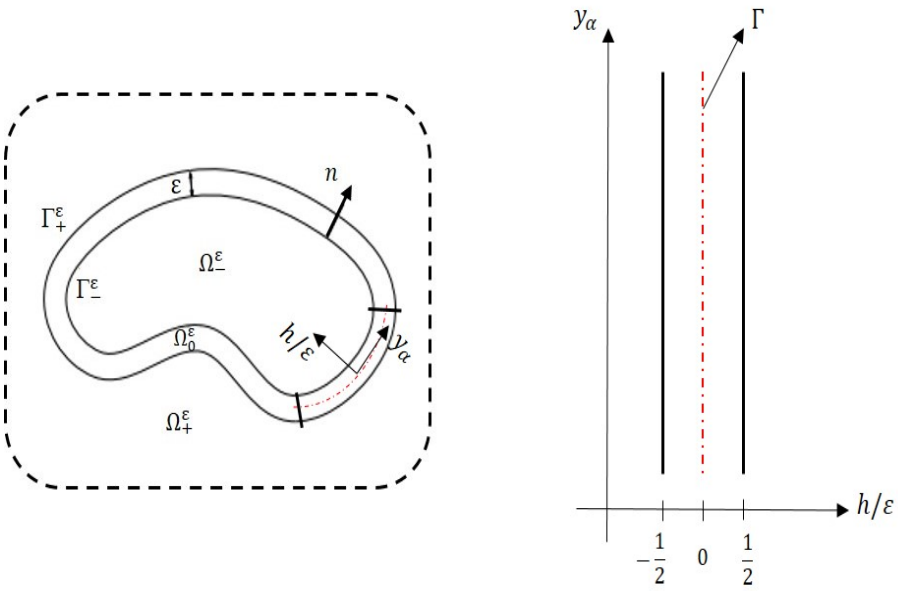

Figure 3.4: Normalised domain

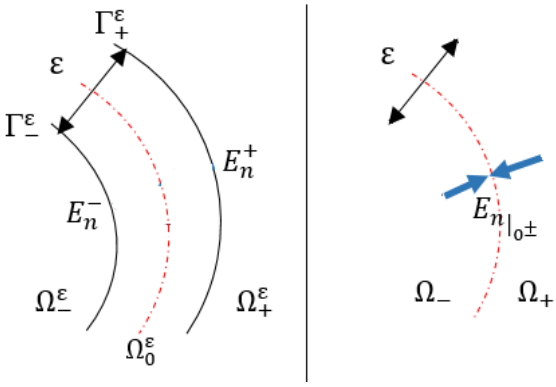

Figure 3.5: Taylor expansion around the mid-surface.

3.3.1 Equations of the coefficients of $E_\pm^\varepsilon/H_0^\varepsilon$

Keep in mind that the hybrid formulation $E_\pm^\varepsilon/H_0^\varepsilon$ satisfies the following

$$\begin{aligned}
\mathrm{curlcurl}E_\pm^\varepsilon &= i\omega\mu_\pm^\varepsilon J_s && \text{in } \Omega_\pm^\varepsilon && (3.13)\\
\mathrm{curlcurl}H_0^\varepsilon - k_0^\varepsilon H_0^\varepsilon &= 0 && \text{in } \Omega_0^\varepsilon && (3.14)\\
i\omega(H_0^\varepsilon \times n) &= \frac{1}{\mu_\pm^\varepsilon}\mathrm{curl}E_\pm^\varepsilon \times n && \text{on } \Gamma_\pm^\varepsilon && (3.15)\\
\mu_0^c H_0^\varepsilon \cdot n &= \frac{1}{i\omega}\mathrm{curl}E_\pm^\varepsilon \cdot n && \text{on } \Gamma_\pm^\varepsilon && (3.16)\\
\mathrm{div}E_\pm^\varepsilon &= 0 && \text{in } \Omega_\pm^\varepsilon && (3.17)\\
\int_{\Gamma_\pm^\varepsilon} E_\pm^\varepsilon \cdot n dS &= 0 && \text{on } \Gamma_\pm^\varepsilon && (3.18)
\end{aligned}$$

Approximating this model by considering just the mid-surface of the thin layer subdomain Ω_0^ε requires us to write the second partial differential equation (3.14) in the thin conductor in the scaled local coordinate system (y_α,Y_3).
We find that the profiles $\boldsymbol{\mathcal{H}}_j$ satisfy the following

$$L[\varepsilon]\sum_{j=0}^{\infty}\varepsilon^j\boldsymbol{\mathcal{H}}_j(y_\alpha,Y_3) \quad = \quad 0 \quad \text{in} \quad \Gamma\times I, \tag{3.19}$$

where L is the second order Maxwell operator defind in Appendix A.1, and $I=(\frac{-1}{2},\frac{1}{2})$. We can easily see that the terms $E_j^\pm$ of the expansion (3.11) depends on ε, because they are evaluated on $\Gamma_\pm^\varepsilon$ when replacing the expansion of E^ε in the transmission conditions across $\Gamma_\pm^\varepsilon$. This is not convenient, and we propose to consider the Taylor expansion of this term towards the surface Γ. This should give a more accurate approximation.

As the expansion of E^ε is assumed to be valid for any small $\varepsilon>0$ the terms $E_j^\pm$ are defined in $\Omega_\pm^\varepsilon$ for all $\varepsilon>0$ and hence in $\Omega_\pm$. According to the assumption that the thin conductors, and its mid-surface Γ are smooth, that $\mu_\pm$, $\sigma_\pm$ are constants, and that the current J_s is zero close to Γ it makes sense to accept that the vector fields $E_j^\pm$ are regular in the neighbourhood of Γ. This can be justified using the regularity theory in [74].
Hence we can use the Taylor expansion and infer for $n\in\mathbf{N}$, that

$$\text{curl}E_n^\pm\times n|_{h=\pm\frac{\varepsilon}{2}} = \text{curl}E_n\times n|_{0\pm} \pm \frac{\varepsilon}{2}\partial_h\Big(\text{curl}E_n\times n|_{0\pm}\Big)+..., \tag{3.20}$$

$$\text{curl}E_n^\pm\cdot n|_{h=\pm\frac{\varepsilon}{2}} = \text{curl}E_n\cdot n|_{0\pm} \pm \frac{\varepsilon}{2}\partial_h\Big(\text{curl}E_n\cdot n|_{0\pm}\Big)+..., \tag{3.21}$$

where $\cdot|_{0\pm}$ means the limit for positive or negative $h\to 0$, respectively.

Proposition 3.3.1 *The components of $L[\varepsilon]\sum_{j=0}^{\infty}\varepsilon^j\boldsymbol{\mathcal{H}}_j(y_\alpha,\,Y_3)$ in $\Gamma\times I$ after performing the identification of terms with the same power of ε are:*

$$L^0(\boldsymbol{\mathcal{H}}_0)=0,$$

$$L^0(\boldsymbol{\mathcal{H}}_1)+L^1(\boldsymbol{\mathcal{H}}_0)=0,$$

and

$$\sum_{l=0}^{k}L^l(\boldsymbol{\mathcal{H}}_{k-l})=0 \quad \textit{for} \;\; n\geq 2,$$

where L^l, $l = 0..k$ are the terms of expansion of L in power series of ε (see Appendix A.1).

Proof. see the Appendix A.2 ■

Proposition 3.3.2 *The profiles $\boldsymbol{\mathcal{H}_n} = (\mathcal{H}_n, \hbar_n)$ and the terms E_n have to satisfy, for all $n \geq 0$*

$$L_3^0(\boldsymbol{\mathcal{H}}_n) = \gamma^2(\hbar_n) = -\sum_{j=1}^{n} L_3^j(\boldsymbol{\mathcal{H}}_{n-j}) \quad \text{in } \Gamma \times I, \tag{3.22}$$

$$L_\alpha^0(\boldsymbol{\mathcal{H}}_n) = -\partial_3^2 \mathcal{H}_{n,\alpha} + \gamma^2 \mathcal{H}_{n,\alpha} = -\sum_{j=1}^{n} L_\alpha^j(\boldsymbol{\mathcal{H}}_{n-j}) \quad \text{in } \Gamma \times I, \tag{3.23}$$

$$\text{curlcurl} E_n^\pm = \delta_n^0 i\omega\mu_\pm J_s \quad \text{in } \Omega_\pm, \tag{3.24}$$

$$\text{curl} E_n^\pm \cdot n|_{0\pm} = i\omega\mu_0^c \boldsymbol{\mathcal{H}}_n \cdot n|_{\pm\frac{1}{2}} - \sum_{j=1}^{n} \frac{1}{(\pm 2)^j} \partial_h^j \Big(\text{curl} E_{n-j}^\pm \cdot n|_{0\pm}\Big) \quad \text{on } \Gamma, \tag{3.25}$$

$$\text{curl} E_n^\pm \times n|_{0\pm} = i\omega\mu_\pm^\varepsilon \boldsymbol{\mathcal{H}}_n \times n|_{\pm\frac{1}{2}} - \sum_{j=1}^{n} \frac{1}{(\pm 2)^j} \partial_h^j \Big(\text{curl} E_{n-j}^\pm \times n|_{0\pm}\Big) \text{ on } \Gamma, \tag{3.26}$$

$$\text{div} E_n^\pm = 0 \quad \text{in } \Omega_\pm^\varepsilon, \tag{3.27}$$

$$\int_{\Gamma_\pm^\varepsilon} E_n^\pm \cdot n dS = 0 \quad \text{on } \Gamma_\pm^\varepsilon, \tag{3.28}$$

where $\cdot|_{\pm\frac{1}{2}}$ abbreviates the trace on $Y_3 = \pm\frac{1}{2}$, and $\delta_n^0 = 1$ if $n = 0$ and zero otherwise. Where $\boldsymbol{\mathcal{H}} = (\mathcal{H}_\alpha, \hbar)$, $\mathcal{H}_\alpha = (\mathcal{H}_1, \mathcal{H}_2)$ and $\hbar$ are the tangential and normal coordinates of $\boldsymbol{\mathcal{H}}$, respectively, and $\gamma = exp(\frac{3i\pi}{4})\sqrt{\omega\mu_0^c\overline{\sigma}}$.

Proof. see the Appendix A.3 ■

Corollary 3.3.1 *The model in (3.3.2) is equivalent to*

$$L_3^0(\boldsymbol{\mathcal{H}}_n) = \gamma^2(\hbar_n) = -\sum_{j=1}^{n} L_3^j(\boldsymbol{\mathcal{H}}_{n-j}) \quad \text{in } \Gamma \times I, \tag{3.29}$$

$$L_\alpha^0(\boldsymbol{\mathcal{H}}_n) = -\partial_3^2 \mathcal{H}_{n,\alpha} + \gamma^2 \mathcal{H}_{n,\alpha} = -\sum_{j=1}^{n} L_\alpha^j(\boldsymbol{\mathcal{H}}_{n-j}) \quad \text{in } \Gamma \times I, \tag{3.30}$$

$$\text{curlcurl} E_n^\pm = \delta_n^0 i\omega\mu_\pm J_s \quad \text{in } \Omega_\pm, \tag{3.31}$$

$$\text{curl} E_n^\pm \cdot n|_{0\pm} = i\omega\mu_0^c \hbar_n|_{\pm\frac{1}{2}} - \sum_{j=1}^{n} \frac{1}{(\pm 2)^j} \partial_h^j \Big(\text{curl} E_{n-j}^\pm \cdot n|_{0\pm}\Big) \quad \text{on } \Gamma, \tag{3.32}$$

$$i\omega\mu_\pm^\varepsilon \boldsymbol{\mathcal{H}}_n|_{\pm\frac{1}{2}} = n \times \text{curl}\mathcal{E}_n^\pm \times n|_{0\pm} + \sum_{j=1}^{n} \frac{1}{(\pm 2)^j} \partial_h^j \Big(n \times \text{curl}\mathcal{E}_{n-j}^\pm \times n|_{0\pm}\Big) \text{ on } \Gamma, \tag{3.33}$$

$$\text{div} E_n^\pm = 0 \quad \text{in } \Omega_\pm, \tag{3.34}$$

$$\int_{\Gamma_\pm} E_n^\pm \cdot n dS = 0 \quad \text{on } \Gamma_\pm, \tag{3.35}$$

where $\mathcal{E}_n^{\pm}$ *is the trace of* E_n *on* $\Gamma_{\pm}$.

3.4 Equivalent Models up to order 2

In the previous section we derived the coupled systems for the terms of the asymptotic expansions to any order n. Hence we can determine now the first terms $\boldsymbol{\mathcal{H}}_n = (\mathcal{H}_n, \mathcal{h}_n)$ and E_n by induction.

3.4.1 Equivalent Model of Order 1

For $n = 0$ in the previous system (see corollary 3.3.1), it is straightforward that $\boldsymbol{\mathcal{H}}_0 = (\mathcal{H}_0, \mathcal{h}_0)$ and the terms E_0 satisfy

$$\begin{aligned}
\gamma^2(\mathcal{h}_0) &= 0 && \text{in } \Gamma \times I, && (3.36)\\
-\partial_3^2\mathcal{H}_{0,\alpha} + \gamma^2\mathcal{H}_{0,\alpha} &= 0 && \text{in } \Gamma \times I, && (3.37)\\
\mathrm{curlcurl}E_0^{\pm} &= i\omega\mu_{\pm}J_s && \text{in } \Omega_{\pm}, && (3.38)\\
\mathrm{curl}E_0^{\pm}\cdot n|_{0\pm} &= i\omega\mu_0^c\mathcal{h}_0|_{\pm\frac{1}{2}} && \text{on } \Gamma, && (3.39)\\
i\omega\mu_{\pm}\boldsymbol{\mathcal{H}}_0|_{\pm\frac{1}{2}} &= n\times\mathrm{curl}\mathcal{E}_0^{\pm}\times n|_{0\pm} && \text{on } \Gamma, && (3.40)\\
\mathrm{div}E_0^{\pm} &= 0 && \text{in } \Omega_{\pm}, && (3.41)\\
\int_{\Gamma_{\pm}} E_0^{\pm}\cdot n dS &= 0 && \text{on } \Gamma_{\pm}. && (3.42)
\end{aligned}$$

Obviously 3.36 implies that $\mathcal{h}_0 = 0$ by the fact that $\gamma \neq 0$ and in view of (3.38), (3.39), (3.41), and (3.42) we can obtain the following limit system for $E_0^{\pm}$

$$\left\{\begin{array}{lcll}
\mathrm{curlcurl}E_0^{-} &= i\omega\mu_- J_s & \text{in} & \Omega_-,\\
\mathrm{curl}E_0^{-}\cdot n &= 0 & \text{on} & \Gamma,\\
\mathrm{curlcurl}E_0^{+} &= i\omega\mu_+ J_s & \text{in} & \Omega_+,\\
\mathrm{curl}E_0^{+}\cdot n &= 0 & \text{on} & \Gamma,\\
\mathrm{div}E_0^{\pm} &= 0 & \text{in} & \Omega_{\pm},\\
\int_{\Gamma_{\pm}} E_0^{\pm}\cdot n dS &= 0 & \text{on} & \Gamma_{\pm}.
\end{array}\right. \tag{3.43}$$

3.4.2 Equivalent Model of Order 2

In the same way we find that $\boldsymbol{\mathcal{H}}_1 = (\mathcal{H}_1, \hbar_1)$ and the terms E_1 satisfy

$$\begin{aligned}
\gamma^2(\hbar_1) &= -L_3^1(\boldsymbol{\mathcal{H}}_0) && \text{in } \Gamma \times I, && (3.44)\\
-\partial_3^2\mathcal{H}_{1,\alpha} + \gamma^2\mathcal{H}_{1,\alpha} &= -L_\alpha^1(\boldsymbol{\mathcal{H}_0}) && \text{in } \Gamma \times I, && (3.45)\\
\mathrm{curlcurl}E_1^\pm &= 0 && \text{in } \Omega_\pm, && (3.46)\\
\mathrm{curl}E_1^\pm \cdot n|_{0\pm} &= i\omega\mu_0^c\boldsymbol{\mathcal{H}_1}\cdot n|_{\pm\frac{1}{2}} \mp \frac{1}{2}\partial_h\Big(\mathrm{curl}E_0^\pm \cdot n|_{0\pm}\Big) && \text{on } \Gamma, && (3.47)\\
i\omega\mu_\pm\boldsymbol{\mathcal{H}_1}|_{\pm\frac{1}{2}} &= n \times \mathrm{curl}\mathcal{E}_1^\pm \times n|_{0\pm} \pm \frac{1}{2}\partial_h\Big(n \times \mathrm{curl}\mathcal{E}_0^\pm \times n|_{0\pm}\Big) && \text{on } \Gamma, && (3.48)\\
\mathrm{div}E_1^\pm &= 0 && \text{in } \Omega_\pm, && (3.49)\\
\int_{\Gamma_\pm} E_1^\pm \cdot n dS &= 0 && \text{on } \Gamma_\pm^\varepsilon. && (3.50)
\end{aligned}$$

According to (3.44), and proposition (A.4.1) we obtain

$$\hbar_1(y_\beta, Y_3) = -\gamma^{-1}\Big(D_\alpha\Big\{\frac{1}{i\omega\mu}\mathrm{curl}\mathcal{E}_0^\alpha\Big\}_\Gamma(y_\beta)\frac{\sinh\gamma Y_3}{\cosh(\frac{\gamma}{2})} + D_\alpha\Big[\frac{1}{i\omega\mu}\mathrm{curl}\mathcal{E}_0^\alpha\Big]_\Gamma(y_\beta)\frac{\cosh\gamma Y_3}{2\sinh(\frac{\gamma}{2})}\Big),$$

where $\mathcal{E}_0^\alpha$ is the tangential components of $\mathcal{E}_0$, and D_α is the covariant derivative.

Now, inserting this explicit representation into the condition (3.47), we find that the term $E_1^\pm$ satisfies the following problem:

$$\begin{cases}
\mathrm{curlcurl}E_1^- &= 0 \quad \text{in} \quad \Omega_-,\\
\mathrm{curl}E_1^- \cdot n &= e_1^- \quad \text{on} \quad \Gamma,\\
\mathrm{curlcurl}E_1^+ &= 0 \quad \text{in} \quad \Omega_+,\\
\mathrm{curl}E_1^+ \cdot n &= e_1^+ \quad \text{on} \quad \Gamma,\\
\mathrm{div}E_1^\pm &= 0 \quad \text{in} \quad \Omega_\pm,\\
\int_{\Gamma_\pm} E_1^\pm \cdot n dS &= 0 \quad \text{on} \quad \Gamma_\pm,
\end{cases} \tag{3.51}$$

where

$$\begin{aligned}
e_1^\pm := &-\gamma^2 i\omega\mu_0^c\Big(\pm D_\alpha\Big\{\frac{1}{i\omega\mu}\mathrm{curl}\mathcal{E}_0^\alpha\Big\}_\Gamma(y_\beta)\tanh(\frac{\gamma}{2}) + D_\alpha\Big[\frac{1}{i\omega\mu}\mathrm{curl}\mathcal{E}_0^\alpha\Big]_\Gamma(y_\beta)\frac{1}{2\tanh(\frac{\gamma}{2})}\Big)\\
&\mp \frac{1}{2}\partial_h\Big(\mathrm{curl}E_0^\pm \cdot n|_{0\pm}\Big).
\end{aligned} \tag{3.52}$$

According to [73, Prop. 3.36] we can write

$$\partial_h \mathrm{curl} E_0^{\pm} \cdot n = -\mathrm{div}_\Gamma (\mathrm{curl} E_0^{\pm})_T \tag{3.53}$$

$$\mathrm{div}_\Gamma (\mathrm{curl} E)_T = D_\alpha \mathrm{curl} \mathcal{E}^\alpha \tag{3.54}$$

Substituting (3.53) and (3.54) in (3.52), we get

$$\begin{aligned} e_1^{\pm} := &- \gamma^2 i\omega\mu_0^c \Big(\pm D_\alpha \Big\{ \frac{1}{i\omega\mu} \mathrm{curl} \mathcal{E}_0^\alpha \Big\}_\Gamma (y_\beta) \tanh(\frac{\gamma}{2}) + D_\alpha \Big[\frac{1}{i\omega\mu} \mathrm{curl} \mathcal{E}_0^\alpha \Big]_\Gamma (y_\beta) \frac{1}{2\tanh(\frac{\gamma}{2})} \Big) \\ &\pm \frac{1}{2} \mathrm{div}_\Gamma (\mathrm{curl} E_0^{\pm})_T. \end{aligned} \tag{3.55}$$

After simple calculations, the boundary conditions for E_1 in (3.51) can be written as

$$[\mathrm{curl} E_1 \cdot n]_\Gamma = \Big(\{\mu\} - 2\frac{\mu_0^c}{\gamma} \tanh(\frac{\gamma}{2}) \Big) \mathrm{div}_\Gamma \Big\{ \frac{1}{\mu} (\mathrm{curl} E_0)_T \Big\}_\Gamma + \Big(\frac{1}{4} [\mu] \Big) \mathrm{div}_\Gamma \Big[\frac{1}{\mu} (\mathrm{curl} E_0)_T \Big]_\Gamma, \tag{3.56}$$

and

$$\{\mathrm{curl} E_1 \cdot n\}_\Gamma = \Big(\frac{\{\mu\}}{4} - \frac{\mu_0^c}{2\gamma} \coth(\frac{\gamma}{2}) \Big) \mathrm{div}_\Gamma \Big[\frac{1}{\mu} (\mathrm{curl} E_0)_T \Big]_\Gamma + \Big(\frac{1}{4} [\mu] \Big) \mathrm{div}_\Gamma \Big\{ \frac{1}{\mu} (\mathrm{curl} E_0)_T \Big\}_\Gamma. \tag{3.57}$$

Adding the obtained equations (3.56-3.57) multiplied by ε to the conditions for E_0 (4.33) and by replacing $E_0 + \varepsilon E_1$ on the left side by E_ε^1 and by replacing εE_0 on the right hand side by $\varepsilon E_1^\varepsilon$, we obtain the second order approximate solution E_ε^1 that solves the system

$$\begin{cases} \mathrm{curl}\mathrm{curl} E_\varepsilon^1 &= i\omega\mu J_s & \text{in} \quad \Omega_\pm, \\ [\mathrm{curl} E_\varepsilon^1 \cdot n]_\Gamma &= \varepsilon \Big(\Big(\{\mu\} - 2\frac{\mu_0^c}{\gamma} \tanh(\frac{\gamma}{2}) \Big) \mathrm{div}_\Gamma \Big\{ \frac{1}{\mu} (\mathrm{curl} E_0)_T \Big\}_\Gamma \\ & \quad + \Big(\frac{1}{4} [\mu] \Big) \mathrm{div}_\Gamma \Big[\frac{1}{\mu} (\mathrm{curl} E_0)_T \Big]_\Gamma \Big) & \text{on} \quad \Gamma, \\ \{\mathrm{curl} E_\varepsilon^1 \cdot n\}_\Gamma &= \varepsilon \Big(\Big(\frac{\{\mu\}}{4} - \frac{\mu_0^c}{2\gamma} \coth(\frac{\gamma}{2}) \Big) \mathrm{div}_\Gamma \Big[\frac{1}{\mu} (\mathrm{curl} E_0)_T \Big]_\Gamma \\ & \quad + \Big(\frac{1}{4} [\mu] \Big) \mathrm{div}_\Gamma \Big\{ \frac{1}{\mu} (\mathrm{curl} E_0)_T \Big\}_\Gamma \Big) & \text{on} \quad \Gamma. \end{cases} \tag{3.58}$$

Which is equivalent to

$$\begin{cases} \text{curlcurl}E^1_\varepsilon & = & i\omega\mu J_s & & \text{in} & \Omega_\pm, \\ E^1_\varepsilon & = & O(\frac{1}{|x|}) & & \text{as} & |x| \to \infty, \\ \begin{pmatrix} [\text{curl}E^1_\varepsilon \cdot n]_\Gamma \\ \{\text{curl}E^1_\varepsilon \cdot n\}_\Gamma \end{pmatrix} & = & \varepsilon \begin{pmatrix} D_1 & D_3 \\ D_3 & D_2 \end{pmatrix} \begin{pmatrix} \{\frac{1}{\mu}(\text{curl}E^1_\varepsilon)_T\}_\Gamma \\ [\frac{1}{\mu}(\text{curl}E^1_\varepsilon)_T]_\Gamma \end{pmatrix} & & \text{on} & \Gamma, \end{cases}$$

where

$$D_i = C_i \text{div}\, \mathbb{I}d \qquad \text{for } i = 1, .., 3,$$

and

$$C_1 = \{\mu\} - 2\frac{\mu_0^c}{\gamma}\tanh(\frac{\gamma}{2}), \quad , \quad C_2 = \frac{\{\mu\}}{4} - \frac{\mu_0^c}{2\gamma}\coth(\frac{\gamma}{2}),$$

$$C_3 = \frac{1}{4}[\mu].$$

Note that $\mathbb{I}d$ is an identity operator.

3.4.2.1 Impedance Transmission Conditions in function of Dirichlet and Neumann Traces of Electric Field

Using Faraday's law $(H^1_\varepsilon)_T = \frac{1}{i\omega\mu}(\text{curl}E^1_\varepsilon)_T$ and using the Stokes formula $\mu H^1_\varepsilon \cdot n = \frac{1}{iw}\text{div}_\Gamma(E^1_\varepsilon \times n)$, we get

$$\text{curl}E^1_\varepsilon \cdot n = \text{div}_\Gamma(E^1_\varepsilon \times n).$$

Using this relation, and applying "the inverse" of the operator div_Γ, we obtain

$$\begin{cases} \text{curlcurl}E^1_\varepsilon & = & i\omega\mu J_s & & \text{in} & \Omega_\pm, \\ E^1_\varepsilon & = & O(\frac{1}{|x|}) & & \text{as} & |x| \to \infty, \\ \begin{pmatrix} [E^1_\varepsilon \times n]_\Gamma \\ \{E^1_\varepsilon \times n\}_\Gamma \end{pmatrix} & = & \varepsilon \begin{pmatrix} C_1 & C_3 \\ C_3 & C_2 \end{pmatrix} \begin{pmatrix} \{\frac{1}{\mu}(\text{curl}E^1_\varepsilon)_T\}_\Gamma \\ [\frac{1}{\mu}(\text{curl}E^1_\varepsilon)_T]_\Gamma \end{pmatrix} & & \text{on} & \Gamma. \end{cases}$$

Applying $n \times \mathbb{I}$ operator, we obtain the following transmission conditions in function of the Neumann and Dirichlet trace of the electric field, we can say that it is in function of

the transverse magnetic field and the transverse electric field. we get

$$\begin{cases} \text{curlcurl}E^1_\varepsilon &= i\omega\mu J_s & \text{in} \quad \Omega_\pm, \\ E^1_\varepsilon &= O(\frac{1}{|x|}) & \text{as} \quad |x| \to \infty, \\ \begin{pmatrix} [\gamma_D E^1_\varepsilon]_\Gamma \\ \{\gamma_D E^1_\varepsilon\}_\Gamma \end{pmatrix} &= -\varepsilon \begin{pmatrix} C_1 & C_3 \\ C_3 & C_2 \end{pmatrix} \begin{pmatrix} \{\frac{1}{\mu}(\gamma_N E^1_\varepsilon)\}_\Gamma \\ [\frac{1}{\mu}(\gamma_N E^1_\varepsilon)]_\Gamma \end{pmatrix} & \text{on} \quad \Gamma. \end{cases}$$

3.4.2.2 Symmetric case with permeability μ_0

For $\mu_- = \mu_+ = \mu_0$, E_1 satisfies

$$\begin{cases} \text{curlcurl}E_1 &= 0 & \text{in} \quad \Omega_\pm, \\ \text{div}E_1 &= 0 & \text{in} \quad \Omega_\pm, \\ E_1 &= O(\frac{1}{|x|}) & \text{as} \quad |x| \to \infty, \\ \begin{pmatrix} [\gamma_D E_1]_\Gamma \\ \{\gamma_D E_1\}_\Gamma \end{pmatrix} &= \begin{pmatrix} K_1 & 0 \\ 0 & K_2 \end{pmatrix} \begin{pmatrix} \{(\gamma_N E_0)\}_\Gamma \\ [(\gamma_N E_0)]_\Gamma \end{pmatrix} & \text{on} \quad \Gamma, \end{cases} \tag{3.59}$$

and E^1_ε satisfies

$$\begin{cases} \text{curlcurl}E^1_\varepsilon &= i\omega\mu J_s & \text{in} \quad \Omega_\pm, \\ E^1_\varepsilon &= O(\frac{1}{|x|}) & \text{as} \quad |x| \to \infty, \\ \begin{pmatrix} [\gamma_D E^1_\varepsilon]_\Gamma \\ \{\gamma_D E^1_\varepsilon\}_\Gamma \end{pmatrix} &= \varepsilon \begin{pmatrix} K_1 & 0 \\ 0 & K_2 \end{pmatrix} \begin{pmatrix} \{(\gamma_N E^1_\varepsilon)\}_\Gamma \\ [(\gamma_N E^1_\varepsilon)]_\Gamma \end{pmatrix} & \text{on} \quad \Gamma, \end{cases} \tag{3.60}$$

where

$$K_1 = -1 + 2\frac{1}{\gamma}\tanh(\frac{\gamma}{2}) \quad , \quad K_2 = -\frac{1}{4} + \frac{1}{2\gamma}\coth(\frac{\gamma}{2}).$$

3.5 Discretisation by the Boundary Element Method

As out of the layer we mainly consider a non-conductive linear homogeneous domain and an open boundary problem, we can avoid the volume mesh required in the FEM by using the BEM that uses only 2D elements on the surfaces. Moreover, the BEM is adapted to general field problems with unbounded structures because no artificial boundaries are needed. After introducing the functional spaces, the potentials, and the general representation formula in sections 3.5.1, 3.5.2 and 3.5.3 respectively. We formulate the integral equations, the variational formulations, and the Galerkin discretisation using special basis functions of the terms of expansion E_0 in section 3.5.4, E_1 in section 3.5.5, and the equivalent model of order 2 E^1_ε in section 3.5.6. Note that we consider $\mu_- = \mu_+ = \mu_0$ all

over this section.

3.5.1 Functional Spaces

The spaces that are related to the traces of vector fields in $H(\mathrm{curl}, \Omega_\pm)$ onto Γ must be considered using Boundary Integral Equations. We will use the following spaces of tangential vector fields on Γ, which are defined in [61],

- $H_\parallel^{\frac{1}{2}}(\Gamma)$ which represents the tangential surface vector fields that are in $H^{\frac{1}{2}}(\Gamma_i)$ for each smooth component Γ_i of Γ, and provides the weak tangential continuity across the edges of Γ_i,

- $H_\perp^{\frac{1}{2}}(\Gamma)$ which provides the weak normal continuity.

Note that for a smooth boundary Γ, these spaces coincide with that of tangential surface vector fields in $H^{\frac{1}{2}}(\Gamma)$. We denote by $H_\parallel^{-\frac{1}{2}}(\Gamma)$, and $H_\perp^{-\frac{1}{2}}(\Gamma)$ the dual spaces of $H_\parallel^{\frac{1}{2}}(\Gamma)$ and $H_\perp^{\frac{1}{2}}(\Gamma)$, respectively. These dual spaces can be considered as the images of tangential traces of vector fields.

These surface differential operators are used to define the spaces $H_\perp^{-\frac{1}{2}}(\mathrm{curl}_\Gamma, \Gamma)$, and $H_\parallel^{-\frac{1}{2}}(\mathrm{div}_\Gamma, \Gamma)$ introduced in [61] by

$$H_\perp^{-\frac{1}{2}}(\mathrm{curl}_\Gamma, \Gamma) = \{v \in H_\perp^{-\frac{1}{2}}(\Gamma), \mathrm{curl}_\Gamma v \in H^{-\frac{1}{2}}(\Gamma)\},$$

$$H_\parallel^{-\frac{1}{2}}(\mathrm{div}_\Gamma, \Gamma) = \{w \in H_\parallel^{-\frac{1}{2}}(\Gamma), \mathrm{div}_\Gamma w \in H^{-\frac{1}{2}}(\Gamma)\}.$$

Another property in [62, sec. 4] is that $H_\perp^{-\frac{1}{2}}(\mathrm{curl}_\Gamma, \Gamma)$ and $H_\parallel^{-\frac{1}{2}}(\mathrm{div}_\Gamma, \Gamma)$ are dual of each others, when the space of L^2-integrable vector fields $L^2(\Gamma)$ is used as pivot space [75]. According to [60, sec. 3], $H_\perp^{-\frac{1}{2}}(\mathrm{curl}_\Gamma, \Gamma)$, $H_\parallel^{-\frac{1}{2}}(\mathrm{div}_\Gamma 0, \Gamma)$ and $H^{\frac{1}{2}}(\Gamma)$ are the suitable spaces for the Dirichlet data $\gamma_D \cdot$, the Neumann data $\gamma_N \cdot$, and the normal data $\gamma_n \cdot$ respectively, where $H_\parallel^{-\frac{1}{2}}(\mathrm{div}_\Gamma 0, \Gamma) = \mathrm{Ker}(\mathrm{div}_\Gamma, H_\parallel^{-\frac{1}{2}}(\mathrm{div}_\Gamma, \Gamma))$.

3.5.2 Potentials

For any tangential vector field λ on Γ we define the vectorial single-layer potential Ψ_A by

$$\Psi_A(\lambda)(x) = \int_\Gamma \lambda(y) G(x, y) d\Gamma_y, \quad x \notin \Gamma, \tag{3.61}$$

the vectorial Newton-potential

$$N(\lambda)(x) = \int_{\mathbb{R}^3} \lambda(y) G(x,y) dy,$$

and the vectorial double-layer potential

$$\Psi_M(u) = \mathrm{curl}\Psi_A(Ru), \qquad Ru = n \times u. \tag{3.62}$$

Recall that $G(x,y)$ is defined in (1.53), and denote by Ψ_V the scalar single layer potential defined in (1.57).

3.5.3 Boundary Integral Equations

Let $E \in L^2(\mathbb{R}^3)$ with $\mathrm{curl}E \in L^2(\Omega_\pm)$.

Theorem 3.5.1 *If a vector field $E : \Omega_\pm \longrightarrow \mathbb{C}^3$ satisfies*

$$\begin{cases} \mathrm{curlcurl}E &= 0 & in \quad \Omega_\pm, \\ \mathrm{div}E &= 0 & in \quad \Omega_\pm, \\ E(x) &= \mathcal{O}(\frac{1}{|x|}) & as \quad |x| \to \infty, \end{cases}$$

then it satisfies the following transmission formula [60]

$$E = \Psi_M([\gamma_D E]_\Gamma) + \Psi_A([\gamma_N E]_\Gamma) - \mathrm{grad}\Psi_V([\gamma_n E]_\Gamma).$$

Applying the trace operators $\gamma_D \cdot$ to the representation formula leads to the boundary-integral equations. For this reason we define the following operators

$$\begin{aligned} K &= \{\gamma_D \Psi_M\}_\Gamma \quad , \quad V = \{\gamma_D \Psi_A\}_\Gamma, \\ Q &= \{\gamma_D \Psi_V\}_\Gamma. \end{aligned}$$

As the potentials Ψ_A, Ψ_M, and Ψ_V are not necessarily continuous across Γ, it is useful to provide the jump relations (see Appendix A.5).

3.5.4 Equivalent Model of Order 1

3.5.4.1 Integral Equations for E_0

In order to write the integral equation in the case where we have an excitation by J_s, we introduce the Newton potential representing the source term

$$E_s(x) = i\omega\mu \int_{\mathbb{R}^3} J_s(y)G(x,y)dy.$$

It is sufficient to consider the representation formula of E_0 in Ω_+, using Theorem 3.5.1 we state the representation formula as

$$E_0 = -\Psi_M(\gamma_D^+ E_0) - \Psi_A(\gamma_N^+ E_0) - \mathrm{grad}\Psi_v(\gamma_n^+ E_0) + E_s.$$

Applying γ_D^+ to the representation formula, we find for E_0

$$\gamma_D^+ E_0 = \left(\frac{1}{2}\mathbb{I} - K\right)(\gamma_D^+ E_0) - V(\gamma_N^+ E_0) - \mathrm{grad}Q(\gamma_n E_0) + \gamma_D^+ E_s,$$

this equation is set in $H_\perp^{-\frac{1}{2}}(\mathrm{curl}_\Gamma, \Gamma)$ which is the appropriate space for Dirichlet data.

3.5.4.2 Variational Formulation for E_0

We obtain an equivalent variational formulation by testing against function from the dual space of $H_\perp^{-\frac{1}{2}}(\mathrm{curl}_\Gamma, \Gamma)$. The dual space of $H_\perp^{-\frac{1}{2}}(\mathrm{curl}_\Gamma, \Gamma)$ is the space $H_\parallel^{-\frac{1}{2}}(\mathrm{div}_\Gamma, \Gamma)$.
Find $\gamma_N^+ E_0 \in H_\parallel^{-\frac{1}{2}}(\mathrm{div}_\Gamma 0, \Gamma)$, such that

$$\langle V(\gamma_N^+ E_0), B_1\rangle_\Gamma = \langle \gamma_D^+ E_s, B_1\rangle_\Gamma, \tag{3.63}$$

for every $B_1 \in H_\parallel^{-\frac{1}{2}}(\mathrm{div}_\Gamma 0, \Gamma)$.
Since

$$\langle \mathrm{grad}Q(\Phi), v\rangle_\Gamma = 0 \quad \text{for every} \quad v \in H_{||}^{-\frac{1}{2}}(\mathrm{div}_\Gamma 0, \Gamma),$$

[60, eq 7.4]

$$\gamma_D^+ E_0 = 0.$$

3.5.4.3 Galerkin Discretisation

Let $\lambda = \gamma_N^+ E_0$ be the rotated tangential field of the electric field E_0. Conforming boundary element discretisation of (3.63) has to be selected in a finite dimensional subspace H_h of $H_{\|}^{-\frac{1}{2}}(\mathrm{div}_\Gamma 0, \Gamma)$. In fact, the suitable functional space for E_0 is $H(\mathrm{curl}, \Omega)$ which is usually discretised by the edge basis functions. So one may think that rotating these functions by 90° is enough. But because of the divergence constraint, we have to search for a basis function that satisfies $\{\phi_h \in E_h \times n, \mathrm{div}_\Gamma \phi_h = 0\}$ where E_h is a subspace of $H(\mathrm{curl}, \Omega)$. Then the Neumann data λ can be approximated by the space of divergence-free lowest order Raviart-Thomas elements $\mathbf{RT}(\Gamma)$ on Γ [63 ; 76]. If Γ is simply connected, then $\mathbf{RT}(\Gamma)$=$\mathbf{curl}_\Gamma N_1(\Gamma)$, where $N_1(\Gamma)$ is the space of nodal functions of degree 1 [69](see Figure 3.6).

λ is approximated as :

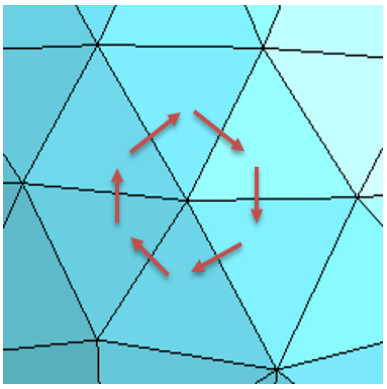

Figure 3.6: Basis function of H_h associated with a vertex

$$\lambda_h = \sum_{i=1}^{N} \lambda^i W^i_{curlN},$$

where N is the number of nodes, the coefficients λ^i's are the values of λ_h at node i, and W^i_{curlN} is the surface rotational operator of the nodal shape function of degree 1 corresponding to the node i.

Applying the Galerkin method, the test functions B_1 should be replaced by the basis functions W^j_{curlN}. We can now state the discretised formulation as:

Find $\lambda^i \in \mathbb{R}^n$, such that

$$\sum_{i=1}^{N} \lambda^i \langle V(W^i_{curlN}), W^j_{curlN} \rangle_\Gamma = \langle \gamma_D^+ E_s, W^j_{curlN} \rangle_\Gamma, \tag{3.64}$$

for $j = 1, .., N$.

The assembly of the linear system of equations is the following:

$$\left[\ M1\ \right]\left[\ \lambda\ \right] = \left[\ S1\ \right],$$

where

$$M1_{ji} = -\int_{\Gamma_j} V(W^i_{curlN})W^j_{curlN}d\Gamma_j,$$

and

$$S1_j = \int_{\Gamma_j} (\gamma_D^+ E_s)\cdot W^j_{curlN}d\Gamma_j.$$

3.5.5 Strong Formulation for E_1

Recall that E_1 satisfies (3.59).

3.5.5.1 Variational Formulation for E_1

Using Theorem 3.5.1, we write the representation formula of E_1 in Ω_+ as

$$E_1 = -\Psi_M(\gamma_D^+ E_1) - \Psi_A(\gamma_N^+ E_1) - \mathrm{grad}\Psi_v(\gamma_n^+ E_1).$$

Applying the Dirichlet trace, we arrive at

$$\gamma_D^+ E_1 = \left(\frac{1}{2}\mathbb{I} - K\right)(\gamma_D^+ E_1) - V(\gamma_N^+ E_1) - \mathrm{grad}Q(\gamma_n E_1). \tag{3.65}$$

By the transmission conditions of the E_1 model (3.59), we can write:

$$\gamma_D^+ E_1 = \frac{K_1}{4}\gamma_N^+ E_0 + K_2\gamma_N^+ E_0. \tag{3.66}$$

Replacing $\gamma_D^+ E_1$ in (3.65) by the formula (3.66) and testing against a function B_1 in $H_{\|}^{-\frac{1}{2}}(\mathrm{div}_\Gamma 0, \Gamma)$, we obtain the variational formulation:
Find $\gamma_N^+ E_1 \in H_{\|}^{-\frac{1}{2}}(\mathrm{div}_\Gamma 0, \Gamma)$, such that

$$\langle V(\gamma_N^+ E_1), B_1\rangle_\Gamma = \langle(-\frac{1}{2}\mathbb{I} - K)(\frac{K_1}{4}\gamma_N^+ E_0 + K_2\gamma_N^+ E_0), B_1\rangle_\Gamma, \tag{3.67}$$

for every $B_1 \in H_{\|}^{-\frac{1}{2}}(\mathrm{div}_\Gamma 0, \Gamma)$.

3.5.5.2 Galerkin Discretisation

Let $\alpha = \gamma_N^+ E_1$, α is approximated as $\alpha_h = \sum_{i=1}^N \alpha^i W^i_{curlN}$ where N is the number of nodes, the coefficients α^i's are the values of α_h at node i. Applying Galerkin Method, we can

state the discretised formulation as:
Find $\alpha^i \in \mathbb{R}^n$, such that

$$\sum_{i=1}^{N} \alpha^i \langle V(W^i_{curlN}), W^j_{curlN}\rangle_\Gamma = \langle(-\frac{1}{2}\mathbb{I} - K)(\frac{K_1}{4}\gamma_N^+ E_0 + K_2\gamma_N^+ E_0), W^j_{curlN}\rangle_\Gamma, \tag{3.68}$$

for $j = 1, ..., N$.
The assembly of the linear system of equations is the following:

$$\left[\ M2\ \right]\left[\ \alpha\ \right] = \left[\ S2\ \right],$$

where

$$M2_{ji} = -\int_{\Gamma_j} V(W^i_{curlN}) W^j_{curlN} d\Gamma_j,$$

and

$$S2_j = \int_{\Gamma_j} (-\frac{1}{2}\mathbb{I} - K)\Big(\frac{K_1}{4}\gamma_N^+ E_0 + K_2\gamma_N^+ E_0\Big) W^j_{curlN} d\Gamma_j.$$

3.5.6 Equivalent Model of Order 2

Recall that E^1_ε satisfies (3.60).

3.5.6.1 Variational Formulation for E^1_ε

For $E^1_\varepsilon \in L^2(\mathbb{R}^3)$, the representation formulas can be given by

$$E^1_\varepsilon \;=\; -\Psi_M(\gamma_D^+ E^1_\varepsilon) - \Psi_A(\gamma_N^+ E^1_\varepsilon) - \mathrm{grad}\Psi_V(\gamma_n^+ E^1_\varepsilon) + E_s \quad \text{in} \quad \Omega_+, \tag{3.69}$$

$$E^1_\varepsilon \;=\; \Psi_M(\gamma_D^- E^1_\varepsilon) + \Psi_A(\gamma_N^- E^1_\varepsilon) + \mathrm{grad}\Psi_V(\gamma_n^- E^1_\varepsilon) \quad \text{in} \quad \Omega_-. \tag{3.70}$$

Applying the Dirichlet trace on (3.69) and (3.70), we get the following integral equations

$$V(\gamma_N^+ E^1_\varepsilon) + (\tfrac{1}{2}\mathbb{I} + K)(\gamma_D^+ E^1_\varepsilon) \;= \gamma_D^+ E_s - \mathrm{grad}_\Gamma Q(\gamma_n^+ E^1_\varepsilon), \tag{3.71}$$

$$-V(\gamma_N^- E^1_\varepsilon) + (\tfrac{1}{2}\mathbb{I} - K)(\gamma_D^- E^1_\varepsilon) \;= \mathrm{grad}_\Gamma Q(\gamma_n^+ E^1_\varepsilon). \tag{3.72}$$

Using the transmission conditions, we obtain the following equalities

$$\gamma_D^+ E^1_\varepsilon = D_0\gamma_N^+ E^1_\varepsilon + D_1\gamma_N^- E^1_\varepsilon, \tag{3.73}$$

$$\gamma_D^- E^1_\varepsilon = -D_1\gamma_N^+ E^1_\varepsilon - D_0\gamma_N^- E^1_\varepsilon, \tag{3.74}$$

where $D_0 = \varepsilon(\frac{K_1}{4} + K_2)$, and $D_1 = \varepsilon(\frac{K_1}{4} - K_2)$.

Substitute the transmission conditions (3.73) and (3.74) in the integral equations (3.71) and (3.72), we find the variational formulation
Find $\gamma_N^+ E_\varepsilon^1, \gamma_N^- E_\varepsilon^1 \in H_{\|}^{-\frac{1}{2}}(\mathrm{div}_\Gamma 0, \Gamma)$, such that

$$\langle (V + \frac{1}{2} D_0 \mathbb{I} + D_0 K)(\gamma_N^+ E_\varepsilon^1), B_1 \rangle_\Gamma + \langle (\frac{1}{2} D_1 \mathbb{I} + D_1 K)(\gamma_N^- E_\varepsilon^1), B_1 \rangle_\Gamma = \langle \gamma_D^+ E_s, B_1 \rangle_\Gamma, \quad (3.75)$$

$$\langle (-\frac{1}{2} D_1 \mathbb{I} + D_1 K)(\gamma_N^+ E_\varepsilon^1), B_2 \rangle_\Gamma + \langle (-V - \frac{1}{2} D_0 \mathbb{I} + D_0 K)(\gamma_N^- E_\varepsilon^1), B_2 \rangle_\Gamma = 0, \quad (3.76)$$

for every $B_1, B_2 \in H_{\|}^{-\frac{1}{2}}(\mathrm{div}_\Gamma 0, \Gamma)$.

3.5.6.2 Galerkin Discretisation

Let $\beta = \gamma_N^+ E_\varepsilon^1$ and $\beta' = \gamma_N^- E_\varepsilon^1$. β and β' are approximated as $\beta_h = \sum_{i=1}^N \beta^i W_{curlN}^i$ and $\beta_h' = \sum_{i=1}^N \beta'^i W_{curlN}^i$ respectively, where N is the number of nodes, the coefficients β^i's and β'^i's are the values of β_h and β_h' respectively at node i. Applying the Galerkin method, we can state the discretised formulation as:
Find $\beta^i, \beta'^i \in \mathbb{R}^n$, such that

$$\sum_{i=1}^N \beta^i \langle (V + \tfrac{1}{2} D_0 \mathbb{I} + D_0 K)(W_{curlN}^i), W_{curlN}^j \rangle_\Gamma + \sum_{i=1}^N \beta'^i \langle (\tfrac{1}{2} D_1 \mathbb{I} + D_1 K)(W_{curlN}^i), W_{curlN}^j \rangle_\Gamma = \langle \gamma_D^+ E_s, W_{curlN}^j \rangle_\Gamma, \quad (3.77)$$

$$\sum_{i=1}^N \beta^i \langle (-\frac{1}{2} D_1 \mathbb{I} + D_1 K)(W_{curlN}^i), W_{curlN}^j \rangle_\Gamma + \sum_{i=1}^N \beta'^i \langle (-V - \frac{1}{2} D_0 \mathbb{I} + D_0 K)(W_{curlN}^i), W_{curlN}^j \rangle_\Gamma = 0. \quad (3.78)$$

The assembly of the linear system of equations:

$$\left[\begin{array}{c|c} M11 & M12 \\ \hline M21 & M22 \end{array}\right] \left[\begin{array}{c} \beta \\ \hline \beta' \end{array}\right] = \left[\begin{array}{c} S1 \\ \hline S2 \end{array}\right],$$

where

$$M11_{ji} = \int_{\Gamma_j} (V + \frac{1}{2} D_0 \mathbb{I} + D_0 K)(W_{curlN}^i) W_{curlN}^j d\Gamma_j,$$

$$M12_{ji} = \int_{\Gamma_j} (\frac{1}{2} D_1 \mathbb{I} + D_1 K)(W_{curlN}^i) W_{curlN}^j d\Gamma_j,$$

$$M21_{ji} = \int_{\Gamma_j} (-\frac{1}{2} D_1 \mathbb{I} + D_1 K)(W^i_{curlN}) W^j_{curlN} d\Gamma_j,$$

$$M22_{ji} = \int_{\Gamma_j} (-V - \frac{1}{2} D_0 \mathbb{I} + D_0 K)(W^i_{curlN}) W^j_{curlN} d\Gamma_j,$$

$$S1_j = \int_{\Gamma_j} (\gamma_D^+ E_s) \cdot W^j_{curlN} d\Gamma_j,$$

and

$$S2_j = \int_{\Gamma_j} (\gamma_N^+ E_s) \cdot W^j_{curlN} d\Gamma_j = 0.$$

3.5.7 Implementation

We implement our model in the platform "MIPSE" of the G2Elab. For actual implementation, we need integral representations for the boundary integral operators.

Proposition 3.5.1 *[69] For $\lambda \in L^\infty(\Gamma)$*

- $V(\lambda) = \{\gamma_D\} \circ \Psi_A(\lambda) = \int_\Gamma \lambda(y) G(x,y) dS(y)$,

- $\tilde{K}(\lambda) = \{\gamma_N\} \circ \Psi_A(\lambda) = \int_\Gamma (\frac{\partial G(x,y)}{\partial n(x)} \lambda(y) - \mathrm{grad}_x G(x,y)(\lambda(y) \cdot n(x))) dS(y)$.

Theorem 3.5.2 *[60] If $Re(k^2) \geq 0$, the boundary operators $\tilde{K}$ and K satisfy*

$$< \tilde{K}\mu, v >_\Gamma = - < \mu, Kv >_\Gamma$$

for every $\mu \in H_{\parallel}^{-\frac{1}{2}}(div_\Gamma 0, \Gamma)$ and $v \in H_{\perp}^{-\frac{1}{2}}(curl_\Gamma, \Gamma)$.

3.6 Numerical Results

In this section, we study the accuracy of the integral equations by considering the problem with PEC (Perfect Electric Conductor) conditions, as well as the validity of the asymptotic expansion. Then we provide many examples to validate our model, examples 1, 2, and 3 satisfy the theoretical condition where closed curved thin layer is considered. Particularly,

example 2 is done to show the robustness of the equivalent models versus the parameter $\tilde{\sigma}$. However, example 4 is provided to show the effectiveness of our model even in open domains that do not satisfy the theoretical condition.

3.6.1 Validation of Integral Equations

To verify the efficiency of the integral equations, we consider the eddy-current problem in a sphere of radius $r_1 = 1$m with PEC boundary conditions. As it is the conditions satisfied by the model of order 1. We compare the numerical solution of the magnetic field to an analytical solution calculated on the arc of radius r_2 1.3m (see Figure 3.7). The curves

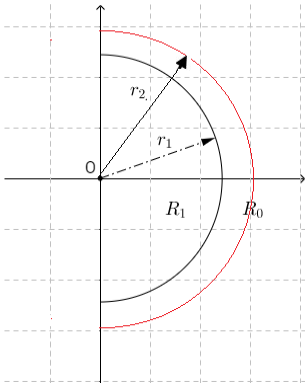

Figure 3.7: A cross section of the domain

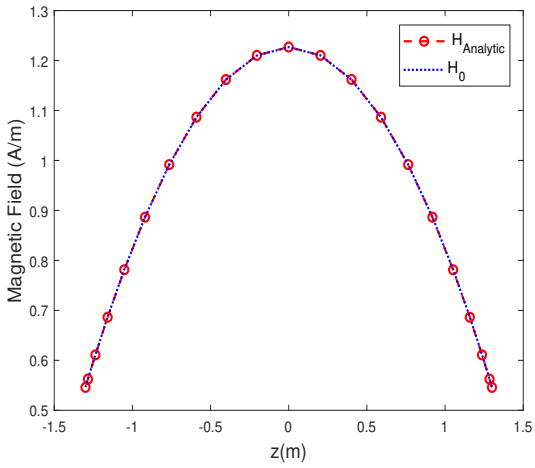

Figure 3.8: The magnetic field H_0 on the arc of radius 1.3m compared to the analytical solution

coincide (see figure 3.8) with L^2-relative error $||H_{analytic} - H_0||_2/||H_{analytic}||_2 = 3.9 \times 10^{-4}$ (where $||U - V||_2 = \sqrt{\sum_i (U_i - V_i)^2}$) which shows a great success of the integral equations.

Details about the calculation of the analytical solution and the postprocessing to calculate the external magnetic field are given in the Appendix A.

3.6.2 Verification of the consistency of H^1_ε with H_0 and $H_0 + \varepsilon H_1$

In order to validate the robustness of the asymptotic expansion and thus the equivalent models, we consider a spherical thin layer with a frequency $f = 10$kHz, and a conductivity $\tilde{\sigma} = 10^3$S/m. In Figure 3.9 we show the relative L^2-error of the solution $H^1_\varepsilon = H_0 + \varepsilon H_1 +$

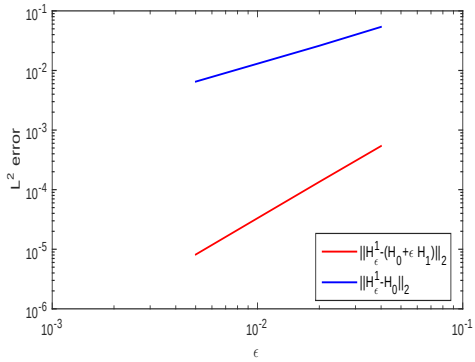

Figure 3.9: L^2 error of the solution H^1_ε with respect to H_0 and $H_0 + \varepsilon H_1$

$\mathcal{O}(\varepsilon^2)$ versus the thickness ε in comparison with the first term of expansion H_0 and $H_0 + \varepsilon H_1$. Comparing H^1_ε and H_0 we can see that the error behaves like ε. Moreover, the error between H^1_ε and $H_0 + \varepsilon H_1$ behaves like ε^2. These error orders validate the consistency of H^1_ε with H_0 and $H_0 + \varepsilon H_1$.

3.6.3 Example 1

We consider a sphere with a radius $0.99m$, surrounded by a conductive sheet of thickness $\varepsilon = 2$cm with $\tilde{\sigma} = 1000$S/m and $f = 1$kHz. The skin depth is $\delta = 0.001$cm and the source is excited by a uniform magnetic field in $\vec{z}$ direction $H^s_0 = 1\vec{z}$ (A/m).

In figure 3.10, we visualize the real and imaginary parts of $\gamma^+ E^1_\varepsilon$ and $\gamma^- E^1_\varepsilon$. We calculate the external magnetic field on an arc of circle at radius 1.3m using a mesh of 384 elements, and we compare the results to the analytical solution. The results are represented in Figure 3.11 that shows a good agreement with L^2-relative error

$$||H_{analytic} - H_0||_2 / ||H_{analytic}||_2 = 0.0047,$$

$$||H_{analytic} - H^1_\varepsilon||_2 / ||H_{analytic}||_2 = 5 \times 10^{-4}.$$

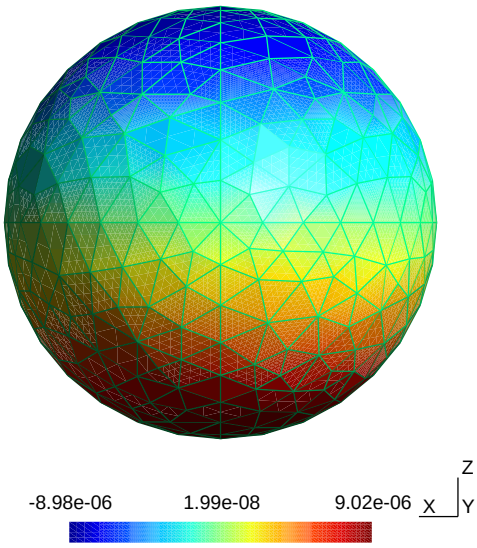

Real part of $\gamma_N^- E_\varepsilon^1$.

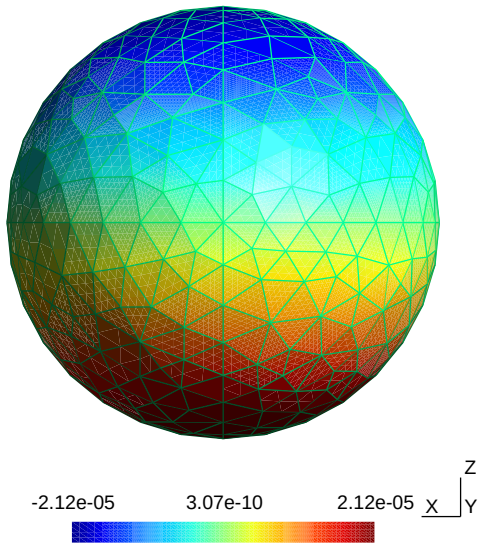

Imaginary part of $\gamma_N^- E_\varepsilon^1$.

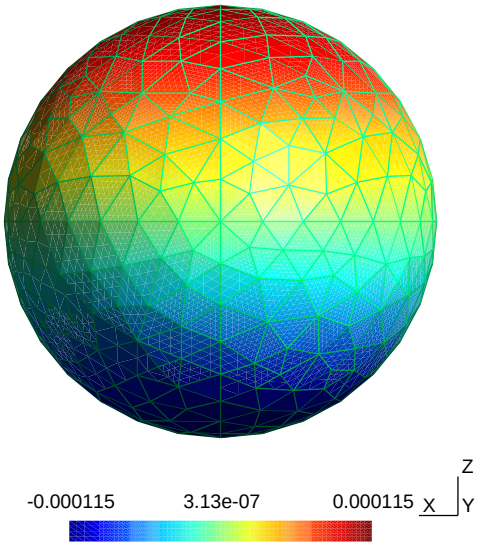

Real part of $\gamma_N^+ E_\varepsilon^1$.

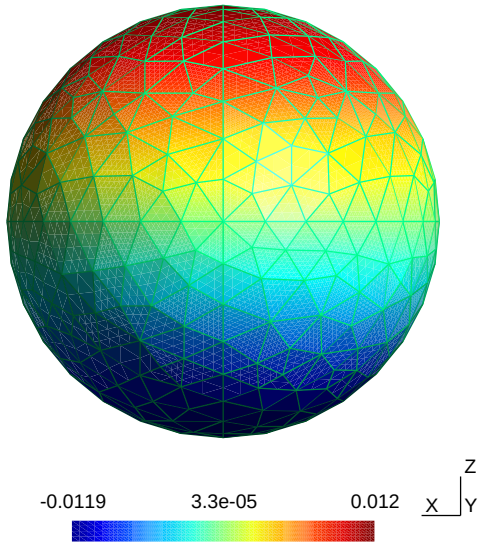

Imaginary part of $\gamma_N^+ E_\varepsilon^1$.

Figure 3.10: The real and imaginary part $\gamma^+ E_\varepsilon^1$ and $\gamma^- E_\varepsilon^1$ for a spherical thin layer of radius 0.99m and thickness 0.02m.

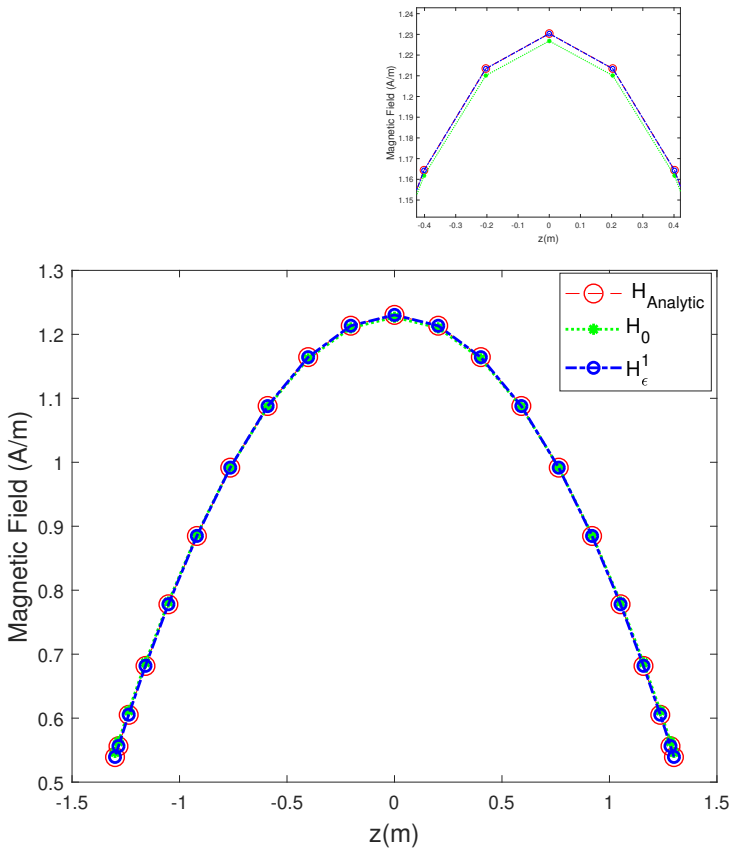

Figure 3.11: The magnetic fields H_0 and H_ε^1 on the arc of radius 1.3m compared to the analytical solution.

We calculate the internal magnetic field on an arc of circle at radius $0.7m$ in order to study the influence of the thin layer on the interior domain i.e. to validate the effect of the thin conductive layer on the interior domain. We compare the results to the analytical solution. These results are represented in Figure 3.12 which affirm the shielding function required by the thin layer with error

$$||H_{analytic} - H_\varepsilon^1||_2/||H_{analytic}||_2 = 6 \times 10^{-2}.$$

3.6.4 Example 2

The aim of this example is to show the robustness of the equivalent models versus the parameter $\tilde{\sigma}$. Fixing the frequency $f = 10$kHz and the radius of the sphere $r = 0.98$m surrounded by a conductive sheet of thickness $\varepsilon = 4$cm, the skin depth is a function of $\tilde{\sigma}$, and the source is a uniform magnetic field $H_0^s = 1\vec{z}$(A/m).

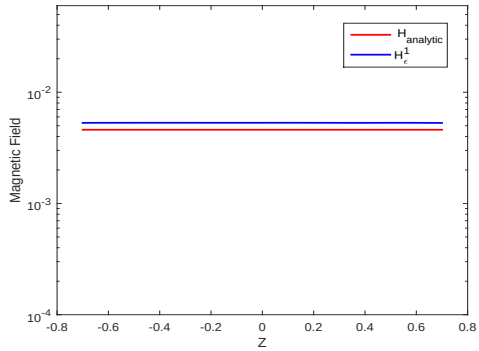

Figure 3.12: The magnetic fields $H_{analytic}$ and H^1_ε in the interior domain of the sphere.

Similarly the error is calculated on an arc of circle at a radius 1.3m. In Figure 3.13 we show the relative L^2 errors of the solutions H_0 and H^1_ε of the equivalent models of order 1 and 2 versus the parameter $\tilde{\sigma}$. The equivalent model of order 1 shows a good

Figure 3.13: Relative L^2 errors of the solutions H_0 and H^1_ε of the equivalent models of order 1 and 2 versus the parameter $\tilde{\sigma}$ for $\varepsilon = 4$cm

agreement, we observe a small error in a wide range of skin depths, the interval where the skin depths is small compared to ε or of the same order, this result corresponds to the theoretical assumption. The same interpretation is observed after the correction by H_1, smaller errors are obtained in the region of small skin depth. This result can be explained by the direct dependence of H_1 on H_0, and the theoretical assumptions. The equivalent model of order 2 gives few errors for all ranges of the skin depth, from very small to very large.

3.6.5 Example 3

Here, we consider a spherical conductive thin sheet of thickness 1cm, radius 1m, conductivity $\tilde{\sigma} = 55\text{S/m}$, and permeability μ_0. The source current is excited by a cylindrical coil of radius 1.5m, height 2m, thickness 1cm, and current 1A (see Figure 3.14).

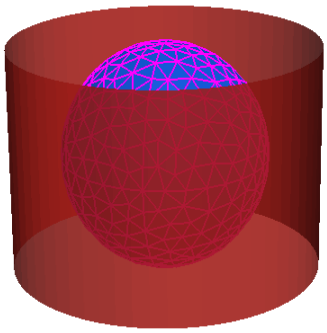

Figure 3.14: A spherical thin sheet with a cylindrical Coil

This problem has been solved using the two equivalent models of order 1 and 2, in Figures 3.15 and 3.16 we visualize the real and the imaginary part of the solution $\gamma_N^+ E_\varepsilon^1$ of the integral equations, respectively. In the Figures 3.17, 3.19, 3.18 and 3.20, we trace

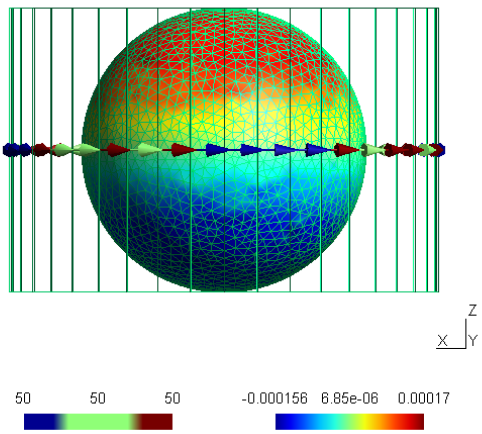

Figure 3.15: The real part of $\gamma_N^+ E_\varepsilon^1$

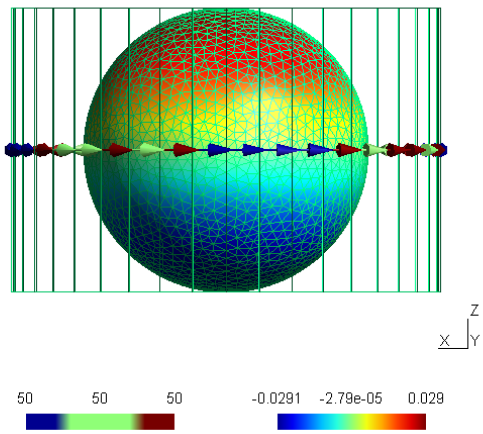

Figure 3.16: The imaginary part of $\gamma_N^+ E_\varepsilon^1$

the x and z components of magnetic fields calculated on the segment that connect the two points $(1.1, 0, -1)$ and $(1.1, 0, +1)$. In Figures 3.17 and 3.19, the model of order 1 is compared to the simulation performed by Comsol in 2D axisymmetry H_{Comsol}, where the

results obtained by the model of order 2 are shown in Figures 3.18 and 3.20.

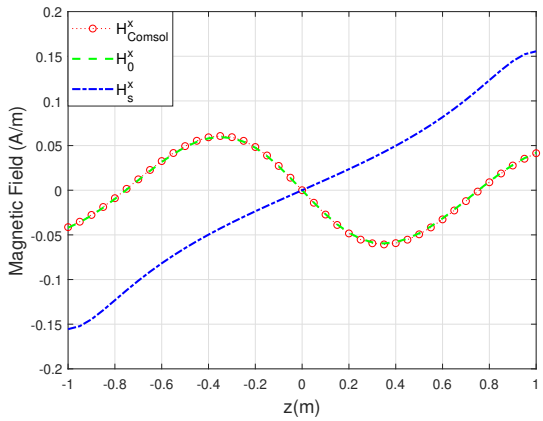

Figure 3.17: The x component of H_0, H_{Comsol}, and the source field H_s.

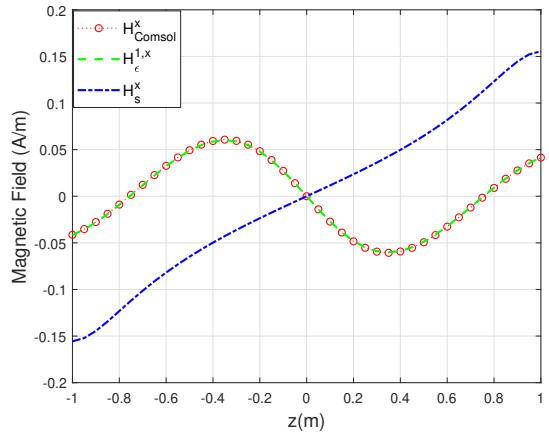

Figure 3.18: The x component of H^1_ε, H_{Comsol}, and the source field H_s.

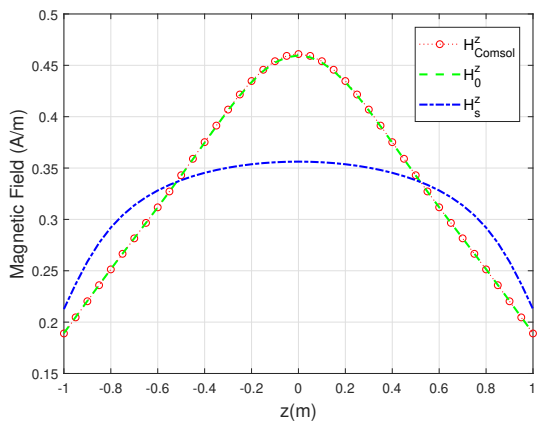

Figure 3.19: The z component of H_0, H_{Comsol}, and the source field H_s.

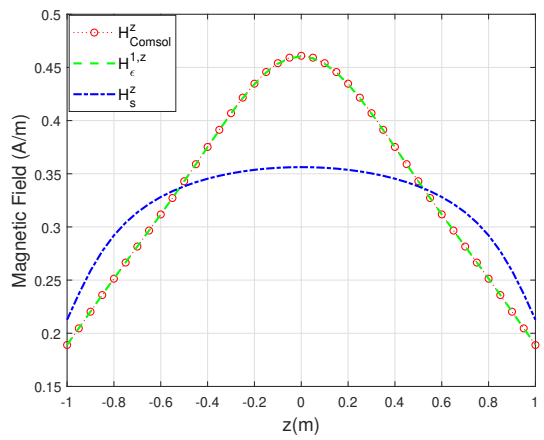

Figure 3.20: The z component of H^1_ε, H_{Comsol}, and the source field H_s.

Comparing the L^2-relative errors calculated on the same segment in Table 3.1, we validate the efficiency of the two models, in addition to the better accuracy obtained using the model of second order.

Table 3.1: L^2-relative errors of H_0 and H^1_ε

$\frac{\|\|H_{Comsol}-H_0\|\|_2}{\|\|H_{Comsol}\|\|_2}$	$\frac{\|\|H_{Comsol}-H^1_\varepsilon\|\|_2}{\|\|H_{Comsol}\|\|_2}$
0.0021	0.0008

3.6.6 Example 4

In this example we provide an open boundary problem which does not satisfy the theoretical assumption, i.e. the surface of the thin layer is not simply connected. We consider a cylinder of $r = 1$m, $h = 3$m and thickness 2cm. The source is excited by a spire of radius $R = 1.1$m and a current of 10A. We compute the norm of the magnetic field on a segment that connect the two points $(1.3, 0, -2)$ and $(1.3, 0, +2)$ (see Fig.3.22) and we compare the results to the 2D axisymmetric formulation in Comsol that is discretised using the Finite Element Method (see Figure 3.21). Note that, discretising using the FEM requires a very fine mesh near the surface of the thin layer and the maximum size of the local element must not exceed $\delta/2$ in order to accurately describe well the flow of current near the surface.

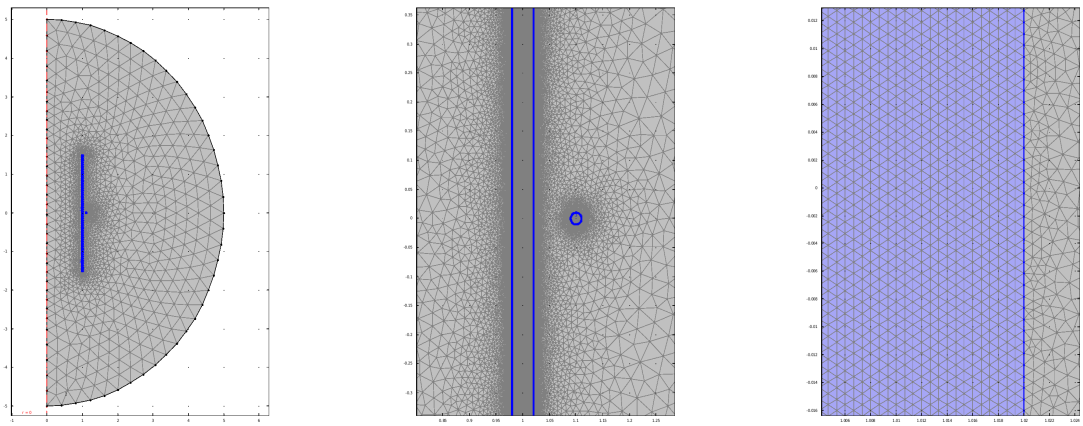

Figure 3.21: Meshing the domain in Comsol

Figure 3.23 shows the magnetic fields H_0 and H^1_ε and the solution obtained by Comsol H_{com} on the segment. The corresponding L^2-relative errors are reported in Table 3.2 and we observe that the model of order 2 still works well, that improves the effectiveness of the second order model even in open domains. In Table 3.3 we compare the computational time and the number of elements of the mesh used by each method, we deduce that the boundary element method may reduce the computational time as it needs a reduced number of elements for the discretisation, note that the error is less than 5% with a mesh of 816 elements. The obtained results will be more important if we compare with the same problem using a 3D discretisation.

The errors obtained are strongly lower than the amplitude of the components of the reaction magnetic fields, see Figure 3.24 for the x-component and see Figure 3.25 for the

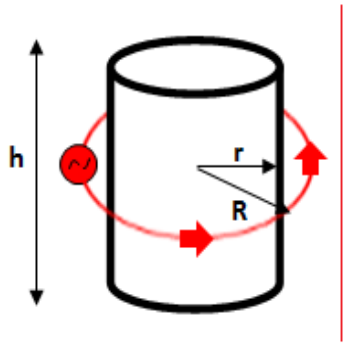

Figure 3.22: A cylindrical thin layer with an exterior spire

z-component. This seems to indicate that, in this configuration, no particular care has to be taken, even if the surface is not simply connected.

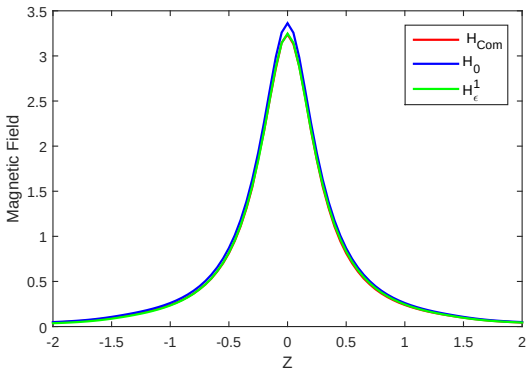

Figure 3.23: The magnetic fields H_0 and H_ε^1 on the segment compared to Comsol (H_{com})

$\frac{\|\|H_{ref}-H_0\|\|_2}{\|\|H_{ref}\|\|_2}$	$\frac{\|\|H_{ref}-H_\varepsilon^1\|\|_2}{\|\|H_{ref}\|\|_2}$
0.045	0.008

Table 3.2: L^∞-errors of H_0 and H_ε^1

Table 3.3: Computational time of our models comparing with Comsol

	Nb of elements	**Time**
Comsol	1771542	132s
Model Order 1	544	25s
Model Order 2	544	56s

3.7 Conclusion

A second order equivalent model for eddy current problems with a thin layer in $3D$ is proposed and discretised using the Boundary Element Method. The model is validated

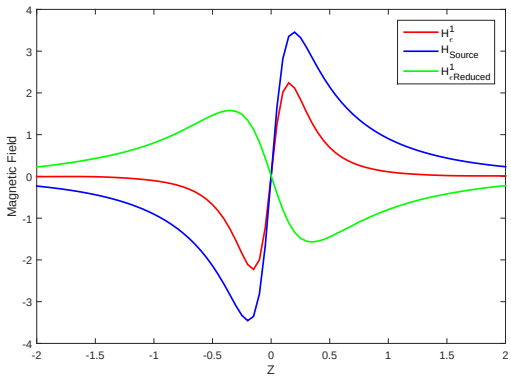

Figure 3.24: The $x-$component of the real part of the total magnetic fields H^1_ε, the reduced magnetic fields $H^1_{\varepsilon Reduced}$ and the source field H_{Source}.

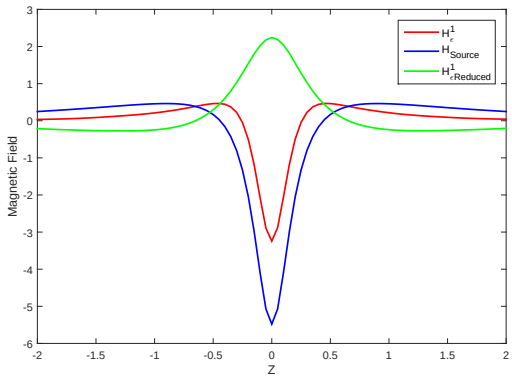

Figure 3.25: The $z-$component of the real part of the total magnetic fields H^1_ε, the reduced magnetic fields $H^1_{\varepsilon Reduced}$ and the source field H_{Source}.

and shows a good agreement with reference results. The discretisation method shows a great success in the accuracy of results and in reducing the computational time.

CHAPTER 4

Homogenisation and boundary correction of laminar stacks in vector potential formulation.

Contents

4.1 Mathematical Formulation **86**

4.2 Procedure **88**

4.3 The 1D model problem **88**

4.3.1 Expansion of $\mathcal{M}^\varepsilon$ 89

4.3.2 Classical homogenisation of the laminar stacks in Ω_L 89

4.3.3 Numerical validation in Ω_L 91

4.3.4 Accounting of the interface 92

4.3.5 Numerical validation in Ω 94

4.4 The 2D model problem **95**

4.4.1 Expansion of $\mathcal{M}^\varepsilon$ 96

4.4.2 Classical homogenisation of the laminar stacks in Ω_L 96

4.4.3 Recombination of the results 100

4.4.4 Numerical results 100

4.5 Conclusion **101**

Many electrical equipments such as motors or transformers use lamination stacks to form the core of coils. These laminated cores are commonly used in order to reduce the eddy current losses, as it increase resistivity in the direction the current would flow. The simulation of these lamination stacks requires many elements and leads to a large system of equations, mostly when the skin depth is smaller or equal to the thickness of one sheet. A homogenisation method is proposed here for an efficient numerical modeling of the laminated sheets in eddy-current problems.

In the last few decades, these laminated cores have been modeled by one solid medium to save computational costs [92]. In this case, the laminated cores have been modeled as a homogeneous medium, indeed, but not always neglecting the eddy currents. This is only the case if this homogeneous block is considered as non-conducting without equivalent complex permeability and conductivity. In order to consider the eddy current losses inside the laminated cores, this lamination is modeled by a homogeneous medium with conductivity and permeability calculated by the analytical solution of the magnetic field inside the sheet [98–100]. The resulting complex permeability are then embedded in either an integral formulation [99] or a differential formulation [98 ; 100].

Many papers have provided approximate formulas for eddy-current losses by means of a posteriori computations. These formulas are given for either low frequencies [94 ; 97] where the thickness of a sheet is greater than the skin depth or high frequencies [95 ; 96]. Starting from these formulas, an equivalent electric conductivity has been provided in [93] permitting to replace the laminated cores with a homogeneous isotropic or anisotropic medium.

A two-scale finite element method based on the magnetic vector potential A has been developed to describe eddy currents in laminar stacks with linear materials [87]- [89], and non-linear materials [86]. In [90], some multiscale finite-element formulations for the eddy current problem in laminated iron in 2D are introduced. They provide multiscale formulations based on the magnetic vector potential, the single component current vector potential and on a mixed formulation of the magnetic vector potential and the current density. They considered the case where the main magnetic flux is parallel to the laminates and assumed to be perpendicular to the plane of projection to study the performance

of multiscale finite element formulations.

In [106], a time-domain homogenisation technique for laminated iron cores in 3D finite element models in terms of the magnetic vector potential was proposed. This approach based on an approximate 1D solution in the time domain is applicable to linear and non-linear materials. The time-domain homogenisation is also adopted in [103] where the net current feature is added. The homogenisation approach presented is based on a finite element model in terms of the magnetic vector potential and the expansion of the induction throughout the lamination thickness using a set of basis functions.

Another finite element computational homogenisation for modeling non-linear multiscale materials in 2D magnetostatics and magnetodynamics problems are presented in [105] and [104] respectively. In these papers, the modeling of the laminated cores is based on heterogeneous multiscale method (HMM) which is based on the transformation of information between macroscale problem, microscale problem, and mesoscale problems.

In the presence of conductive laminar sheets, the fields oscillate strongly. The classical homogenisation [88] is an efficient method to simplify the numerical simulation of such periodic heterogeneous materials, as it leads to an equivalent equation that is generally simpler and describes the behavior of the solution. In fact, the classical homogenisation is an asymptotic homogenisation proceeds by introducing the fast variable and posing a formal expansion. Thus, the formal two-scale expansion considered in chapter 3 to study the behavior of the field in a conductive thin layer will be also adopted to model the lamination stacks.

In this chapter, we present an effective model of a lamination stack using a classical homogenisation approach (section 4.3.2) and a correction for the interface between the air and the lamination stack (section 4.3.4). We consider the case where the skin depth is kept less than or equal to the thickness of one metal sheet.

4.1 Mathematical Formulation

Consider a lamination stack composed of insulating and metal sheets of permeability μ_0 and μ_1, and conductivity $\sigma_0 = 0$ and σ_1 respectively. The thickness of one metal sheet and an insulating sheet together is ε, which is small compared with the whole domain Ω (see Fig. 4.1). We consider also that the thickness of an insulating sheet is negligible compared with the metal sheet.

For simplicity, we consider $\Omega = (-1, 1) \times [0, 1)$, the air is the interval $\Omega_A = (-1, 0) \times [0, 1)$, and the laminar stack domain is $\Omega_L = (0, 1) \times [0, 1)$. Let Γ be the interface between the air region and the lamination stacks.

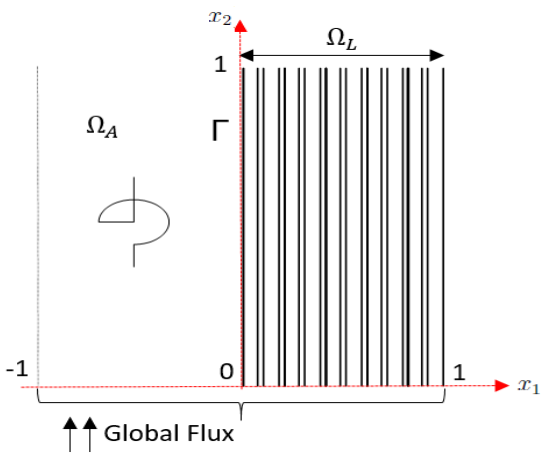

Figure 4.1: Representation of the whole domain Ω which consists of an air domain Ω_A and a lamination stack Ω_L. A global magnetic flux and a current source will be enforced.

In this problem, we consider electrically isolated sheets. They are isolated from any exterior circuit, and each sheet is isolated from the others. We thus express the conservation of the current, and the global net current is zero.

The formulation of the magnetic potential in the air region is:

$$\Delta A_\varepsilon = \mu_0 J_s, \qquad \text{in } \Omega_A. \tag{4.1}$$

In each sheet i, the magnetic potential can be written as the sum $A_\varepsilon + A_i$, where $A_i = \mathcal{M}^\varepsilon(A_\varepsilon)$ is a constant related to the sheet i [91]. Using this fact, the formulation of the

magnetic potential in Ω_L can be written as

$$\Delta A_\varepsilon - i\omega\sigma_1\mu_1(A_\varepsilon - \mathcal{M}^\varepsilon(A_\varepsilon)) = 0, \qquad \text{in } \Omega_L, \tag{4.2}$$

where $\mathcal{M}^\varepsilon$ is an average operator in each sheet defined by

$$\mathcal{M}^\varepsilon(f) : (x_1, x_2) \to \frac{1}{\varepsilon}\int_0^1 \int_{\varepsilon\lfloor x_1/\varepsilon\rfloor}^{\varepsilon\lfloor x_1/\varepsilon\rfloor+\varepsilon} f(s,y)dsdx_2, \qquad \forall f \in C(\Omega). \tag{4.3}$$

Note that $\lfloor\cdot\rfloor$ is the floor function.
This constant (4.3) in each sheet is chosen to ensure the continuity of A_ε between all the interfaces of the sheets, i.e. on both sides of the sheet. As well as the continuity of its Neumann trace related to the tangential magnetic field between two layers.

A global magnetic flux is enforced on the whole domain in a manner that the total flux in the domain is zero, that is to say what enters from the bottom get out of the top. It will be expressed by the following boundary conditions:

$$A_\varepsilon|_{x_1=-1} = g(x_2), \qquad A_\varepsilon|_{x_1=1} = h(x_2), \tag{4.4}$$

$$\partial_{x_2}A_\varepsilon|_{x_2=0} = \partial_{x_2}A_\varepsilon|_{x_2=1} = 0. \tag{4.5}$$

In addition, we have also to take into account the continuity condition at the interface between the lamination stack and the air Γ

$$\frac{1}{\mu_0}\frac{\partial A_\varepsilon}{\partial n}|_{\Gamma^-} = \frac{1}{\mu_1}\frac{\partial A_\varepsilon}{\partial n}|_{\Gamma^+}, \tag{4.6}$$

$$A_\varepsilon|_{\Gamma^-} = A_\varepsilon|_{\Gamma^+}. \tag{4.7}$$

We are interested in the case where the skin depth is smaller or equal to the thickness ε. Because we will study the limit case ($\varepsilon \to 0$), we should assume an explicit dependence of the layer conductivity σ_1 on ε

$$\sigma_1\mu_1 = \varepsilon^{-2}\bar{\alpha}, \tag{4.8}$$

where $\bar{\alpha}$ is a constant, that enables δ/ε to remain constant when ε goes to zero (the same assumption as in Chapter 3).

4.2 Procedure

Our methodology is based on two points:

- Applying the classical 2-scale homogenisation method in the domain of lamination stacks Ω_L.
- Studying the influence of the interface Γ on the vector potential to treat the problem in the whole domain Ω.

The derivation of the asymptotic terms in Ω_L is based on:

1. The expansion of $\mathcal{M}^\varepsilon$ for any function a of $\Omega \times \mathbb{R}/\mathbb{Z}$.
2. A standard formal 2-scale expansion for A_ε.
3. Identifying the terms of same powers of ε in the governing PDE.

In order to validate the possibility of adopting this methodology to model the lamination stacks, we will start by a 1D problem then we proceed in 2D.

4.3 The 1D model problem

The magnetic vector potential satisfies (in a 1D assumption we simply denote $x = x_1$):

$$\partial_x^2 A_\varepsilon = 0, \qquad \text{in } \Omega_A, \tag{4.9}$$

$$\partial_x^2 A_\varepsilon - i\omega\sigma_1\mu_1(A_\varepsilon - \mathcal{M}^\varepsilon(A_\varepsilon)) = 0, \qquad \text{in } \Omega_L, \tag{4.10}$$

where $\mathcal{M}^\varepsilon$ is an average operator in each sheet defined by

$$\mathcal{M}^\varepsilon(f) : x \to \frac{1}{\varepsilon}\int_{\varepsilon\lfloor x/\varepsilon\rfloor}^{\varepsilon\lfloor x/\varepsilon\rfloor+\varepsilon} f(s)ds, \qquad \forall f \in C(\Omega), x \in (0,1). \tag{4.11}$$

A global flux is enforced on the whole domain and expressed by the boundary conditions

$$A_\varepsilon|_{x=-1} = 0, \qquad A_\varepsilon|_{x=1} = 1. \tag{4.12}$$

Moreover, we have the continuity condition at the interface

$$\frac{1}{\mu_0}\partial_x A_\varepsilon|_{x=0^-} = \frac{1}{\mu_1}\partial_x A_\varepsilon|_{x=0^+}. \tag{4.13}$$

4.3.1 Expansion of $\mathcal{M}^\varepsilon$

By changing of variable in (4.11), we observe that

$$\mathcal{M}^\varepsilon(f)(x) = \int_0^1 f(\varepsilon\lfloor x/\varepsilon\rfloor + \varepsilon y)dy, \ \ \forall f \in C(\Omega). \tag{4.14}$$

Therefore the function f has the following expansion with respect to ε

$$\begin{aligned} f(\varepsilon\lfloor x/\varepsilon\rfloor + \varepsilon y) =& f(x) + \varepsilon\Big(\frac{1}{2} - \frac{x-\varepsilon\lfloor x/\varepsilon\rfloor}{\varepsilon}\Big)\partial_x f(x) + \varepsilon^2\Big(\frac{1}{3} \\ &- \frac{x-\varepsilon\lfloor x/\varepsilon\rfloor}{\varepsilon}\Big(1 - \frac{x-\varepsilon\lfloor x/\varepsilon\rfloor}{\varepsilon}\Big)\Big)\partial_x^2 f(x) + ... \end{aligned} \tag{4.15}$$

Now we can observe that for any function a defined on $\Omega \times \mathbb{R}/\mathbb{Z}$ one has

$$\mathcal{M}^\varepsilon(a)(x) = \int_0^1 a(x,s)ds + \varepsilon\int_0^1 \Big(\frac{1}{2} - \frac{x-\varepsilon\lfloor x/\varepsilon\rfloor}{\varepsilon}\Big)\partial_x a(x,s)ds + ... \tag{4.16}$$

Therefore one can define the sequence of operators $(\mathfrak{M}_i)_{i\in\mathbb{N}}$ defined on the space of functions of $\Omega \times \mathbb{R}/\mathbb{Z}$ such that

$$\mathfrak{M}_0(a)(x,y) = \int_0^1 a(x,s)ds, \tag{4.17}$$

$$\mathfrak{M}_1(a)(x,y) = (\frac{1}{2} - y)\int_0^1 \partial_x a(x,s)ds, \tag{4.18}$$

$$\mathfrak{M}_2(a)(x,y) = (\frac{1}{3} - y(1-y))\int_0^1 \partial_x^2 a(x,s)ds. \tag{4.19}$$

The operators $(\mathfrak{M}_i)_{i\in\mathbb{N}}$ satisfy for any function of $\Omega \times \mathbb{R}/\mathbb{Z}$

$$\mathbf{M}^\varepsilon(a(\cdot,\cdot/\varepsilon))(x) = \mathfrak{M}_0(a)(x,x/\varepsilon) + \varepsilon\mathfrak{M}_1(a)(x,x/\varepsilon) + \varepsilon^2\mathfrak{M}_2(a)(x,x/\varepsilon) + .., \tag{4.20}$$

for all $x \in \Omega$.

4.3.2 Classical homogenisation of the laminar stacks in Ω_L

The problem (4.10)-(4.12) in Ω_L can be reformulated by the following

$$\partial_x^2 A_\varepsilon - \frac{i\omega\bar{\alpha}}{\varepsilon^2}(A_\varepsilon - \mathcal{M}^\varepsilon(A_\varepsilon)) = 0, \tag{4.21}$$

$$A_\varepsilon|_{x=0} = 0, \qquad A_\varepsilon|_{x=1} = 1. \tag{4.22}$$

As standard in classical asymptotic homogenisation assumes that A_ε has the following 2-scale expansion:

$$A_\varepsilon(x) = A_0(x, x/\varepsilon) + \varepsilon A_1(x, x/\varepsilon) + \varepsilon^2 A_2(x, x/\varepsilon) + ..., \tag{4.23}$$

where $A_i(x, y)$ are assumed to be 1-periodic with respect to the y variable.
Note that each term of the expansion depends on both the slow variable $x = x_1$ and the fast variable $y = x/\varepsilon$.

Replacing (4.23) in (4.21), we obtain (see the Appendix B.1.1)

$$\begin{aligned}(4.21) :&\partial_x^2 A_0 + \varepsilon^{-2}\partial_y^2 A_0 + 2\varepsilon^{-1}\partial_{yx}^2 A_0 + \varepsilon\partial_x^2 A_1 + \varepsilon^{-1}\partial_y^2 A_1 + 2\partial_{yx}^2 A_1 + \varepsilon^2\partial_x^2 A_2 \\ &+ \partial_y^2 A_2 + 2\varepsilon\partial_{yx}^2 A_2 - i\omega\frac{\bar{\alpha}}{\varepsilon^2}\Big(A_0 + \varepsilon A_1 + \varepsilon^2 A_2 - \mathfrak{M}_0(A_0) - \varepsilon\mathfrak{M}_1(A_0) - \varepsilon^2\mathfrak{M}_2(A_0) \\ &- \varepsilon\mathfrak{M}_0(A_1) - \varepsilon^2\mathfrak{M}_1(A_1) - \varepsilon^3\mathfrak{M}_2(A_1) - \varepsilon^2\mathfrak{M}_0(A_2) - \varepsilon^3\mathfrak{M}_1(A_2) - \varepsilon^4\mathfrak{M}_2(A_2)\Big) = 0.\end{aligned} \tag{4.24}$$

Identifying the terms of same order in powers of ε, the expansion (4.23) leads to the following

- Order ε^{-2}: we have

$$\partial_y^2 A_0 - i\omega\bar{\alpha}(A_0 - \mathfrak{M}_0(A_0)) = 0, \ \ \forall(x, y) \in \Omega \times \mathbb{R}/\mathbb{Z} \tag{4.25}$$

  Using the assumption that $A_0(x, \cdot)$ is 1-periodic, the solution A_0 is a constant function with respect to y but it may depend on x (see the appendix B.1.2)

$$A_0(x, y) = A_0(x). \tag{4.26}$$

- Order ε^{-1}: we have

$$\partial_y^2 A_1 + \partial_y\partial_x A_0 - i\omega\bar{\alpha}(A_1 - \mathfrak{M}_1(A_0) - \mathfrak{M}_0(A_1)) = 0, \tag{4.27}$$

  using (4.26), we get

$$\partial_y^2 A_1 - i\omega\bar{\alpha}(A_1 - \mathfrak{M}_0(A_1)) = -i\omega\bar{\alpha}(\mathfrak{M}_1(A_0)), \tag{4.28}$$

then,

$$\partial_y^2 A_1 - i\omega\bar{\alpha}(A_1 - \mathfrak{M}_0(A_1)) = i\omega\bar{\alpha}(y - \frac{1}{2})\partial_x A_0. \tag{4.29}$$

We call W a periodic function (unique up to an additive constant) solution of

$$\partial_y^2 W - i\omega\bar{\alpha}(W - \mathfrak{M}_0(W)) = i\omega\bar{\alpha}(y - \frac{1}{2}), \tag{4.30}$$

and deduce by linearity that

$$A_1(x, y) = W(y)\partial_x A_0(x). \tag{4.31}$$

The solution of (4.30) in a unit cell is

$$W(y) = \left(\frac{1}{2} - y\right) + \frac{1}{2}\frac{\sinh(\kappa(y - 1/2))}{\sinh(\kappa/2)}, \tag{4.32}$$

where $\kappa^2 = i\omega\bar{\alpha}$.

- Order ε^0: we have

$$\partial_y^2 A_2 - i\omega\bar{\alpha}(A_2 - \mathfrak{M}_0(A_2)) = -\partial_x^2 A_0 - 2\partial_x\partial_y A_1 + i\omega\bar{\alpha}(\mathfrak{M}_2(A_0) + \mathfrak{M}_1(A_1)) \tag{4.33}$$

Integrating (4.33) on $y \in (0, 1)$, we get (see the appendix B.1.3)

$$\left(-1 + \frac{i\omega\bar{\alpha}}{6}\right)\partial_x^2 A_0 = 0. \tag{4.34}$$

The solution of (4.34) considering the boundary condition (4.22) is

$$A_0(x) = x. \tag{4.35}$$

For clarity, we denote by $A_\varepsilon^k = A_0 + \varepsilon A_1 + ... + \varepsilon^k A_k$.
Using (4.23), (4.31), and (4.35), the magnetic vector potential in the lamination stack can be written as

$$A_\varepsilon^1(x) = A_0(x) + \varepsilon W(y)\partial_x A_0(x), \tag{4.36}$$

$$A_\varepsilon^1(x) = x + \varepsilon W(y). \tag{4.37}$$

4.3.3 Numerical validation in Ω_L

We consider $\varepsilon = 0.1$ (10 toles), $\bar{\alpha} = 1$. We show in Figs. 4.2 and 4.3 the magnetic vector potential expansion $A_\varepsilon^1(x) = A_0(x) + \varepsilon W(y)\partial_x A_0(x)$, the first term of the expansion $A_0(x)$, and the magnetic potential $A_{Analytic}$ calculated analytically (see the appendix B.1.4), for

different frequencies. The results show a good agreement as the curves coincides, and their relative error is given in Table 4.1:.

ω	$\|\|A_{analytic} - A^1_\varepsilon\|\|_2$
50	0.0398
10^3	0.0183

Table 4.1: Relative L^2-errors of the solution A^1_ε for several ω.

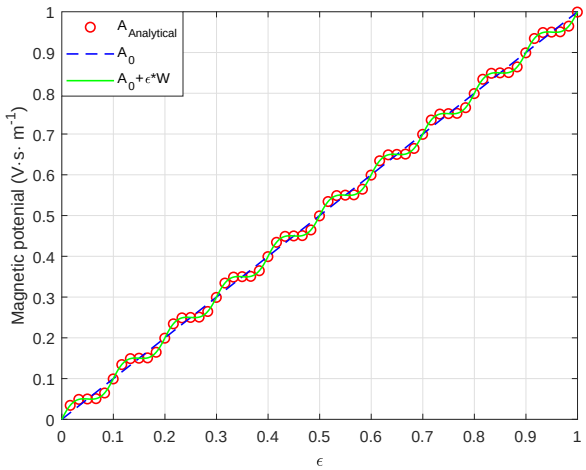

Figure 4.2: The magnetic vector potential in Ω_L for $\omega = 50$.

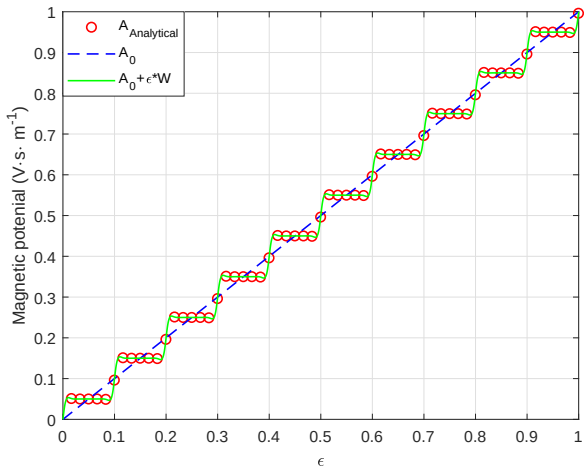

Figure 4.3: The magnetic vector potential in Ω_L for $\omega = 10^3$.

The relative L^2-errors

$$\frac{||A_{analytic} - A^1_\varepsilon||_2}{||A_{analytic}||_2}$$

are shown in Fig. (4.4) versus the thickness ε, for $\omega = 800$. The result shows a convergence of $\mathcal{O}(\varepsilon)$ as expected by the 2-scale expansion.

4.3.4 Accounting of the interface

Recall that the magnetic potential in Ω satisfies (4.9-4.13).
Considering the coupling between the air and the lamination stack, we are seeking for an expansion such as:

$$A_\varepsilon(x) = A_0^-(x) + \varepsilon K^-(x/\varepsilon)\partial_x A_0^-(x) + ..., \text{ in } \Omega_A \tag{4.38}$$

$$A_\varepsilon(x) = A_0^+(x) + \varepsilon K^+(x/\varepsilon)\partial_x A_0^+(x) + ... \text{ in } \Omega_L \tag{4.39}$$

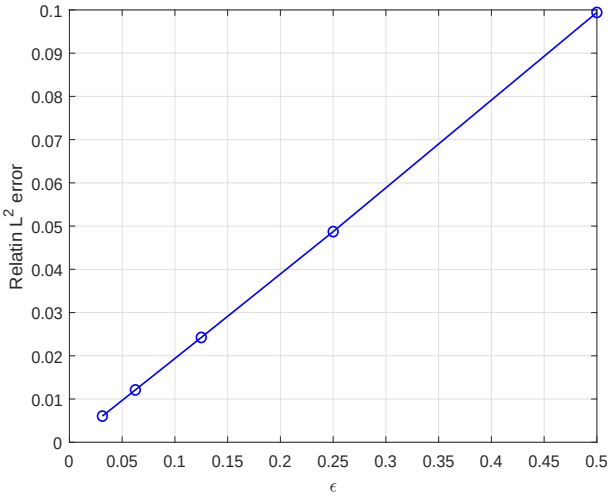

Figure 4.4: Relative L^2-errors of the solution A^1_ε versus the thickness ε.

Knowing that in the presence of infinite thin sheets, the effect of the interface with air will decrease as we go far from Γ. Consequently, K must behave like $x \mapsto W(\frac{x}{\varepsilon} - \lfloor \frac{x}{\varepsilon} \rfloor)$ at ∞, as it can be deduced from (4.36).

Note that we do not know the problem satisfied by A_0^- and A_0^+. We just know that they are harmonic, should satisfy the boundary conditions at $x = -1$, $x = 1$, and the continuity and Neumann conditions at the interface.

Using the fact that $W(0) = 0$, we get that

$$A^1_\varepsilon(x) = \begin{cases} A_0^-(x), \text{if } x \in \Omega_A \\ A_0^+(x) + \varepsilon W(x/\varepsilon)\partial_x A_0^+(x), \text{if } x \in \Omega_L \end{cases} \tag{4.40}$$

is continuous and satisfies

$$\partial_x^2 A^1_\varepsilon - \frac{i\omega\bar{\alpha}}{\varepsilon^2}(A^1_\varepsilon - \mathcal{M}^\varepsilon(A^1_\varepsilon)) = o(\varepsilon). \tag{4.41}$$

Thus, we simply have to adjust the Neumann condition at $x = 0$ to adopt the approximation (4.40)

$$\frac{1}{\mu_0}\partial_x A_0^-(0) = \frac{(1 + \partial_y W(0))}{\mu_1}\partial_x A_0^+(0). \tag{4.42}$$

This condition combined to the conditions defines A_0^- and A_0^+ (4.9), (4.12), (4.34) and the continuity condition at the interface put up the following system

$$\partial_x^2 A_0^\pm = 0, \qquad \text{in } \Omega, \tag{4.43}$$

$$A_0^-(-1) = 0, \qquad A_0^+(1) = 1, \tag{4.44}$$

$$\frac{1}{\mu_0}\partial_x A_0^-(0) = \frac{(1+\partial_y W(0))}{\mu_1}\partial_x A_0^+(0), \tag{4.45}$$

$$A_0^-(0) = A_0^+(0), \tag{4.46}$$

which gives

$$A_0(x) = \begin{cases} \frac{\mu_0(1+\partial_y W(0))}{\mu_1+\mu_0(1+\partial_y W(0))}(x+1), & \text{if } x \in \Omega_A, \\ \frac{1}{\mu_1+\mu_0(1+\partial_y W(0))}(\mu_1 x + \mu_0(1+\partial_y W(0))), & \text{if } x \in \Omega_L, \end{cases} \tag{4.47}$$

and

$$A_\varepsilon^1(x) = \begin{cases} A_0(x), & \text{if } x \in \Omega_A, \\ A_0(x) + \varepsilon\frac{\mu_1}{\mu_1+\mu_0(1+\partial_y W(0))}W(x/\varepsilon), & \text{if } x \in \Omega_L. \end{cases} \tag{4.48}$$

4.3.5 Numerical validation in Ω

Considering $\varepsilon = 0.1$ (10 toles), $\mu_1^r = 50$H/m, and $\sigma_1 = 10^5$S/m. The magnetic vector potential expansion $A_0(x) + \varepsilon W(y)\partial_x A_0(x)$ shows a good agreement. A comparison with the analytical solution $A_{Analytical}$ is shown in Figs. 4.5 and 4.6.

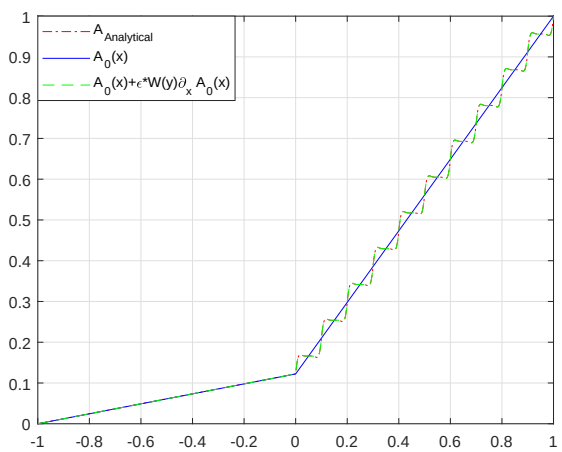

Figure 4.5: The magnetic vector potential in Ω for $\omega = 50$

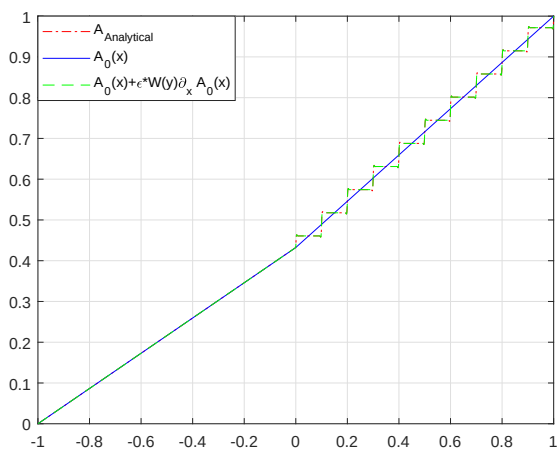

Figure 4.6: The magnetic vector potential in Ω for $\omega = 10^3$

The relative L^2-errors versus the thickness ε are shown in Fig. 4.7 , for $\omega = 10$, $\bar{\alpha} = \mu_r = 1$. The result shows a convergence of $\mathcal{O}(\varepsilon)$ as expected by the 2-scale expansion.

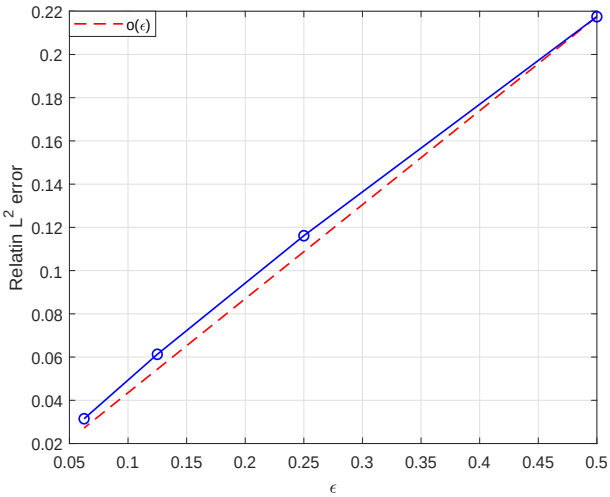

Figure 4.7: Relative L^2-errors of the solution A^1_ε versus the thickness ε.

Finally, the robustness of the result with respect to $\bar{\alpha}$ is studied. In Figure 4.8, we show the relative L^2-error in dependence of the parameter $\bar{\alpha}$ for $\omega = 10$, and $\mu_r = 1$. Fixing $\varepsilon = 0.1$ or $\varepsilon = 0.2$ as well as the other parameters, the skin depth depends on $\bar{\alpha}$, varying $\bar{\alpha}$ corresponds to a variation of the skin depth and so these experiments study the accuracy for a large range of skin depths, from very small to very large. In Figure 4.8, we observe an error reduction for any small or large value of $\bar{\alpha}$, in other words, for large and small skin depths. The error reduction is higher for large values of $\bar{\alpha}$, or equivalently for $\frac{\delta}{\varepsilon} \ll 1$ (factor 2 for $\bar{\alpha} \to \infty$), than for small values of $\bar{\alpha}$ where $\frac{\delta}{\varepsilon} \gg 1$ (factor 1.6 for $\bar{\alpha} \to 0$).

4.4 The 2D model problem

The formulation based on the magnetic vector potential in 2D is provided in section 4.1.

Remark: To avoid singularities, it is important, in a first step, to consider g such that $g'(0) = g'(1) = 0$.

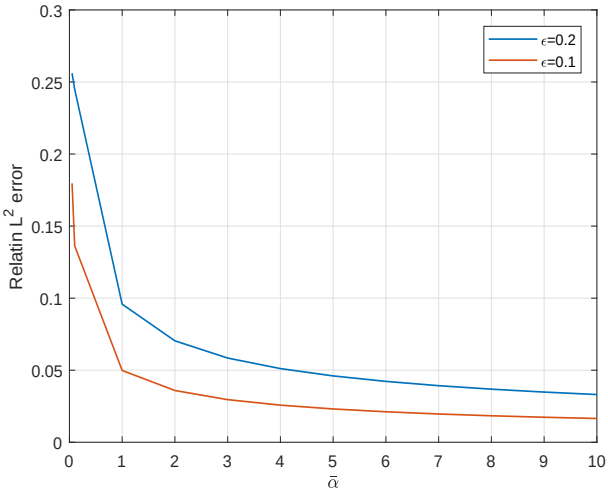

Figure 4.8: Relative L^2-errors of the solution A_ε^1 versus $\bar{\alpha}$.

4.4.1 Expansion of $\mathcal{M}^\varepsilon$

Using the same development of $\mathcal{M}^\varepsilon$ used in 1D in the direction x_1 (see section 4.3.1), and by integrating on $x_2 \in (0,1)$ we get:

$$\mathcal{M}^\varepsilon(a(x,y)) = \mathfrak{M}_0(a)(x,y) + \varepsilon\mathfrak{M}_1(a)(x,y) + \varepsilon^2\mathfrak{M}_2(a)(x,y) + .. \tag{4.49}$$

for all $x = (x_1, x_2) \in \Omega$ and $y \in \mathbb{R}/\mathbb{Z}$, where

$$\mathfrak{M}_0(a)(x,y) = \int_0^1 \int_0^1 a(x,s)dsdx_2, \tag{4.50}$$

$$\mathfrak{M}_1(a)(x,y) = (\frac{1}{2} - y)\int_0^1 \int_0^1 \partial_{x_1} a(x,s)dsdx_2, \tag{4.51}$$

$$\mathfrak{M}_2(a)(x,y) = (\frac{1}{3} - y(1-y))\int_0^1 \int_0^1 \partial_{x_1}^2 a(x,s)dsdx_2, \tag{4.52}$$

4.4.2 Classical homogenisation of the laminar stacks in Ω_L

Considering the domain of the laminated stacks Ω_L, the problem in 2D can be written as the following:

$$\Delta A_\varepsilon - \frac{i\omega\bar{\alpha}}{\varepsilon^2}(A_\varepsilon - \mathcal{M}^\varepsilon(A_\varepsilon)) = 0, \qquad \text{in } \Omega_L, \tag{4.53}$$

$$A_\varepsilon(0,x_2) = g(x_2), \qquad A_\varepsilon(1,x_2) = 0, \ \text{ for } \ x_2 \in (0,1), \tag{4.54}$$

$$\partial_{x_2} A_\varepsilon(x_1,0) = 0, \qquad \partial_{x_2} A_\varepsilon(x_1,1) = 0, \ \text{ for } \ x_1 \in (0,1). \tag{4.55}$$

A_ε admits the following two-scale expansion:

$$A_\varepsilon(x) = A_0(x, x_1/\varepsilon) + \varepsilon A_1(x, x_1/\varepsilon) + \varepsilon^2 A_2(x, x_1/\varepsilon) + ..., \tag{4.56}$$

where $A_i(x, y)$ are assumed to be 1-periodic with respect to the y variable.
Note that each term of the expansion depends on both the slow variable $x = (x_1, x_2)$ and the fast variable $y = x_1/\varepsilon$.

Replacing (4.56) in (4.53) and equating all terms of the same orders in powers of ε, the expansion (4.56) leads to the following:

- Order ε^{-2}: we have

$$\partial_y^2 A_0 - i\omega\bar{\alpha}(A_0 - \mathfrak{M}_0(A_0)) = 0, \;\; \forall (x, y) \in \Omega \times \mathbb{R}/\mathbb{Z} \tag{4.57}$$

  The solution A_0 is a constant function with respect to y but it may depend on x

$$A_0(x, y) = A_0(x).$$

- Order ε^{-1}: we have

$$\partial_y^2 A_1 + \partial_y \partial_{x_1} A_0 - i\omega\bar{\alpha}(A_1 - \mathfrak{M}_1(A_0) - \mathfrak{M}_0(A_1)) = 0, \tag{4.58}$$

$$\partial_y^2 A_1 - i\omega\bar{\alpha}(A_1 - \mathfrak{M}_0(A_1)) = -i\omega\bar{\alpha}(\mathfrak{M}_1(A_0)), \tag{4.59}$$

  then,

$$\partial_y^2 A_1 - i\omega\bar{\alpha}(A_1 - \mathfrak{M}_0(A_1)) = i\omega\bar{\alpha}(y - \frac{1}{2}) \int_0^1 \partial_{x_1} A_0 dx_2. \tag{4.60}$$

  We call $W(y)$ a periodic vector (unique up to an additive constant) solution to

$$\partial_y^2 W - i\omega\bar{\alpha}(W - \mathfrak{M}_0(W)) = i\omega\bar{\alpha}(y - \frac{1}{2}), \tag{4.61}$$

  and deduce by linearity that

$$A_1(x, y) = W(y) \int_0^1 \partial_{x_1} A_0(x) dx_2. \tag{4.62}$$

- Order ε^0: we have

$$\partial_y^2 A_2 - i\omega\bar{\alpha}(A_2 - \mathfrak{M}_0(A_2)) = -\partial_{x_1}^2 A_0 - \partial_{x_2}^2 A_0 - 2\partial_{x_1}\partial_y A_1 + i\omega\bar{\alpha}(\mathfrak{M}_2(A_0) + \mathfrak{M}_1(A_1)) \tag{4.63}$$

Integrating (4.63) on $y \in (0,1)$, we get:

$$\partial_{x_1}^2 A_0 + \partial_{x_2}^2 A_0 - i\omega\bar{\alpha}\Big(\int_0^1 A_2(x,y)dy - \int_0^1\int_0^1 A_2(x,y)dx_2dy\Big) = \frac{i\omega\bar{\alpha}}{6}\int_0^1 \partial_{x_1}^2 A_0(x)dx_2 \tag{4.64}$$

Then, we try to eliminate the coefficients of the term A_2. For this reason, we integrate the equation (4.64) on $x_2 \in (0,1)$. we get:

$$\Big(1 - \frac{i\omega\bar{\alpha}}{6}\Big)\int_0^1 \partial_{x_1}^2 A_0 dx_2 + \partial_{x_2} A_0|_{x_2=0}^{x_2=1} = 0. \tag{4.65}$$

Considering the equation (4.65), the term A_0 cannot be obviously determined. Thus, we propose to decompose the main problem and calculate the terms $\partial_{x_2} A_\varepsilon$ and $\int_0^1 A_\varepsilon dx_2$ separately.

4.4.2.1 Approximation of the derivative of A_ε along x_2 by the asymptotic expansion in power series of δ

Denote by $b = \partial_{x_2} A_\varepsilon$ the derivative of A_ε along x_2. The problem satisfied by b can be written as follows:

$$\Delta b - \frac{i\omega\bar{\alpha}}{\varepsilon^2} b = 0, \qquad \text{in } (0,1)\times(0,1), \tag{4.66}$$

$$b(0,x_2) = \partial_{x_2} g(x_2) = g', \qquad b(1,x_2) = \partial_{x_2} h(x_2) = h', \ \text{ for } x_2 \in (0,1), \tag{4.67}$$

$$b(x_1,0) = 0, \qquad b(x_1,1) = 0, \ \text{ for } x_1 \in (0,1). \tag{4.68}$$

According to the conditions at the boundaries and knowing that the total flux in the domain is zero, we can simply consider infinite sheets in x_2 direction. Moreover, as the width of the domain is much larger than δ, we can take into account only the left interface (see Figure 4.9).

Then, we can rewrite the problem as follows

$$-\Delta b_\delta + \frac{i}{\delta^2} b_\delta = 0, \qquad \text{in } \Gamma\times(0,1), \tag{4.69}$$

$$b_\delta(0,\cdot) = g', \qquad \text{on } \Gamma. \tag{4.70}$$

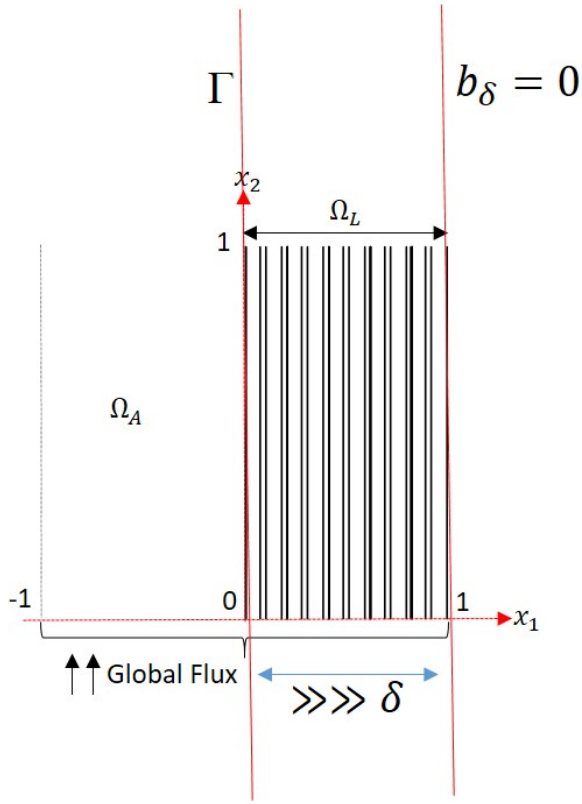

Figure 4.9

It is possible to derive a multiscale expansion in power series of the small complex parameter δ

$$b_\delta(x) = b_0(x,\delta) + \delta b_1(x,\delta) + \delta^2 b_2(x,\delta) + ..., \forall x \in \mathbb{R}^2 \tag{4.71}$$

with $b_j(x,\delta) = \chi(\nu) w_j(t, \nu/\delta)$, where t and ν are the tangential and normal variation in a neighborhood $\chi(\nu)$ of Γ.

Following the work in [102], we obtain (see Appendix B.1.5)

$$b(x_1, x_2) = g'(x_2) e^{-x_1 \kappa/\varepsilon} + O(\varepsilon). \tag{4.72}$$

4.4.2.2 Approximation of the mean value of A_ε along x_2

Denote now the mean value of A_ε along x_2 by $\bar{A}_\varepsilon : x_1 \mapsto \int_0^1 A^\varepsilon(x_1, x_2)dx_2$. The function $\bar{A}_\varepsilon$ satisfies the following 1D problem

$$\partial_{x_1}^2 \bar{A}_\varepsilon - \frac{\kappa^2}{\varepsilon^2}\left(\bar{A}_\varepsilon - \frac{1}{\varepsilon}\int_{\varepsilon\lfloor x_1/\varepsilon\rfloor}^{\varepsilon(\lfloor x_1/\varepsilon\rfloor+1)} \bar{A}_\varepsilon(s,t)\,dsdt\right) = 0, \quad \text{in } \cup_{k=1}^{\lfloor 1/\varepsilon\rfloor}(\varepsilon(k-1), \varepsilon k) \times (0,1) \tag{4.73a}$$

$$\bar{A}_\varepsilon|_{x_1=0} = \int_0^1 g(x_2)dx_2 := \bar{g}, \quad \bar{A}_\varepsilon|_{x_1=1} = 0. \tag{4.73b}$$

Using the 1D expansion in section 4.3.2, the solution of the differential equation (4.34) considering the interface conditions (4.73b) is

$$\bar{A}_0 = \bar{g}\,(1 - x_1)\,, \tag{4.74}$$

which leads to

$$\bar{A}_\varepsilon^1(x_1) = \bar{g}\,(1 - x_1 - \varepsilon W(x_1/\varepsilon))\,. \tag{4.75}$$

4.4.3 Recombination of the results

The magnetic potential A_ε can be written, using simple calculations, in the following way:

$$A_\varepsilon(x_1, x_2) = \int_0^{x_2} b(x_1, s)ds - \int_0^1\int_0^{x_2} b(x_1, s)dsdx_2 + \bar{A}_\varepsilon(x_1). \tag{4.76}$$

Hence, using the approximations (B.22)–(4.75), we obtain

$$A_\varepsilon^1(x_1, x_2) = (g(x_2) - \bar{g})e^{-x_1\kappa/\varepsilon} + \bar{g}\,(1 - x_1 - \varepsilon W(x_1/\varepsilon))\,, \tag{4.77}$$

where $\bar{g} = \int_0^1 g(x_2)dx_2$.

4.4.4 Numerical results

We consider $\varepsilon = 0.1$ (10 toles), $\bar{\alpha} = 1$, $\omega = 50$, $g(x_2) = 1 + \cos(\pi x_2)$, and $\delta = 0.014$. In Figure 4.10, we show the approximate magnetic vector potential $A_\varepsilon^1(x)$ compared to the magnetic potential A_{FDM} calculated numerically using the finite difference method.
The result shows a good agreement as we have the correct oscillations far from the interface

($x_1 = 0$), a good behavior in its neighborhood which is due to the presence of the term b, and a relative L^2-error $\frac{||A_{FDM} - A^1_\varepsilon||_2}{||A_{FDM}||_2} = 0.007$.

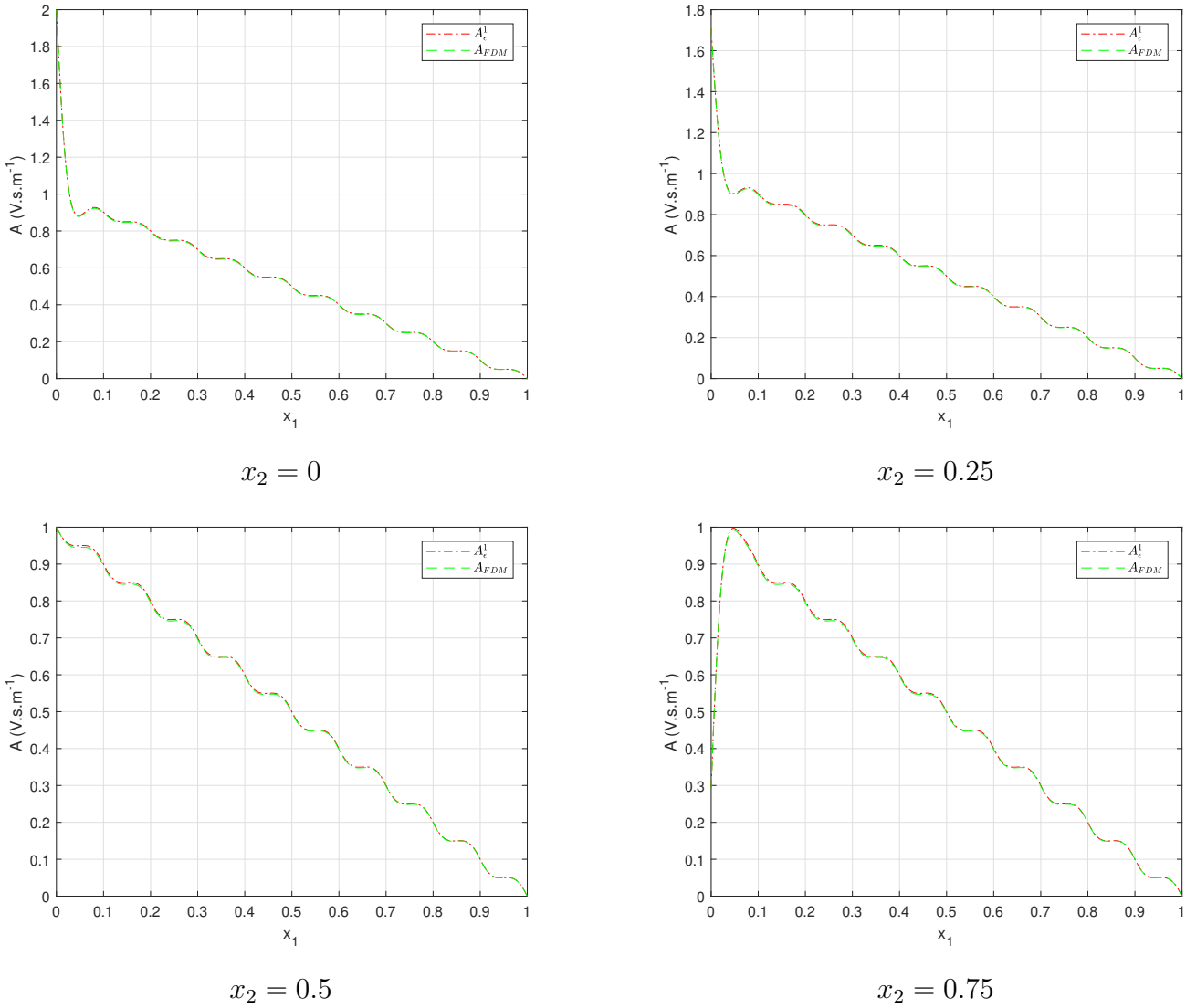

Figure 4.10: The magnetic vector potential A^1_ε in Ω_L compared to the numerical solution A_{FDM}.

4.5 Conclusion

A solution is provided by classical homogenization in 1D and a correction at the interface with the air. Another solution is also provided in 2D in the domain of the lamination stacks, while the correction at the interface with air have to be added

Conclusion and Perspectives

Conclusion

In this thesis, we presented an asymptotic modelling and discretisation techniques for eddy current problems in electromagnetism. This coupling between the two notions led to an accurate result with less computational time.

In chapter 2, we provided a FEM/BEM coupling for magnetostatic and magnetodynamic problems using different mathematical formulations. The results validate the interest of the coupling by reducing the discretisation elements with a good accuracy.

In chapter 3, an asymptotic modelling of a conductive thin layer in eddy-current problem is accomplished. An equivalent models of high order is derived by replacing the thin layer by its mid-surface with an impedance transmission conditions that connects the electromagnetic fields. Moreover, these models are discretised by the BEM. Both models show a good agreement, and the equivalent model of second order show an accuracy for all range of the skin depth. Thus, the modelisation and discretisation techniques together lead to a high reduction of the number of mesh elements, as well as to a good precision comparing with analytical solutions.

In chapter 4, a homogenisation technique with an interface correction is proposed for modeling a lamination of conductive sheets in eddy-current problems. The 1D case is validated by comparing the results to an analytical solution. However, the 2D case is actually in progress.

Perspectives

Firstly, we aim to implement and test the FEM/BEM coupling for 3D eddy current problems in non-linear medium. Taking into account the nonlinearity of the magnetic materials is necessary for the computation of the electromagnetic fields in many direct applications, like the analysis of large power transformers.

Another aspect to consider concerns the conductive thin layers in open domain (i.e. with holes) and take into account the vicinity of the corners of the conducting layer. For this purpose, there are two steps to be done:

1. Test the equivalent models with transmission conditions on some complex geometries in order to validate or to detect if they do not work in specific cases.

2. Make an appropriate modification on the discretization technique to treat the problem near the corners.

Finally, we aim to consider the direct continuation of the work presented in chapter 4 by proceeding in the following plan:

1. Complete and validate the homogenization technique of laminated stacks in 2D.
2. Proceed with this technique to treat a 3D case.
3. Consider the case of connected sheets to go towards foil windings.

APPENDIX A

Annex

A.1 Expansion of differential operators inside the conductive sheet Ω_0^ε [59, section 5.1]

The derivatives in the normal and tangential directions scale differently in ε, due to the small thickness of the conductor. Thus, it is more convenient to use the local normal coordinate system in Ω_0^ε.
For this coordinate system, we denote by D_α the covariant derivative which specifies the derivative along the tangent vectors of the mean surface Γ. The covariant derivative at a point $p \in \Gamma$ depends on a small neighborhood of p, and thus it considers the information on the neigbourhood of p and allows us to transport vectors along surfaces that are parallel with respect to Γ. Denote also ∂_3^h the partial derivative with respect to the normal coordinate $y_3 = h$.
We use the covariant derivative as partial derivative when it acts on a scalar function: $D_\alpha w = \partial_\alpha w$, where $\alpha = 1, 2$ refers to the tangential coordinates on Γ.

Let Γ_h be the surface contained in $\Omega_+^\varepsilon \cup \Omega_-^\varepsilon$ at a distance h of Γ. We denote by $a_{\alpha\beta}(h)$ and $b_{\alpha\beta}(h)$ the metric tensor and the curvature tensor of the manifold Γ_h, respectively. The metric tensor generalizes many of the familiar properties of the dot product of vectors, $a_{\alpha\beta}(h)$ is the restriction of the metric of Γ on Γ_h , in such a coordinate system it writes

$$a_{\alpha\beta}(h) = a_{\alpha\beta} - 2b_{\alpha\beta}h + b_\alpha^\gamma b_{\gamma\beta}h^2,$$

and its inverse expands in power series of h

$$a^{\alpha\beta}(h) = a^{\alpha\beta} - 2b^{\alpha\beta}h + \mathcal{O}(h^2).$$

The curvature tensor describes the curvature of a Riemannian manifold, given in terms of Christoffel symbols.

Let $L(y_\alpha, h; D_\alpha, \partial_3^h)$ be the second order Maxwell operator

$$\text{curlcurl} - (k_0^\varepsilon)^2\mathbb{I},$$

in Ω_0^ε in the normal coordinate system and by $B(y_\alpha, h; D_\alpha, \partial_3^h) = (B_\alpha(y_\alpha, h; D_\alpha, \partial_3^h), 0)$ the tangent trace operator curl $\cdot \times n$ on $\Gamma_\pm^\varepsilon$, with [[73], chapter 3, prop 3.36]

$$B_\alpha(y_\alpha, h; D_\alpha, \partial_3^h)\boldsymbol{\mathcal{H}} = \partial_3^h \mathcal{H}_\alpha - D_\alpha \hbar,$$

for $\boldsymbol{\mathcal{H}} = (\mathcal{H}_\alpha, \hbar)$, where $\mathcal{H}_\alpha = (\mathcal{H}_1, \mathcal{H}_2)$ and $\hbar$ are the tangential and normal coordinates of $\boldsymbol{\mathcal{H}}$, respectively.

These two operators L and B expand in power series of h with intrinsic coefficients with respect to Γ.
In order to obtain a coordinate which does not depend on ε we can scale the normal coordinate $Y_3 = \varepsilon^{-1}h$. We use from now on the same symbol $\boldsymbol{\mathcal{H}}$ for three dimensional one-form field in these scaled coordinates i.e. the linear combination of the differentials of theses coordinates, and call $L[\varepsilon]$ and $B[\varepsilon]$ the respective three dimensional harmonic Maxwell operators in Ω_0^ε. These operators expand in power of ε

$$L[\varepsilon] = \varepsilon^{-2} \sum_{n=0}^{\infty} \varepsilon^n L^n,$$

and

$$B[\varepsilon] = \varepsilon^{-1} B^0 + B^1,$$

whose coefficients are intrinsic operators on Γ, which are completely determined by the shape of Γ and the material parameters of the conducting sheet. Let L_α^n and B_α^n be the surface components of L^n and B^n, respectively. Defined as follows

$$L_\alpha^0(\boldsymbol{\mathcal{H}}) = -\partial_3^2 \mathcal{H}_\alpha + \gamma^2 \mathcal{H}_\alpha,$$

$$L_\alpha^1(\boldsymbol{\mathcal{H}}) = -2b_\alpha^\beta \partial_3 \mathcal{H}_\beta + b_\beta^\beta \partial_3 \mathcal{H}_\alpha,$$

$$B_\alpha^0(\boldsymbol{\mathcal{H}}) = \partial_3 \mathcal{H}_\alpha, \quad \text{and} \quad B_\alpha^1(\boldsymbol{\mathcal{H}}) = -D_\alpha \hbar.$$

Here, ∂_3 is the partial derivative with respect to Y_3. We denote by L_3^n the transverse components of L^n, they satisfy

$$L_3^0(\boldsymbol{\mathcal{H}}) = \gamma^2 \hbar,$$

and

$$L_3^1(\boldsymbol{\mathcal{H}}) = \gamma_\alpha^\alpha (\partial_3 \mathcal{H}) + b_\beta^\beta \partial_3 \hbar,$$

where $\gamma_{\alpha\beta}(\boldsymbol{\mathcal{H}}) = \frac{1}{2}(D_\alpha \mathcal{H}_\beta + D_\beta \mathcal{H}_\alpha) - b\alpha\beta\hbar$ is the change of metric tensor and $\gamma_\alpha^\alpha = a^{\alpha\beta}\gamma_{\alpha\beta}$ and $\gamma = \exp(\frac{3i\pi}{4})\sqrt{\omega\mu_0^c\bar{\sigma}}$ γ is defined such that $(k_0^\varepsilon)^2 = -\varepsilon^{-2}\gamma^2$.

A.2

Applying the Cauchy product of the formal series $\sum_{n\geq 0} \varepsilon^n L^n$ associated to the operator $L[\varepsilon]$, with the formal series $\sum_{j\geq 0} \varepsilon^j \boldsymbol{\mathcal{H}}_j$.
we get:

$$\Big(\sum_{n\geq 0} \varepsilon^n L^n\Big)\Big(\sum_{j\geq 0} \varepsilon^j \boldsymbol{\mathcal{H}}_j\Big) = \sum_{n\geq 0} \varepsilon^n \Big[\sum_{l=0}^{n} L^l \boldsymbol{\mathcal{H}}_{n-l}\Big].$$

Clearly the coefficient for each ε^k-term is $\sum_{l=0}^{k} L^l \boldsymbol{\mathcal{H}}_{k-l}$.

A.3

Considering the first equation of the system (3.19): $L[\varepsilon]\sum_{j=0}^{\infty}\varepsilon^j\boldsymbol{\mathcal{H}}_j(y_\alpha,Y_3)=0$.
And using Proposition (3.3.1), we get that $\sum_{j=0}^{n}L^j(\boldsymbol{\mathcal{H}}_{n-j})=0$ for all $n\geq 0$
Taking into account the surface and transverse components of L^n, we get

$$\sum_{j=0}^{k}L_3^j(\boldsymbol{\mathcal{H}}_{k-j})=0,$$

$$\sum_{j=0}^{k}L_\alpha^j(\boldsymbol{\mathcal{H}}_{k-j})=0.$$

Using the expression of the operators, and substituting the first term of the operator $L[\varepsilon]$, we obtain the first two equations (3.22) and (3.23).
Expanding E^ε, we get (3.24).
Finally, the equation (3.26) is obtained from (3.20) and the transmission condition (3.15).

A.4

Proposition A.4.1 *[72] According to equations (3.37), (3.40) when $n=0$, the tangential field $\mathcal{H}_{0,\alpha}$ satisfies the following ODE*

$$\begin{cases}\partial_3^2\mathcal{H}_{0,\alpha}(\cdot,Y_3)-\gamma^2\mathcal{H}_{0,\alpha}(\cdot,Y_3) &= 0 \qquad\qquad for \quad Y_3\in I,\\ i\omega\mu_\pm\boldsymbol{\mathcal{H}}_0|_{\pm\frac{1}{2}} &= n\times curl\mathcal{E}_0^\pm\times n|_{0\pm},\end{cases}$$

and has a unique solution

$$\mathcal{H}_{0,0}\cosh(\gamma Y_3)+\mathcal{H}_{0,1}\sinh(\gamma Y_3),$$

with

$$\mathcal{H}_{0,0}=\frac{1}{\cosh(\frac{\gamma}{2})}\left\{\frac{1}{i\omega\mu}\mathrm{curl}\mathcal{E}_0\right\}_\Gamma,$$

$$\mathcal{H}_{0,1}=\frac{1}{2\sinh(\frac{\gamma}{2})}\left[\frac{1}{i\omega\mu}\mathrm{curl}\mathcal{E}_0\right]_\Gamma.$$

A.5

Theorem A.5.1 *The potentials satisfy the jump relations*

$$\begin{array}{lllllll}[\gamma_D\Psi_M] &=& -\mathbb{I}d &,& [\gamma_D\Psi_A] &=& 0,\\ [\gamma_N\Psi_M] &=& 0 &,& [\gamma_N\Psi_A] &=& -\mathbb{I}d,\\ [\gamma_D\Psi_V] &=& 0. & & & & \end{array}$$

A.6 Calculation of the External Field

The representation formula of any vector field E for all $x \in \Omega_\pm$ is

$$E(x) = \Psi_M([\gamma_D E]_\Gamma)(x) + \Psi_A([\gamma_N E]_\Gamma)(x) - \mathrm{grad}\Psi_V([\gamma_n E]_\Gamma)(x).$$

where Ψ_M, Ψ_A, and Ψ_V are defined in section 3.5.2.
Moreover

$$H(x) = -(i\omega\mu_0)^{-1}\mathrm{curl}E(x),$$

then

$$H(x) = -(i\omega\mu_0)^{-1}\Big(\mathrm{curlcurl}\int_\Gamma (n \times [\gamma_D E]_\Gamma)G(x,y)dS(y) + \mathrm{curl}\int_\Gamma [\gamma_N E]_\Gamma G(x,y)dS(y)\Big),$$

which is equivalent to :

$$H(x) = -(i\omega\mu_0)^{-1}\Big(\int_\Gamma \mathrm{div}_\Gamma(n\times[\gamma_D E]_\Gamma)\nabla_x G(x,y)dS(y) + \int_\Gamma (\nabla_x G(x,y)\times[\gamma_N E]_\Gamma)dS(y)\Big),$$

or

$$H(x) = -(i\omega\mu_0)^{-1}\Big(\int_\Gamma -\mathrm{curl}_\Gamma([\gamma_D E]_\Gamma)\nabla_x G(x,y)dS(y) + \int_\Gamma (\nabla_x G(x,y)\times[\gamma_N E]_\Gamma)dS(y)\Big).$$

Concerning the terms of asymptotic expansion introduced in 4.33, 3.59, and 3.60, we will consider the following formulas.

A.6.1 First term H_0

As $[\gamma_D E_0] = 0$,

$$\widetilde{H}_0(x) = -(i\omega\mu_0)^{-1}\Big(\int_\Gamma (\nabla_x G(x,y)\times[\gamma_N \widetilde{E}_0]_\Gamma)dS(y)\Big),$$

and so

$$H_0 = \widetilde{H}_0 + H_s.$$

A.6.2 Second term H_1

$$H_1(x) = -(i\omega\mu_0)^{-1}\Big(-\int_\Gamma \mathrm{curl}_\Gamma([\gamma_D E_1]_\Gamma)\nabla_x G(x,y)dS(y) + \int_\Gamma (\nabla_x G(x,y)\times[\gamma_N E_1]_\Gamma)dS(y)\Big).$$

But

$$[\gamma_D E_1]_\Gamma = K_1\{\gamma_N E_0\}_\Gamma,$$

then

$$H_1(x) = -(i\omega\mu_0)^{-1}\Big(-K_1\int_\Gamma \mathrm{curl}_\Gamma(\{\gamma_N E_0\}_\Gamma)\nabla_x G(x,y)dS(y) + \int_\Gamma (\nabla_x G(x,y)\times[\gamma_N E_1]_\Gamma)dS(y)\Big).$$

A.6.3 Second order H^1_ε

$$H^1_\varepsilon(x) = -(i\omega\mu_0)^{-1}\Big(-\int_\Gamma \mathrm{curl}_\Gamma([\gamma_D E^1_\varepsilon]_\Gamma)\nabla_x G(x,y)dS(y)+\int_\Gamma(\nabla_x G(x,y)\times[\gamma_N E^1_\varepsilon]_\Gamma)dS(y)\Big).$$

But

$$[\gamma_D E^1_\varepsilon]_\Gamma = \varepsilon K_1\{\gamma_N E^1_\varepsilon\}_\Gamma,$$

then

$$H^\varepsilon_1(x) = -(i\omega\mu_0)^{-1}\Big(-\varepsilon K_1\int_\Gamma \mathrm{curl}_\Gamma(\{\gamma_N E^1_\varepsilon\}_\Gamma)\nabla_x G(x,y)dS(y)+\int_\Gamma(\nabla_x G(x,y)\times[\gamma_N E_1]_\Gamma)dS(y)\Big).$$

A.7 Analytical Solution of the Eddy-Current Problem for a Sphere with a Thin Layer in 3D

Consider a thin layer made of an inner sphere of radius r_2 and an outer spherical shell of radius r_1 (see figure A.1). The source current is provided by a uniform magnetic field in the $\vec{z}$ direction.

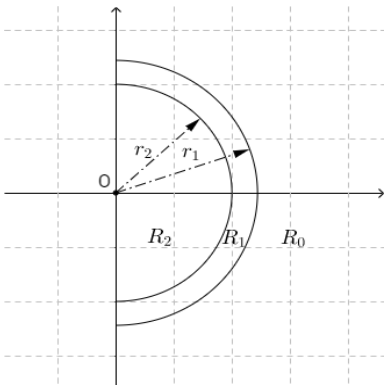

Figure A.1: A cross section of the domain

A.7.1 Formulation of the problem

We introduce the spherical coordinates system (r, θ, ϕ) with a center at O, where θ and ϕ stands for the azimuthal and polar angle respectively.

We consider the three regions R_0, R_1, and R_2 defined as follows:

$R_0 : \{r > r_1, 0 \leq \theta \leq 2\pi, 0 \leq \phi \leq \pi\}$ containing air.
$R_1 : \{r_2 < r < r_1, 0 \leq \theta \leq 2\pi, 0 \leq \phi \leq \pi\}$ which is a conducting medium where σ ans μ are constants.
$R_2 : \{0 \leq r < r_2, 0 \leq \theta \leq 2\pi, 0 \leq \phi \leq \pi\}$ which is a non-conducting medium where $\sigma = 0$ and $\mu_r = \mu_0$.

We introduce the vector potential $\text{curl}A = B$, where B is the magnetic induction vector. Using Ampere's and Faraday's laws the eddy current model can be reduced to the following second order equation for the magnetic vector potential

$$\text{curlcurl}A + i\sigma\omega\mu A = \mu J_e,$$

as

$$\text{div}A = 0,$$

we obtain

$$\Delta A + k^2 A = -\mu J_e \tag{A.1}$$

where $k^2 = -i\sigma\omega\mu$.

Proposition A.7.1 *The source term can be expressed as an initial excitation of a magnetic vector potential A_s, which is written in spherical coordinates as follows*

$$A_s = \frac{\mu}{2} r \sin(\phi) e_\theta$$

Proof. For $H_s = 1e_z$,
We can write the uniform magnetic field in terms of the spherical coordinates using

$$\begin{pmatrix} H_r \\ H_\phi \\ H_\theta \end{pmatrix} = \begin{pmatrix} \sin\phi\cos\theta & \sin\phi\sin\theta & \cos\phi \\ \cos\phi\cos\theta & \cos\phi\sin\theta & -\sin\phi \\ -\sin\theta & \cos\theta & 0 \end{pmatrix} \begin{pmatrix} H_x \\ H_y \\ H_z \end{pmatrix}$$

to obtain that

$$H_s = \cos\phi e_r - \sin\phi e_\phi$$

Using the formula of curl in spherical coordinates we can prove that $\text{curl}A_s = \frac{1}{\mu} H_s$

$$\text{curl}A = \frac{1}{r\sin\phi}\left[\frac{\partial}{\partial\phi}\sin\phi A_\theta - \frac{\partial A_\phi}{\partial\theta}\right]\vec{r} + \frac{1}{r}\left[\frac{1}{\sin\phi}\frac{\partial A_r}{\partial\theta} - \frac{\partial}{\partial r}(rA_\theta)\right]\vec{\phi} + \frac{1}{2}\left[\frac{\partial}{\partial r}(rA_\phi) - \frac{\partial A_r}{\partial\phi}\right]\vec{\theta}$$

■ Taking into account the axial symmetry, we obtain that A has only one non-zero component,

$$A = (0, A(r,\phi), 0)$$

Writing the equation A.1 in spherical coordinates with considering the θ-component of A, we obtain the following equation for the function $A(r,\phi)$

$$\frac{\partial^2 A}{\partial r^2} + \frac{2}{r}\frac{\partial A}{\partial r} + \frac{cot\phi}{r^2}\frac{\partial A}{\partial\phi} + \frac{1}{r^2}\frac{\partial^2 A}{\partial\phi^2} - \frac{A}{r^2\sin^2\phi} + k^2 A = -\mu_0 J_e$$

A.7.2 Mathematical Analysis

We consider the case where σ and μ are defined as a piecewise constant functions

$$\mu = \begin{cases} \mu_0 & \text{in} \quad R_2 \\ \mu_0 & \text{in} \quad R_1 \\ \mu_0 & \text{in} \quad R_0 \end{cases} \qquad and \qquad \sigma = \begin{cases} 0 & \text{in} \quad R_2 \\ \sigma & \text{in} \quad R_1 \\ 0 & \text{in} \quad R_0 \end{cases}$$

Substituting these properties, we obtain the following system of equations:

$$\frac{\partial^2 A_0}{\partial r^2} + \frac{2}{r}\frac{\partial A_0}{\partial r} + \frac{cot\phi}{r^2}\frac{\partial A_0}{\partial \phi} + \frac{1}{r^2}\frac{\partial^2 A_0}{\partial \phi^2} - \frac{A_0}{r^2 \sin^2\phi} = -\mu_0 J_e \tag{A.2}$$

$$\frac{\partial^2 A_1}{\partial r^2} + \frac{2}{r}\frac{\partial A_1}{\partial r} + \frac{cot\phi}{r^2}\frac{\partial A_1}{\partial \phi} + \frac{1}{r^2}\frac{\partial^2 A_1}{\partial \phi^2} - \frac{A_1}{r^2 \sin^2\phi} + k^2 A_1 = 0 \tag{A.3}$$

$$\frac{\partial^2 A_2}{\partial r^2} + \frac{2}{r}\frac{\partial A_2}{\partial r} + \frac{cot\phi}{r^2}\frac{\partial A_2}{\partial \phi} + \frac{1}{r^2}\frac{\partial^2 A_2}{\partial \phi^2} - \frac{A_2}{r^2 \sin^2\phi} = 0 \tag{A.4}$$

whereA_i denotes the θ component of the vector potential in region R_i, for $i = 0, .., 2$.

The boundary conditions are:

$$A_{0_{|r=r_1}} = A_{1_{|r=r_1}}, \quad A_{1_{|r=r_2}} = A_{2_{|r=r_2}}. \tag{A.5}$$

$$\frac{\partial A_0}{\partial r}_{|r=r_1} = \frac{\partial A_1}{\partial r}_{|r=r_1}, \quad \frac{\partial A_1}{\partial r}_{|r=r_2} = \frac{\partial A_2}{\partial r}_{|r=r_2}. \tag{A.6}$$

To solve the problem (A.2)-(A.6), we use the following integral transform [71]:

$$\bar{A}_i(r,n) = \frac{1}{D_n}\int_{-1}^{-1} A_i(r,t) P_n^{(1)}(t) dt \tag{A.7}$$

where $t = cos\phi$, $P_n^{(1)}(t)$ is an associated Legendre function of first kind, and

$$D_n := \int_{-1}^{-1} (P_n^{(1)}(t))^2 dt = \frac{2n(n+1)}{2n+1}$$

Using this integral transform (A.7), and using the fact that $A_0 = A_0^r + A_s$, we obtain

$$\frac{\partial^2 \bar{A}_0^r}{\partial r^2} + \frac{2}{r}\frac{\partial \bar{A}_0^r}{\partial r} - \frac{n(n+1)}{r^2}\bar{A}_0^r = 0 \tag{A.8}$$

$$\frac{\partial^2 \bar{A}_1}{\partial r^2} + \frac{2}{r}\frac{\partial \bar{A}_1}{\partial r} - \frac{n(n+1)}{r^2}\bar{A}_1 + k^2\bar{A}_1 = 0 \tag{A.9}$$

$$\frac{\partial^2 \bar{A}_2}{\partial r^2} + \frac{2}{r}\frac{\partial \bar{A}_2}{\partial r} - \frac{n(n+1)}{r^2}\bar{A}_2 = 0 \tag{A.10}$$

The general solution of (A.8) is:

$$\bar{A}_0^r = C_1 r^{-1-n} + C_1' r^n,$$

But A_0^r should vanish as $r \to \infty$ since the potential goes to zero far away from any charges, so

$$\bar{A}_0^r = C_1 r^{-1-n}. \tag{A.11}$$

The general solution of (A.9) is expressed in terms of Bessel functions:

$$\bar{A}_1 = C_2 r^{-1/2} J_{n+\frac{1}{2}}(kr) + C_3 r^{-1/2} Y_{n+\frac{1}{2}}(kr). \tag{A.12}$$

The general solution of (A.10) is:

$$\bar{A}_2 = C_4 r^n + C_4' r^{-1-n},$$

But the solution must remain bounded as $r \to 0$, thus

$$\bar{A}_2 = C_4 r^n. \tag{A.13}$$

Inverting the integral transform (A.7), we obtain the solution to the problem in the form

$$A_i(r,\phi) = \sum_{n=1}^{\infty} \bar{A}_i(r,n) P_n^{(1)}(\cos\phi) \tag{A.14}$$

Applying (A.14) to (A.20)-(A.22), we obtain the solution of (A.2)-(A.4) in the form

$$\begin{cases} A_0(r,\phi) &= \sum_{n=1}^{\infty} C_1 r^{-1-n} P_n^{(1)}(\cos\phi) + A_s & R_0 \\ A_1(r,\phi) &= \sum_{n=1}^{\infty} (C_2 r^{-1/2} J_{n+\frac{1}{2}}(kr) + C_3 r^{-1/2} Y_{n+\frac{1}{2}}(kr)) P_n^{(1)}(\cos\phi) & R_1 \\ A_2(r,\phi) &= \sum_{n=1}^{\infty} C_4 r^n P_n^{(1)}(\cos\phi) & R_2 \end{cases}$$

The $\sin\phi$ dependence of the excitation source requires that only $n = 1$ be present, with

$$P_1^{(1)}(\cos\phi) = \sin\phi.$$

Therefore, the solution for the vector potential is

$$A_\theta(r,\phi) = \begin{cases} A_0(r,\phi) &= C_1 r^{-2} \sin\phi + \frac{\mu}{2} r \sin\phi & R_0 \\ A_1(r,\phi) &= (C_2 r^{-1/2} J_{\frac{3}{2}}(kr) + C_3 r^{-1/2} Y_{\frac{3}{2}}(kr)) \sin\phi & R_1 \\ A_2(r,\phi) &= C_4 r \sin\phi & R_2 \end{cases}$$

Using the boundary conditions (A.5)-(A.6), we can determine the constants C_i for $i = 1, .., 4$.

A.8 Analytical Solution of the Eddy-Current Problem for a Sphere without Thin Layer

Consider a sphere of radius r_1 (see figure A.2). The source current is given by the excitation of a uniform magnetic field in $\vec{z}$ direction in the domain R_0.

We consider the two regions R_0 and R_1 defined as follows:

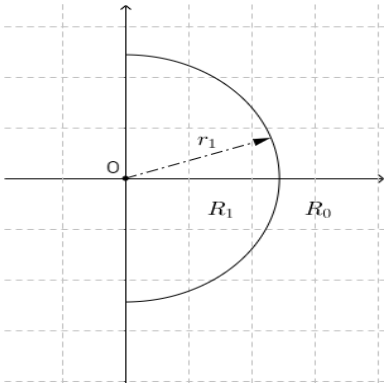

Figure A.2: A cross section of the domain

$R_0 : \{r > r_1, 0 \leq \theta \leq 2\pi, 0 \leq \phi \leq \pi\}$ containing air.
$R_1 : \{0 \leq r < r_1, 0 \leq \theta \leq 2\pi, 0 \leq \phi \leq \pi\}$ which is a conducting medium where σ ans μ are constants.

The solution of the problem satisfy the following system of equations:

$$\frac{\partial^2 A_0}{\partial r^2} + \frac{2}{r}\frac{\partial A_0}{\partial r} + \frac{cot\phi}{r^2}\frac{\partial A_0}{\partial \phi} + \frac{1}{r^2}\frac{\partial^2 A_0}{\partial \phi^2} - \frac{A_0}{r^2 \sin^2 \phi} = -\mu_0 J_e \tag{A.15}$$

$$\frac{\partial^2 A_1}{\partial r^2} + \frac{2}{r}\frac{\partial A_1}{\partial r} + \frac{cot\phi}{r^2}\frac{\partial A_1}{\partial \phi} + \frac{1}{r^2}\frac{\partial^2 A_1}{\partial \phi^2} - \frac{A_1}{r^2 \sin^2 \phi} + k^2 A_1 = 0 \tag{A.16}$$

$A_i(r, \phi)$ denotes the θ component of the vector potential in region R_i, for $i = 0, 1$.

With the boundary conditions

$$A_{0_{|r=r_1}} = A_{1_{|r=r_1}}, \quad \frac{\partial A_0}{\partial r}_{|r=r_1} = \frac{\partial A_1}{\partial r}_{|r=r_1}. \tag{A.17}$$

Using the integral transform (A.7), and using the fact that $A_0 = A_0^r + A_s$, we obtain

$$\frac{\partial^2 \bar{A}_0^r}{\partial r^2} + \frac{2}{r}\frac{\partial \bar{A}_0^r}{\partial r} - \frac{n(n+1)}{r^2}\bar{A}_0^r = 0 \tag{A.18}$$

$$\frac{\partial^2 \bar{A}_1}{\partial r^2} + \frac{2}{r}\frac{\partial \bar{A}_1}{\partial r} - \frac{n(n+1)}{r^2}\bar{A}_1 + k^2 \bar{A}_1 = 0 \tag{A.19}$$

The general solution of (A.18) is:

$$\bar{A}_0^r = C_1 r^{-1-n}. \tag{A.20}$$

The general solution of (A.19) is expressed in terms of Bessel functions:

$$\bar{A}_1 = C_2 r^{-1/2} J_{n+\frac{1}{2}}(kr) + C_2' r^{-1/2} Y_{n+\frac{1}{2}}(kr). \tag{A.21}$$

But the solution must remain bounded as $r \to 0$, so

$$\bar{A}_1 = C_2 r^{-1/2} J_{n+\frac{1}{2}}(kr). \tag{A.22}$$

Applying (A.14) to (A.20)-(A.22), we obtain the solution of (A.15)-(A.16) in the form

$$A_\theta(r,\phi) = \begin{cases} A_0(r,\phi) & = & C_1 r^{-2} sin\phi + \frac{\mu}{2} r \sin\phi & R_0 \\ A_1(r,\phi) & = & C_2 r^{-1/2} J_{\frac{3}{2}}(kr) \sin\phi & R_1 \end{cases}$$

Using the boundary conditions (A.17), we can determine the constants C_i for $i = 1, 2$.

APPENDIX B Annex

B.1 Appendix

B.1.1

Using the derivation of $A_i(x, x/\varepsilon)$

$$\frac{d}{dx}[A_i(x, x/\varepsilon)] = \frac{\partial}{\partial x}A_i(x, x/\varepsilon) + \frac{1}{\varepsilon}\frac{\partial}{\partial y}A_i(x, x/\varepsilon),$$

we get

$$\nabla \cdot (\nabla A_i) = \partial_x^2 A_i + 2\varepsilon^{-1}\partial_y\partial_x A_i + \varepsilon^{-2}\partial_y^2 A_i.$$

B.1.2

Multiplying (4.25) by $\overline{A_0 - \mathfrak{M}_0(A_0)}$ and integrating on $y \in (0, 1)$, we obtain

$$\int_0^1 \Big(|\partial_y A_0|^2 + i\omega\bar{\alpha}(A_0 - \mathfrak{M}_0(A_0))^2\Big)dy = 0. \tag{B.1}$$

Which gives that

$$A_0 = \mathfrak{M}_0(A_0) = A_0(x). \tag{B.2}$$

B.1.3

Details of calculation of (4.34) are as follows:

$$\begin{aligned} -2\int_0^1 \partial_x\partial_y A_1 dy =& -2\int_0^1 \partial_{x_1}\partial_y\Big(W(y)\partial_x A_0(x)\Big)dy = -2\int_0^1 \Big(\partial_x^2 A_0(x)\Big)\partial_y W(y)dy \\ =& -2\Big(\partial_x^2 A_0(x)\Big)W(y)|_0^1 = 0. \end{aligned} \tag{B.3}$$

$$\begin{aligned} \int_0^1 \mathfrak{M}_2(A_0)dy =& \int_0^1 \Big((\frac{1}{3} - y(1-y))\int_0^1 \partial_x^2 A_0(x)ds\Big)dy = \Big(\partial_x^2 A_0(x)\Big)\int_0^1 (\frac{1}{3} - y(1-y))dy \\ =& \frac{1}{6}\partial_x^2 A_0(x). \end{aligned} \tag{B.4}$$

$$\int_0^1 (-\partial_x^2 A_0)dy = -\partial_x^2 A_0. \tag{B.5}$$

$$\begin{aligned} \int_0^1 \mathfrak{M}_1(A_1)dy =& \int_0^1 \Big((\frac{1}{2} - y)\int_0^1 \partial_x A_1(x,s)ds\Big)dy = \int_0^1 (\frac{1}{2} - y)dy\int_0^1 \partial_x A_1(x,s)ds \\ =& 0. \end{aligned} \tag{B.6}$$

$$\int_0^1 (\partial_y^2 A_2 - i\omega\bar{\alpha}(A_2 - \mathfrak{M}_0(A_2)))dy = \partial_y A_2|_0^1 - i\omega\bar{\alpha}\Big(\int_0^1 A_2(x,y)dy - \int_0^1 A_2(x,y)dy\Big) = 0. \tag{B.7}$$

B.1.4 Analytical solution of A_ε in the domain of lamination stack Ω_L

Recall that the magnetic vector potential in 1d assumption satisfies (4.21)-(4.22). Define the vector $a = A_\varepsilon - \mathcal{M}(A_\varepsilon)$ in each sheet. Replacing a in (4.21), we obtain a second order ordinay differential equation

$$\partial_x^2 a - i\omega\sigma_1\mu_1 a = 0. \tag{B.8}$$

The solution of (B.8) is

$$a = C_1^i e^{\kappa x} + C_2^i e^{-\kappa x}, \tag{B.9}$$

in each sheet i, where $\kappa^2 = i\omega\mu_1\sigma_1$.

By integrating $a = A_\varepsilon - \mathcal{M}(A_\varepsilon)$ on each thin layer $(\varepsilon\lfloor x_1/\varepsilon\rfloor, \varepsilon\lfloor x_1/\varepsilon\rfloor + \varepsilon)$, we obtain that the average value of a in each layer is nul. we have then

$$\int_{\varepsilon\lfloor x_1/\varepsilon\rfloor}^{\varepsilon\lfloor x_1/\varepsilon\rfloor+\varepsilon} a(s)ds = 0. \tag{B.10}$$

Let x_i and x_{i+1} be the extremities of the layer i. Integration (B.9) on the sheet i, and using (B.10), we have

$$\int_{x_i}^{x_{i+1}} (C_1^i e^{\kappa s} + C_2^i e^{-\kappa s})ds = 0, \tag{B.11}$$

which gives that

$$C_1^i(e^{\kappa x_{i+1}} - e^{\kappa x_i}) + C_2^i(-e^{-\kappa x_{i+1}} + e^{-\kappa x_i}) = 0, \tag{B.12}$$

in each sheet $i = (x_i, x_{i+1}$.

By considering the continuity conditions of $A_\varepsilon = a + \mathcal{M}$ at the interface of each two consecutive sheets, we obtain the following equalities

$$C_1^i e^{\kappa x_{i+1}} + C_2^i e^{-\kappa x_{i+1}} + \mathcal{M}^i - C_1^{i+1} e^{\kappa x_{i+1}} - C_2^{i+1} e^{-\kappa x_{i+1}} - \mathcal{M}^{i+1} = 0, \tag{B.13}$$

$$C_1^i e^{\kappa x_{i+1}} - C_2^i e^{-\kappa x_{i+1}} - C_1^{i+1} e^{\kappa x_{i+1}} + C_2^{i+1} e^{-\kappa x_{i+1}} = 0, \tag{B.14}$$

where x_{i+1} is the boundary point between the two stacks i and $i+1$.

Adding together the equations (B.12), (B.13), (B.14) and the boundary conditions (4.22) we obtain the coefficients C_1^i,C_2^i and $\mathcal{M}^i$ in each sheet by solving a linear system of equations.

B.1.5 Approximation of the derivative of A_ε along x_2 by the asymptotic expansion in power series of δ

Using the multiscale expansion in power series of the small complex parameter δ

$$b_\delta(x) = b_0(x,\delta) + \delta b_1(x,\delta) + \delta^2 b_2(x,\delta) + ..., \forall x \in \mathbb{R}^2 \tag{B.15}$$

with $b_j(x,\delta) = \chi(\nu)w_j(t,\nu/\delta)$, where t and ν are the tangential and normal variation in a neighborhood $\chi(\nu)$ of Γ.

Rescaling $\Upsilon = \frac{\nu}{\delta}$, the operator Δ expands in power series of δ with coefficients intrinsic operators with respect to Γ [102]:

$$\delta^2\Delta = \partial_\Upsilon^2 + \sum_{n\geq 1} \delta^n A_n, \tag{B.16}$$

where

$$A_1 = -k(t)\partial_\Upsilon,$$
$$A_2 = \partial_t^2 - k(t)^2\Upsilon\partial_\Upsilon.$$

Denote by $v_\delta(t,\Upsilon) = b_\delta(x)$. After scaling $\nu \longrightarrow \Upsilon = \nu/\delta$, we get:

$$(-\partial_\Upsilon^2 + i)v_\delta - \sum_{n\geq 1} \delta^n A_n v_n = 0 \text{ in } \Gamma \times (0,+\infty). \tag{B.17}$$

Inserting $v_\delta = \sum_{n\geq 0} \underline{\delta}^n w_n(t,\nu/\delta)$ with $w_n(.,\Upsilon) \longrightarrow 0$ as $\Upsilon \longrightarrow +\infty$ in (B.17), the terms w_n satisfy the following family of problems coupled by their conditions on the interface $\Gamma(\Upsilon = 0)$

$$\begin{cases} -\partial_\Upsilon^2 w_n + w_n = \sum_{p\geq 1}^n A_p w_{n-p} \text{ in } \Gamma \times (0,+\infty), \\ w_n = g'\delta_n^0 \text{ on } \Gamma, \end{cases} \tag{B.18}$$

where δ_n^0 is the Kronecker symbol.

The first term to be determined in the asymptotics is the profile w_0. According to (B.18) for $n = 0$, w_0 solves the ODE:

$$\begin{cases} -\partial_\Upsilon w_0(\cdot,\Upsilon) + w_0(\cdot,\Upsilon) = 0 \text{ in } \Gamma \times (0,+\infty), \\ w_0(\cdot,\Upsilon) = g'(X(t)) \text{ on } \Gamma, \end{cases} \tag{B.19}$$

i.e.

$$\begin{cases} -\partial_\Upsilon w_0 + w_0 = 0 \text{ in } \Gamma \times (0,+\infty), \\ w_0 = g' \text{ on } \Gamma. \end{cases} \tag{B.20}$$

The general solution of (B.20) is:

$$w_0 = a(t)e^{-\Upsilon}.$$

Using the boundary condition on Γ, we get:

$$w_0 = g'(X(t))e^{-\Upsilon}.$$

Thus,

$$b_0(x,\delta) = g'(x_2)e^{-x_1/\delta}, \tag{B.21}$$

and

$$b(x_1,x_2) = g'(x_2)e^{-x_1\kappa/\varepsilon} + O(\varepsilon). \tag{B.22}$$

Publications

M. Issa, B. Bannwarth, O. Chadebec, G. Meunier, J-R. Poirier, E. Sarraute, R. Perrussel , *Boundary Element Method for 3D Eddy Current Problems With a Conductive Thin Layer*. NUMELEC 2017. https://numelec2017.sciencesconf.org/.

Mohammad Issa, Victor Péron, Ronan Perrussel. *Asymptotic Modelling for 3D Eddy Current Problems with a Conductive Thin Layer*. ACOMEN 2017 - 7th International Conference on Advanced COmputational Methods in ENgineering, Sep 2017, Ghent, Belgium. hal-01679683

Mohammad Issa, Jean-René Poirier, Olivier Chadebec, Victor Péron, Ronan Perrussel. *Boundary Element Method for Conductive Thin Layer in 3D Eddy Current Problems*. IABEM , 2018. Lien : https://project.inria.fr/iabem2018/

Mohammad Issa, Jean-René Poirier, Ronan Perrussel, Olivier Chadebec, Victor Péron, (2019). *Boundary element method for 3D conductive thin layer in eddy current problems*. COMPEL - The international journal for computation and mathematics in electrical and electronic engineering, Vol. 38 Issue: 2, pp.502-521, https://doi.org/10.1108/COMPEL-09-2018-0348

Mohammad Issa, Laurent Krähenbühl, Clair Poignard, Jean-René Poirier, Ronan Perrussel. *Homogenization of lamination stacks based on the vector potential formulation*. Compumag 2019, Jul 2019, Paris, France. hal-02063629

Bibliography

[1] A. Rodríguez, A. Valli. *Eddy Current Approximation of Maxwell Equations: Theory, Algorithms and Applications*. Springer-Verlag: Milan, 2010. *Cited on page 12*

[2] A. Bondeson, T. Rylander, and P. Ingelström. *Computational Electromagnetics*. Texts in Applied Mathematics Vol. 51, Springer, New York, 2005. *2 citations pages 8 and 9*

[3] J M Jin. *The Finite Element Method in Electromagnetics*. New York, NY: John Wiley and Sons, 1993. *Cited on page 17*

[4] J M Jin. *The Finite Element Method in Electromagnetics*. New York, NY: John Wiley and Sons, second edition, 2002. *Cited on page 17*

[5] A F Peterson, S L Ray, and R Mittra. *Computational Methods for Electromagnetics*. New York, NY: IEEE Press, 1997. *Cited on page 17*

[6] A. Kirsch and F. Hettlich. *The mathematical theory of Maxwell's equations*, Lecture Notes, 2009. *pas de citations*

[7] A. Bossavit. *Whitney forms: a class of finite elements for three-dimensional computations in electromagnetism*. IEE Proceedings A - Physical Science, Measurement and Instrumentation, Management and Education - Reviews, vol. 135, no. 8, pp. 493-500, Nov. 1988. *Cited on page 19*

[8] Van Dantzig. *The fundamental equations of electromagnetism, independent of metrical geometry*. Mathematical Proceedings of the Cambridge Philosophical Society, 30(4), 421-427, (1934). doi:10.1017/S0305004100012664 *Cited on page 10*

[9] Alfonzetti, S. , Borzì, G. and Salerno, N. (1998). *Iteratively-improved Robin boundary conditions for the finite element solution of scattering problems in unbounded domains*. Int. J. Numer. Meth. Engng., 42: 601-629. doi:10.1002/(SICI)1097-0207(19980630)42:4<601::AID-NME373>3.0.CO;2-O. *Cited on page 13*

[10] Dan Givoli, Joseph B. Keller. *A finite element method for large domains*. Computer Methods in Applied Mechanics and Engineering, Volume 76, Issue 1, 1989, Pages 41-66, ISSN 0045-7825, https://doi.org/10.1016/0045-7825(89)90140-0. *Cited on page 13*

[11] Hagstrom, T. M., and H. B. Keller. *Asymptotic Boundary Conditions and Numerical Methods for Nonlinear Elliptic Problems on Unbounded Domains*. Mathematics of Computation 48, no. 178 (1987): 449-70. doi:10.2307/2007821. *Cited on page 13*

[12] D. A. Lowther and E. M. Freeman. *Further aspects of the Kelvin transformation method for dealing with open boundaries*. IEEE Transactions on Magnetics, vol. 28, no. 2, pp. 1667-1670, March 1992. doi: 10.1109/20.124022 *Cited on page 13*

[13] X. Brunotte, G. Meunier and J. F. Imhoff. *Finite element modeling of unbounded problems using transformations: a rigorous, powerful and easy solution.* IEEE Transactions on Magnetics, vol. 28, no. 2, pp. 1663-1666, March 1992. doi: 10.1109/20.124021 *Cited on page 13*

[14] V. Radulescu, D. Repovs. *Partial Differential Equations with Variable Exponents: Variational Methods and Qualitative Analysis.* CRC Press, Taylor and Francis Group, Boca Raton *Cited on page 17*

[15] R. D. Graglia. *On the numerical integration of the linear shape functions times the 3-D Green's function or its gradient on a plane triangle.* IEEE Transactions on Antennas and Propagation, vol. 41, no. 10, pp. 1448-1455, Oct. 1993. doi: 10.1109/8.247786 FL, 2015. *Cited on page 25*

[16] P. Alotto, P. Bettini and R. Specogna. *Sparsification of BEM Matrices for Large-Scale Eddy Current Problems.* IEEE Transactions on Magnetics, vol. 52, no. 3, pp. 1-4, March 2016, Art no. 7203204. doi: 10.1109/TMAG.2015.2488699 *Cited on page 25*

[17] J. Smajic, Z. Andjelic and M. Bebendorf. *Fast BEM for Eddy-Current Problems Using H-Matrices and Adaptive Cross Approximation.* IEEE Transactions on Magnetics, vol. 43, no. 4, pp. 1269-1272, April 2007. doi: 10.1109/TMAG.2006.890971 *Cited on page 25*

[18] J. Ostrowski, Z. Andjelic, M. Bebendorf, B. Cranganu-Cretu and J. Smajic. *Fast BEM-solution of Laplace problems with H-matrices and ACA.* IEEE Transactions on Magnetics, vol. 42, no. 4, pp. 627-630, April 2006. doi: 10.1109/TMAG.2006.871642 *Cited on page 25*

[19] G. Meunier, H. T. Luong and Y. Marechal. *Computation of coupled problem of 3D eddy current and electrical circuit by using $T_0 - T - \phi$ formulation.* IEEE Transactions on Magnetics, vol. 34, no. 5, pp. 3074-3077, Sept. 1998. doi: 10.1109/20.717719. *Cited on page 13*

[20] A. Bossavit. *Hybrid electric–magnetic methods in eddy-current problems.* Computer Methods in Applied Mechanics and Engineering, Volume 178, Issues 3–4, 1999. *Cited on page 12*

[21] R. Hiptmair. *Symmetric coupling for eddy current problems.* SIAM J. Numer. Anal., 40, pp. 41-65, 2002. *Cited on page 24*

[22] D. Albertz and G. Henneberger. *Calculation of 3D eddy current fields using both electric and magnetic vector potential in conducting regions.* IEEE Transactions on Magnetics, vol. 34, no. 5, pp. 2644-2647, Sept. 1998. *Cited on page 13*

[23] M. T. Holmberg. *Three-Dimensional Finite Element Computation of Eddy Currents in Synchronous Machines.* Ph.D. dissertation, Chalmers Univ. Technol., Gothenberg, Sweden, Dec. 1998. *Cited on page 26*

[24] J. C. Nédélec. *Mixed finite elements in $\mathbb{R}^3$.* Numer. Math. 35 (1980), 315-341. *Cited on page 25*

[25] G. Mur. *Edge elements, their advantages and their disadvantages.* IEEE Transactions on Magnetics, vol. 30, no. 5, pp. 3552-3557, Sept. 1994. *Cited on page 25*

[26] M. L. Barton and Z. J. Cendes. *New vector finite elements for three dimensional magnetic field computation.* J. Appl. Phys., vol. 61, no.2, pp. 3919–3921, Apr. 1987. *Cited on page 27*

[27] S. Rjasanow, and O. Steinbach. *The Fast Solution of Boundary Integral Equations.* Springer, Berlin 2007. *2 citations pages 21 and 22*

[28] J.T. Katsikadelis and M.S. Nerantzaki. *A Boundary-Only BEM for Linear and Nonlinear Problems.* Transactions on Modelling and Simulation vol 20, 1998. *Cited on page 24*

[29] D. Soares, J. A. M. Carrer, W. J. Mansur. *Non-linear elastodynamic analysis by the BEM: an approach based on the iterative coupling of the D-BEM and TD-BEM formulations.* Engineering Analysis with Boundary Elements, Elsevier, 2005, 29 (8), pp.761 - 774. ff10.1016/j.enganabound.2005.04.005ff. ffhal-01634270 *Cited on page 24*

[30] J. C. Nedelec. *A new family of mixed finite elements in R^3.* Numer. Math., 50 (1986), pp. 57-81. *Cited on page 25*

[31] A.A. Rodriguez, R. Hiptmair, and A. Valli. *Hybrid formulations of eddy current problems.* Numer. Method. Part. Differ. Eq., 21(4):742–763, 2005. *Cited on page 12*

[32] R. Albanese and G. Rubinacci. *Formulation of the eddy-current problem.* IEE Proceedings A - Physical Science, Measurement and Instrumentation, Management and Education, vol. 137, no. 1, pp. 16-22, Jan. 1990. *Cited on page 12*

[33] Z. Ren and A. Razek. *Comparison of some 3D eddy current formulations in dual systems.* IEEE Transactions on Magnetics, vol. 36, no. 4, pp. 751-755, July 2000. *Cited on page 12*

[34] O. C. Zienkiewicz, D. M. Kelly and P. Bettes. *The Coupling of the Finite Element Method and Boundary Solution Procedures.* International Journal for Numerical Methods in Engineering, 11, 355-375, 1977. *Cited on page 30*

[35] M. Costabel. *Symmetric methods for the coupling of finite elements and boundary elements.* Boundary Elements IX, C. Brebbia, W. Wendland, and G. Kuhn (Eds.), Springer, 411–420, 1987. *Cited on page 30*

[36] S. Sirtori, G. Maier, G. Novati and S. Miccoli. *A Galerkin Symmetric Boundary Element Method in Elasticity: Formulation and Implementation.* International Journal for Numerical Methods in Engineering, 35, 255-282, 1992. *Cited on page 30*

[37] U. Langer. *Parallel Iterative Solution of Symmetric Coupled FE/BE-Equation via Domain Decomposition.* Contempory Mathematics, 157, 335-344, 1994. *Cited on page 30*

[38] M. Bonnet. *Regularized Direct and Indirect Symmetric Varaitional BIE Formulations for Three-Dimensional Elasticity.* Engineering Analysis with Boundary Elements, 15, 93-102 (1995). *Cited on page 30*

[39] S. Ganguly, J. B. Layton and C. Balakrishma. *Symmetric coupling of multi-zone curved Galerkin boundary elements with finite elements in elasticity.* International Journal of Numerical Methods in Engineering, 48, 633-654, 2000. *Cited on page 30*

[40] U. Langer, O. Steinbach. *Coupled Boundary and Finite Element Tearing and Interconnecting Methods.* Proceedings of the Fifteenth International Conference on Domain Decomposition, Berlin, 83-98, 2003. *Cited on page 30*

[41] M. Haas, B. Helldörfer and G. Kuhn. *Improved Coupling of Finite Shell Elements and 3D Boundary Elements.* Archive of Applied Mechanics, 75, 649-663, 2006. *Cited on page 30*

[42] R. Springhetti, G. Novati, M. Margonari. *Weak Coupling of the Symmetric Galerkin BEM with FEM for Potential and Elastostatic Problems.* Computer Modeling in Engineering and Sciences, 13, 67-80, 2006. *Cited on page 30*

[43] R. V. Sabariego, J. Gyselinck, P. Dular, C. Geuzaine and W. Legros. *Fast multipole acceleration of the hybrid finite-element/boundary-element analysis of 3-D eddy-current problems.* IEEE Transactions on Magnetics, vol. 40, no. 2, pp. 1278-1281, March 2004. doi: 10.1109/TMAG.2004.825151 *Cited on page 30*

[44] S. Kurz, J. Fetzer, G. Lehner and W. M. Rucker. *A novel formulation for 3D eddy current problems with moving bodies using a Lagrangian description and BEM-FEM coupling.* IEEE Transactions on Magnetics, vol. 34, no. 5, pp. 3068-3073, Sept. 1998. doi: 10.1109/20.717718 *Cited on page 30*

[45] A. Buchau, C. J. Huber, W. Rieger and W. M. Rucker. *Fast BEM computations with the adaptive multilevel fast multipole method.* IEEE Transactions on Magnetics, vol. 36, no. 4, pp. 680-684, July 2000. doi: 10.1109/20.877540 *Cited on page 25*

[46] J-M. Bergheau and Ph. Conraux. *Fem-bem coupling for the modelling of induction heating processes including moving parts.* Journal of Shangai Jiaotong University, June 2000, vol. E-5, pp. 91–99. *Cited on page 30*

[47] T. Steinmetz, N. Godel, G. Wimmer, M. Clemens, S. Kurz and M. Bebendorf. *Efficient Symmetric FEM-BEM Coupled Simulations of Electro-Quasistatic Fields.* IEEE Transactions on Magnetics, vol. 44, no. 6, pp. 1346-1349, June 2008. doi: 10.1109/TMAG.2008.915785 *Cited on page 30*

[48] S. Kurz and S. Russenschuck. *The application of the BEM-FEM coupling method for the accurate calculation of fields in superconducting magnets.* Elect. Engrg., vol. 82, pp. 1–10, 1999. *Cited on page 30*

[49] A. Warszawski, D. Jr. Soares, and W. J. Mansur. *A FEM–BEM coupling procedure to model the propagation of interacting acoustic–acoustic/acoustic– elastic waves through axisymmetric media.* Comput. Methods Appl. Mech. Eng., vol.197, pp. 3828-3835, 2008. *Cited on page 30*

[50] A. Bossavit and J. Vérité. *The TRIFOU code: Solving the 3-D eddy–currents problem by using H as state variable* IEEE Trans. Mag. 19 (1983) 2465–2470. *Cited on page 31*

[51] A. Bossavit. *Two dual formulations of the 3-D eddy-currents problem.* COMPEL 4 (1985) 103–116. *Cited on page 31*

[52] A. Bossavit. *The computation of eddy-currents in dimension 3 by using mixed finite elements and boundary elements in association.* Math. Comput. Modelling 15 (1991) 33–42. *Cited on page 31*

[53] A. Bossavit. *Electromagnétisme, en vue de la modélisation.* Springer-Verlag, Paris, Berlin, Heidelberg, 1993. *Cited on page 31*

[54] G.N. Gatica and G.C. Hsiao. *Boundary-field equation methods for a class of nonlinear problems.* Longman, 1995. *Cited on page 30*

[55] S. Meddahi, J. Valdés, O. Menéndez, P. Pérez. *On the coupling of boundary integral and mixed finite element methods.* Journal of Computational and Applied Mathematics, Volume 69, Issue 1, 1996. *Cited on page 30*

[56] C. Johnson, J.C. Nédélec. *On the coupling of boundary integral and finite element methods.* Mathematics of Computation 35 (1980) 1063–1079. *Cited on page 30*

[57] F. Bruckner, C. Vogler, M. Feischl, D. Praetorius, B. Bergmair, T. Huber, M. Fuger, D. Suess. *3D FEM–BEM-coupling method to solve magnetostatic Maxwell equations.* Journal of Magnetism and Magnetic Materials, Volume 324, Issue 10, Pages 1862-1866, 2012. *Cited on page 33*

[58] W.Hackbusch. *A sparse matrix arithmetic based on H-matrices. Part I: Introduction to H-matrices.* Computing 62, 1999. *Cited on page 36*

[59] Victor Péron, Kersten Schmidt, Marc Duruflé. *Equivalent transmission conditions for the time-harmonic Maxwell equations in 3D for a medium with a highly conductive thin sheet.* SIAM Journal on Applied Mathematics, Society for Industrial and Applied Mathematics, 2016, 76 (3), pp.1031-1052. <10.1137/15M1012116>. <hal-01260111v2>. *3 citations pages xi, 48, and 105*

[60] R. Hiptmair. *Symmetric coupling for eddy current problems.* SIAM J. Numer. Anal. 40 (2002),pp. 41-65. *4 citations pages 64, 65, 66, and 71*

[61] A. Buffa and M. Fortin. *On traces for functional spaces related to Maxwell's equations.Part I: An integration by parts formula in Lipschitz polyhedra.* Tech. Rep. 1147, Instituto di Analisi Numerica, CNR, Pavia, Italy, 1999. *Cited on page 64*

[62] A. Buffa and M. Fortin. *On traces for functional spaces related to Maxwell's equations.Part II: Hodge decompositions on the boundary of Lipschitz polyhedra and applicatons.* Tech. Rep. 1147, Instituto di Analisi Numerica, CNR, Pavia, Italy, 1999. *Cited on page 64*

[63] P. A. Raviart and J. M. Thomas. *A mixed Finite Element Method for second order elliptic problems.* vol. 606 of Springer lecture notes in Mathematics, Springer-Vergal, New York, 1977,pp. 292 315. *Cited on page 67*

[64] Victor Péron. *Impedance transmission conditions for eddy current problems.* 2017. https://hal.inria.fr/hal-01505612. *3 citations pages 48, 52, and 55*

[65] K. Schmidt and A. Chernov.*Robust transmission conditions of high order for thing conducting sheets in two dimensions*, IEEE Trans. Magn., 50(2):41-44, 2014. *Cited on page 47*

[66] S. Rjasanow, O. Steinbach. *The fast solution of boundary integral equations*, Mathematical and Analytical Techniques with Applications to Engineering, Springer, New York, 2007. *Cited on page 48*

[67] K. Schmidt and A. Chernov. *A unified analysis of transmission conditions for thin conducting sheets in the time-harmonic eddy current model*, SIAM J. Appl. Math., 73(6):1980-2003, 2013. *Cited on page 48*

[68] Thanh-Trung Nguyen, Gérard Meunier, Jean-Michel Guichon, and Olivier Chadebec, *3- D Integral Formulation Using Facet Elements for Thin Conductive Shells Coupled With an External Circuit*. IEEE Transactions on Magnetics, Vol. 51, Issue 3, 2015 . *Cited on page 47*

[69] R. Hiptmair and J. Ostrowski. *Coupled boundary-element scheme for eddy-current computation*. Journal of Engineering Mathematics 51:3, 231-250. *2 citations pages 67 and 71*

[70] Ana Alonso Rodríguez, and Alberto Valli. *Eddy Current Approximation of Maxwell Equations: Theory, Algorithms and Applications*. Vol. 4, Springer Science and Business Media, 2010. *Cited on page 53*

[71] A. A. Kolyshkin and R. Vaillancourt. *Series solution of an eddy-current problem for a sphere with varying conductivity and permeability profiles*. IEEE Transactions on Magnetics, vol. 35, no. 6, pp. 4445-4451, 1999. *Cited on page 111*

[72] G. Caloz, M. Dauge, E. Faou, and V. Peron. *On the influence of the geometry on skin effect in electromagnetism*. Comput. methods Appl. Mech. Engrg.,2011. *Cited on page 107*

[73] V. Péron. *Modelisation mathematique de phenomenes electromagnetiques dans des matériaux à fort contraste*. PHD Thesis, Université Rennes 1,2009. *2 citations pages 61 and 105*

[74] W. Mclean. *Strongly Elliptic Systems and Boundary Integral Equations*. Cambridge University Press, 2000. *Cited on page 57*

[75] H. Brezis. *Analyse Fonctionelle*. Paris: Masson, 1980. *Cited on page 64*

[76] S.M. Rao, D.R. Wilton, and A.W. Glisson. *Electromagnetic scattering by surfaces of arbitrary shape*. IEEE Trans. Antennas Propag. AP-30, 409-418, 1982. *Cited on page 67*

[77] C. Geuzaine, P. Dular, and W. Legros. *Dual formulations for the modeling of thin electromagnetic shells using edge elements*. IEEE Transactions on Magnetics, vol. 36, no. 4, pp. 799-803, July 2000. *Cited on page 47*

[78] R. V. Sabariego, P. Sergeant, J. Gyselinck, P. Dular, L. Dupré, and C. Geuzaine. *Finite element analysis of a shielded pulsed-current induction heater - Experimental validation of a time-domain thin shell approach.* COMPEL International Journal for computation and mathetamtics in electrical and electronic engineering, 29(6):1585-1595, 2010. *pas de citations*

[79] P. Sergeant, R. V. Sabariego, C. Crevecoeur, L. Dupré, and C. Geuzaine. *Analysis of perforated magnetic shields for electric power applications.* IET Electric power applications, 3(2): 123-132, March 2009. *Cited on page 47*

[80] R. V. Sabariego, C. Geuzaine, P. Dular, and J. Gyselinck. *h- and a- time-domain formulations for the modelling of thin electromagnetic shells.* IET Science, Measurement & Technology, 2(6):402-408, November 2008. *Cited on page 47*

[81] J. Gyselinck, R. V. Sabariego, P. Dular, and C. Geuzaine. *Time-domain finite-element modeling of thin electromagnetic shells.* IEEE Transactions on Magnetics, 44(6):742-745, June 2008. *Cited on page 47*

[82] M. Issa, B. Bannwarth, O. Chadebec, G. Meunier, J-R. Poirier, E. Sarraute, R. Perrussel , *Boundary Element Method for 3D Eddy Current Problems With a Conductive Thin Layer.* NUMELEC 2017. https://numelec2017.sciencesconf.org/. *Cited on page 4*

[83] Mohammad Issa, Victor Péron, Ronan Perrussel. *Asymptotic Modelling for 3D Eddy Current Problems with a Conductive Thin Layer.* ACOMEN 2017 - 7th International Conference on Advanced COmputational Methods in ENgineering, Sep 2017, Ghent, Belgium. hal-01679683 *Cited on page 4*

[84] Mohammad Issa, Jean-René Poirier, Olivier Chadebec, Victor Péron, Ronan Perrussel. *Boundary Element Method for Conductive Thin Layer in 3D Eddy Current Problems.* IABEM , 2018. Lien : https://project.inria.fr/iabem2018/ *Cited on page 4*

[85] Mohammad Issa, Jean-René Poirier, Ronan Perrussel, Olivier Chadebec, Victor Péron, (2019). *Boundary element method for 3D conductive thin layer in eddy current problems.* COMPEL - The international journal for computation and mathematics in electrical and electronic engineering, Vol. 38 Issue: 2, pp.502-521, https://doi.org/10.1108/COMPEL-09-2018-0348 *Cited on page 4*

[86] K. Hollaus, A. Hannukainen and J. Schöberl. *Two-Scale Homogenization of the Nonlinear Eddy Current Problem With FEM.* IEEE Transactions on Magnetics, vol. 50, no. 2, pp. 413-416, Feb. 2014, Art no. 7010104. *Cited on page 84*

[87] K. Hollaus, M. Huber, J. Schöberl, and P. Hamberger. *A linear FEM benchmark for the homogenization of the eddy currents in laminated media in 3D.* Proc. IFAC, 2012, pp. 1190–1194. *Cited on page 84*

[88] E. Sanchez-Palencia and A. Zaoui. *Homogenization Techniques for Composite Media.* Vol. 272, 1987, doi:10.1007/3-540-17616-0. *Cited on page 85*

[89] K. Hollaus and J. Schöberl. *Homogenization of the eddy current problem in 2D.* Proc. 14th Int. IGTE Symp., Graz, Austria, Sep. 2010, pp. 154–159. *Cited on page 84*

[90] K. Hollaus and J. Schöberl. *Some 2-D Multiscale Finite-Element Formulations for the Eddy Current Problem in Iron Laminates.* IEEE Transactions on Magnetics, vol. 54, no. 4, pp. 1-16, April 2018. *Cited on page 84*

[91] L. Krähenbühl, R. Scorretti, R. Perrussel, and P. Dular. *Approche alternative à l'homogénéisation pour la modélisation des empilements de tôles - le cas harmonique linéaire.* [Rapport de recherche] Laboratoire Ampère; Laboratoire Laplace ; Université de Liège, 2017. < hal01516189v5> *Cited on page 86*

[92] L. Krähenbühl, P. Dular, T. Zeidan and F. Buret. *Homogenization of Lamination Stacks in Linear Magnetodynamics.* IEEE T-Mag 40-2, pp. 912-915, 2004. *Cited on page 84*

[93] A. Bermudez, D. Gomez and P. Salgado. *Eddy-Current Losses in Laminated Cores and the Computation of an Equivalent Conductivity.* IEEE Transactions on Magnetics, vol. 44, no. 12, pp. 4730-4738, Dec. 2008. doi: 10.1109/TMAG.2008.2005118 *Cited on page 84*

[94] Yicheng Chen and P. Pillay. *An improved formula for lamination core loss calculations in machines operating with high frequency and high flux density excitation.* Conference Record of the 2002 IEEE Industry Applications Conference. 37th IAS Annual Meeting (Cat. No.02CH37344), Pittsburgh, PA, USA, 2002, pp. 759-766 vol.2. doi: 10.1109/IAS.2002.1042645 *Cited on page 84*

[95] K. Howard and M. K. Kazimierczuk. *Eddy-current power loss in laminated iron cores.* ISCAS 2001, The 2001 IEEE International Symposium on Circuits and Systems (Cat. No.01CH37196), Sydney, NSW, 2001, pp. 668-671 vol. 2. doi: 10.1109/ISCAS.2001.921399 *Cited on page 84*

[96] T. L. Mthombeni and P. Pillay. *Physical Basis for the Variation of Lamination Core Loss Coefficients as a Function of Frequency and Flux Density.* IECON 2006 - 32nd Annual Conference on IEEE Industrial Electronics, Paris, 2006, pp. 1381-1387. doi: 10.1109/IECON.2006.347545 *Cited on page 84*

[97] J. Xu, A. Lakhsasi, Z. Yao and V. Rajagopalan. *A Practical Modeling Method for Eddy-Current Losses Computation in Laminated Magnetic Cores.* IAS '96. Conference Record of the 1996 IEEE Industry Applications Conference Thirty-First IAS Annual Meeting, San Diego, CA, USA, 1996, pp. 1532-1537. doi: 10.1109/IAS.1996.559270 *Cited on page 84*

[98] L. Krähenbühl and D. Muller. *Thin layers in electrical engineering-example of shell models in analysing eddy-currents by boundary and finite element methods.* IEEE Transactions on Magnetics, vol. 29, no. 2, pp. 1450-1455, March 1993. doi: 10.1109/20.250676 *Cited on page 84*

[99] H. Igarashi, A. Kost and T. Honma. *A three dimensional analysis of magnetic fields around a thin magnetic conductive layer using vector potential.* IEEE Transactions on Magnetics, vol. 34, no. 5, pp. 2539-2542, Sept. 1998. doi: 10.1109/20.717585 *Cited on page 84*

[100] P. Dular, J. Gyselinck, C. Geuzaine, N. Sadowski and J. P. A. Bastos. *A 3-D magnetic vector potential formulation taking eddy currents in lamination stacks into account*. IEEE Transactions on Magnetics, vol. 39, no. 3, pp. 1424-1427, May 2003. doi: 10.1109/TMAG.2003.810386 *Cited on page 84*

[101] Mohammad Issa, Laurent Krähenbühl, Clair Poignard, Jean-René Poirier, Ronan Perrussel. *Homogenization of lamination stacks based on the vector potential formulation*. Compumag 2019, Jul 2019, Paris, France. hal-02063629 *Cited on page 5*

[102] Victor Peron. Asymptotic expansion for the magnetic potential in the eddy current problem : the ferromagnetic case. 2015. ffhal-01253971f *2 citations pages 99 and 117*

[103] J. Gyselinck, P. Dular, L. Krähenbühl and Ruth V. Sabariego. *Finite-element homogenization of laminated iron cores with inclusion of net circulating currents due to imperfect insulation*. IEEE Transactions on Magnetics, vol. 52, no. 3, March 2016. *2 citations pages 47 and 85*

[104] I. Niyonzima, R. V. Sabariego, P. Dular, F. Henrotte and C. Geuzaine. *Computational homogenization for laminated ferromagnetic cores in magnetodynamics*. IEEE Transactions on Magnetics, vol. 49, no. 5, May 2013. *Cited on page 85*

[105] I. Niyonzima, R. V. Sabariego, P. Dular, and C. Geuzaine. *Finite element computational homogenization of nonlinear multiscale materials in magnetostatics*. IEEE Transactions on Magnetics, vol. 48, no. 2, February 2012. *Cited on page 85*

[106] J. Gyselinck, R. V. Sabariego, and P. Dular. *A nonlinear time-domain homogenization technique for laminated iron cores in three-dimensional finite-element models*. IEEE Transactions on Magnetics, vol. 42, no. 4, April 2006. *Cited on page 85*